PROPAGATION AND BREAKING OF WAVE GROUPS

by

JAYARAM VEERAMONY

AND

IB A. SVENDSEN

RESEARCH REPORT NO. CACR-95-03

FEBRUARY, 1995

CENTER FOR APPLIED COASTAL RESEARCH

Ocean Engineering Laboratory
University of Delaware
Newark, Delaware 19716

REPORT DOCUMENTATION PAGE

Public reporting burden for this collection of information is estimated to average 1 hour per response, including the time for reviewing instructions, searching existing data sources, gathering and maintaining the data needed, and completing and reviewing the collection of information. Send comments regarding this burden estimate or any other aspect of this collection of information, including suggestions for reducing this burden, to Washington Headquarters Services, Directorate for Information Operations and Reports, 1215 Jefferson Davis Highway, Suite 1204, Arlington, VA 22202-4302, and to the Office of Management and Budget, Paperwork Reduction Project (0704-0188), Washington, DC 20503.

1. AGENCY USE ONLY (Leave blank)	2. REPORT DATE	3. REPORT TYPE AND DATES COVERED
	2/95	Technical

4. TITLE AND SUBTITLE

PROPAGATION AND BREAKING OF WAVE GROUPS

5. FUNDING NUMBERS

DAAL03-92-G-0116

6. AUTHOR(S)

Jayaram Veeramony and Ib A. Svendsen

7. PERFORMING ORGANIZATION NAME(S) AND ADDRESS(ES)

CENTER FOR APPLIED COASTAL RESEARCH
OCEAN ENGINEERING LABORATORY
UNIVERSITY OF DELAWARE
NEWARK, DE 19716

8. PERFORMING ORGANIZATION REPORT NUMBER

9. SPONSORING/MONITORING AGENCY NAME(S) AND ADDRESS(ES)

U.S. Army Research Office
P.O. Box 12211
Research Triangle Park, NC 27709-2211

10. SPONSORING/MONITORING AGENCY REPORT NUMBER

ARO 30379.28-GS-URI

11. SUPPLEMENTARY NOTES

The views, opinions and/or findings contained in this report are those of the author(s) and should not be construed as an official Department of the Army position, policy, or decision, unless so designated by other documentation.

12a. DISTRIBUTION/AVAILABILITY STATEMENT

Approved for public release; distribution unlimited.

12b. DISTRIBUTION CODE

13. ABSTRACT (Maximum 200 words)

ABSTRACT IN REPORT

14. SUBJECT TERMS

	15. NUMBER OF PAGES
	142
	16. PRICE CODE

17. SECURITY CLASSIFICATION OF REPORT	18. SECURITY CLASSIFICATION OF THIS PAGE	19. SECURITY CLASSIFICATION OF ABSTRACT	20. LIMITATION OF ABSTRACT
UNCLASSIFIED	UNCLASSIFIED	UNCLASSIFIED	UL

PROPAGATION AND BREAKING OF WAVE GROUPS

by

JAYARAM VEERAMONY

AND

IB A. SVENDSEN

RESEARCH REPORT NO. CACR-95-03

FEBRUARY, 1995

CENTER FOR APPLIED COASTAL RESEARCH
OCEAN ENGINEERING LABORATORY
UNIVERSITY OF DELAWARE
NEWARK, DE 19716

TABLE OF CONTENTS

Chapter

LIST OF FIGURES

iii

LIST OF TABLES

ABSTRACT

It is well known that long waves and currents in the cross-shore and long-shore directions are generated due to the process of wave breaking. Numerous authors have worked on the mechanisms for the generation of long waves; all these studies show that wave groupiness is a primary factor in the generation of long waves in the offshore as well as in the nearshore region. To predict the long waves, a comprehensive model is required which can predict the time varying wave height and frequency.

An attempt has been made in this thesis to develop a one-dimensional model using the kinematic and the dynamic conservation equations along with the dispersion relation to predict the time and space dependent behavior of the wave averaged quantities, c, ω and H. Cnoidal theory is used in the region before breaking. Inside the surf zone, hydraulic jump theory, as applicable to waves, is used. Experiments were conducted in order to test the validity of the model. Wave groups consisting of individual cnoidal waves were generated and measurements of the water surface elevation were obtained at a number of locations around the breaking region and inside the surf zone.

The experimental data shows that there is a time variation of the break point as a result of the wave groups. Furthermore, the group structure is not completely destroyed by the variation of the break point and part of the groupiness is transferred to the surf zone. The variation of the wave height within a group

does not remain the same as the group propagates, due to the fact that the groups generated are not of permanent from. Long waves were generated in the wave tank at the group frequency.

Within the limitations of the model, reasonable agreement is found between the model results and data for the wave height, wave period and wave speed of the individual waves. The model also performs reasonably well for the time varying wave height and wave periods.

ACKNOWLEDGEMENT

Chapter 1

INTRODUCTION

The prediction of coastal processes such as beach erosion depends on the capability to predict the waves and currents in the nearshore region. In the past two decades, tremendous advances have been achieved towards understanding the hydrodynamic aspects of the nearshore flow.

It is known that in the region between breaking point and the shoreline, strong currents are generated in both the longshore and the cross-shore directions. Energy is also transferred from the short waves to the long waves in the nearshore region. The strength of the currents and long waves are dependent, among other factors, on the time variation of the incident wave heights and the wave periods.

The group structure of waves has been commonly used as the driving mechanism in models for the generation of long waves in the offshore region (Longuet-Higgins & Stewart 1962b, 1964) as well as in the nearshore region (e.g., Symonds et al. 1982, Schäffer & Svendsen 1988, Schäffer 1990). Symonds et al. assumed a time varying break point due to the groupiness of the incident wave field; and a fixed wave height to water depth ratio in the surf zone. Using linearized, depth-integrated continuity and momentum equations to analyze the flow, they concluded that the variation in the break point was a probable cause for the generation of long waves. Seaward of the breaking region, free wave solutions were

1

obtained; and standing wave solutions were obtained shoreward of the break point. It was also found that the amplitude of standing wave was not affected much by the incident wave field. Experiments were conducted with wave groups formed by two waves with slightly different frequencies by Kostense (1984), who found that the surf beat could be considered as two waves, an incident bound wave and a reflected free wave. The results from these experiments agreed qualitatively with the theoretical findings of Symonds. Schäffer & Svendsen (1988) assumed a fixed break point, thereby preserving the group structure in the surf zone, and found that the group structure allowed the generation of free long waves even inside the surf zone. Schäffer et al. (1989) combined the above two models, with a more general wave field, allowing for the variation of groupiness inside the surf zone and concluded that the mechanism for long wave generation is a combination of the above two models. List (1991) analyzed field data and concluded that a substantial level of groupiness survived the breaking process. In all, it has been found that the group structure of the incident waves play an important role in coastal processes.

In the present work, a model was developed to describe the time variation of the wave height and wave period, given the wave field at any offshore location. The model results give the instantaneous wave heights and wave periods at any arbitrary location from the offshore position to a water depth of one centimeter. The model is based on the equations for kinematic and dynamic conservation of waves along with the dispersion relation. The kinematic conservation of waves describes the variation of the wave number and the frequency (e.g., Phillips 1980) as the waves propagate through the region considered. Conservation of energy gives the variation of the wave heights in the same region. The development of the model is described in Chapter 2.

Experiments were conducted to study the model performance as well the propagation of wave groups in the surf zone. The wave groups consisted of cnoidal waves, whose heights were computed so as to obtain a sinusoidal variation of heights in a group. The water surface elevation was measured at a number of locations in the tank with emphasis on obtaining data near the breaking region and in the surf zone. The setup of the experiment and the data acquisition systems are described in Chapter 3.

The analysis of the data is presented and discussed in Chapter 4. The variation of wave heights, phase speeds and the frequencies of the individual waves as well as of the group is discussed. The long waves in the tank are also analyzed. The comparison of the model to the experimental data is presented in Chapter 5. The model results were compared to the individual waves in the group and to the wave group as a whole.

Chapter 2

MODEL EQUATIONS AND FORMULATION

In this chapter, the equations for modeling the wave averaged quantities, the wave number k, frequency ω and the wave height H, are derived and discussed for short waves in the presence of long waves. Normally incident short waves, approaching a plane beach with a constant slope are studied. The model equations are the conservation equations (Sections 2.1 and 2.3) along with the dispersion relation (Section 2.2). The finite difference scheme for numerically integrating the model equations is presented in Section 2.4. The physical and numerical boundary conditions are discussed in Section 2.5.

2.1 The kinematic conservation equation.

Assuming oscillatory waves, the water surface elevation can be described by

$$\eta = \frac{H(x,t)}{2} \cos \theta(x,t) \tag{2.1}$$

where $H(x,t)$ is the local wave height and $\theta(x,t)$ is the local phase of the wave. The local wave number k and local frequency ω are defined as

$$k = \frac{\partial \theta}{\partial x}; \ \omega = -\frac{\partial \theta}{\partial t}. \tag{2.2}$$

The variables, k and ω, are related by a dispersion relation of the form

$$\omega = f(k, h, H) \tag{2.3}$$

4

where h is the local water depth. Eliminating θ from (2.2), we get

$$\frac{\partial k}{\partial t} + \frac{\partial \omega}{\partial x} = 0 \qquad (2.4)$$

which is the kinematic wave conservation equation.

The short wave amplitudes and wave number are modified by the presence of long waves. Assuming that the wavelengths of the long waves are much larger than those of the short waves ($k_l \ll k_s$) and the frequency of the long waves much smaller than that of the short waves ($\omega_l \ll \omega_s$), the frequency at any location is given by (e.g., Garrett & Smith 1976, Abdelrehman & Thornton 1988)

$$\omega = \omega_s + k_s u_l \qquad (2.5)$$

where the subscript s and l refer to the short waves and the long waves respectively and where u is the horizontal component of the particle velocity under a wave. It has also been assumed that the long wave amplitudes are small in comparison to the short wave amplitudes ($a_l \ll a_s$). These assumptions, in effect, allow the long waves to be treated in a manner similar to uniform currents. The second term on the righthand side of (2.5) is the Doppler shift due to the long waves.

Assuming linear long waves and also hydrostatic pressure under the long wave, the momentum equation for the long waves in the cross-shore direction can be written as

$$\frac{\partial u_l}{\partial t} = -g\frac{\partial \eta_l}{\partial x} \qquad (2.6)$$

where we assume the stresses to be negligible. It has also been implicitly assumed that the long and short waves can be separated. This gives the orbital velocity under the long wave as

$$u_l = -\int g\frac{\partial \eta_l}{\partial x}\,dt \qquad (2.7)$$

provided the form of the long wave, i.e. η_l, is known.

Substituting (2.5) in (2.4), and using the definition of the wave speed

$$c_s = \frac{\omega_s}{k_s},\qquad(2.8)$$

we get the kinematic conservation equation as

$$\frac{\partial k_s}{\partial t} + \frac{\partial \left(c_s + u_l\right) k_s}{\partial x} = 0 \qquad (2.9)$$

2.2   The dispersion relation.

Outside the surf zone, the dispersion relation for the short waves can be obtained from the appropriate wave theory. Here, the individual waves in a group are cnoidal waves, the reason for which is discussed in detail in Section 3.4. The dispersion relation outside the surf zone for a cnoidal wave is (Svendsen 1974)

$$\frac{c_s^2}{gh} = 1 + \frac{H}{mh}\left(2 - m - 3\frac{E(m)}{K(m)}\right)\qquad(2.10)$$

where m is the elliptic parameter, $E(m)$ is the elliptic integral of the second kind and $K(m)$ is the elliptic integral of the first kind.

Inside the surf zone, we assume that the wave is of the same form as a propagating hydraulic jump or bore. Figure 2.1 shows the features of the two flows. Assuming depth-independent velocities and hydrostatic pressure, the bore speed, with respect to a fixed frame of reference, is (e.g., Henderson 1966)

$$c_b^2 = \frac{1}{2}g d_t \xi(\xi + 1),\qquad(2.11)$$

where $\xi = \frac{d_c}{d_t} \equiv \frac{\eta_c + h}{\eta_t + h}$ is the ratio of the total water depth at the crest to the total water depth at the trough. A broken wave, however, propagates into an opposing velocity due to the wave trough in front of it. The continuity equation gives

$$\frac{\partial \eta}{\partial t} + \frac{\partial \left(h + \eta\right) u}{\partial x} = 0 \qquad (2.12)$$

Assuming constant form waves traveling with speed c, we have

$$\frac{\partial \eta}{\partial t} + c_s \frac{\partial \eta}{\partial x} = 0 \tag{2.13}$$

Substituting (2.13) in (2.12) and integrating, the velocity is obtained as

$$u = c \frac{\eta}{\eta + h} \tag{2.14}$$

Therefore, under a wave trough for a wave with speed c_s, we have

$$u_t = c_s \frac{\eta_t}{\eta_t + h} \tag{2.15}$$

Therefore, we have the breaker speed given by

$$c_s = c_b + u_t \tag{2.16}$$

which gives

$$c_b = c_s - u_t = c_s \frac{h}{d_t} \quad \Rightarrow \quad c_s = c_b \frac{d_t}{h} \tag{2.17}$$

Substituting (2.11) into (2.17), we obtain

$$c_s^2 = \frac{1}{2} g h \left(\frac{d_t}{h} \right)^3 \xi(\xi + 1) \tag{2.18}$$

which can be expressed in terms of the wave height $H = d_c - d_t$ and the crest height of the wave η_c. After some algebraic manipulation, we obtain the dispersion relation in the surf zone as

$$\frac{c_s^2}{gh} = 1 + \left(-\frac{3}{2} + 3\delta \right) \frac{H}{h} + \left(\frac{1}{2} - 3\delta + 3\delta^2 \right) \left(\frac{H}{h} \right)^2 + \left(\frac{1}{2}\delta - \frac{3}{2}\delta^2 + \delta^3 \right) \left(\frac{H}{h} \right)^3 \tag{2.19}$$

where $\delta \equiv \frac{\eta_c}{H}$.

The dispersion relation used in the model is therefore

$$\frac{c_s^2}{gh} = \begin{cases} 1 + \frac{H}{mh} \left(2 - m - 3\frac{E(m)}{K(m)} \right) & \text{for } h > h_b \\ \\ 1 + \left(-\frac{3}{2} + 3\delta \right) \frac{H}{h} + \left(\frac{1}{2} - 3\delta + 3\delta^2 \right) \left(\frac{H}{h} \right)^2 \\ + \left(\frac{1}{2}\delta - \frac{3}{2}\delta^2 + \delta^3 \right) \left(\frac{H}{h} \right)^3 & \text{for } h \leq h_b \end{cases} \tag{2.20}$$
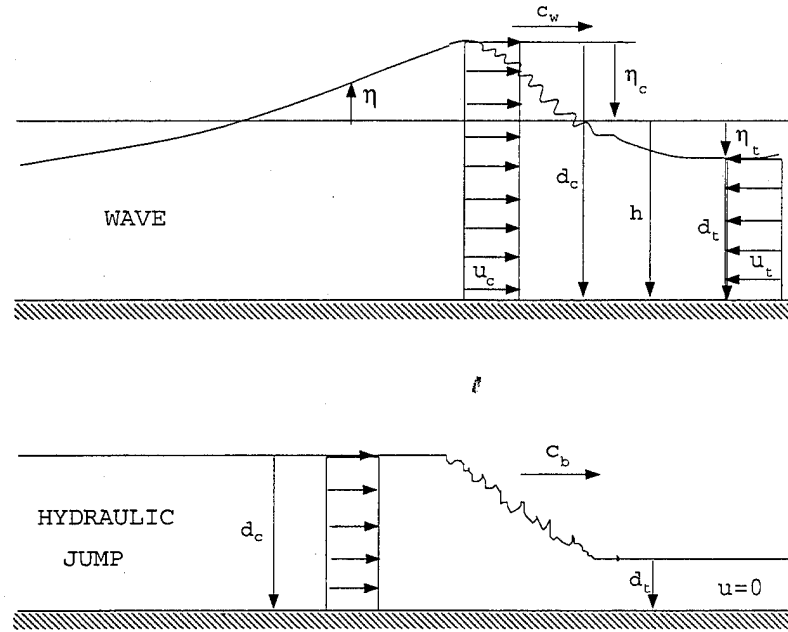
Figure 2.1: Comparison between a wave and a bore.

where h_b is the depth at which wave breaking occurs.

2.3 The energy conservation equation.

Assuming that $\frac{H}{h} \ll 1$; that all the energy in the low frequency motion is due to the fluctuating (oscillatory) motion; and that the mean energy flux is due to the fluctuating motion alone, the equation for the conservation of short wave energy is (Phillips 1980)

$$\frac{\partial \mathcal{E}}{\partial t} + \frac{\partial \left[\mathcal{E} \left(u_l + c_g \right) \right]}{\partial x} + S_{xx} \frac{\partial u_l}{\partial x} = \mathcal{D} \qquad (2.21)$$

where $\mathcal{E}$ is the short wave energy density, c_g is the speed at which the energy is propagated, or more commonly the group velocity, S_{xx} is the radiation stress and $\mathcal{D}$ is the energy dissipation. The term involving the radiation stress describes the momentum transfer between the long and short waves. The above form of the energy equation was first given by Longuet-Higgins and Stewart (1960, 1961). Phillips (1980) derives the same equation using the continuity and momentum equations.

The wave averaged energy density, the sum of potential energy and kinetic energy, is

$$\mathcal{E} = \frac{1}{T} \int_0^T \left[\frac{1}{2}\rho g \eta^2 + \int_{-h}^{\eta} \frac{1}{2}\rho \left(u^2 + w^2\right) dz \right] dt \qquad (2.22)$$

where T is the wave period, η is the instantaneous water surface elevation, u and w are the horizontal and vertical components of the orbital velocity under the wave. Assuming shallow water, which implies $u \simeq c\frac{\eta}{h}$ and $w \ll u$, we can write

$$\mathcal{E} = \frac{1}{T} \int_0^T \left[\frac{1}{2}\rho g \eta^2 + \int_{-h}^{\eta} \frac{1}{2}\rho \frac{c^2 \eta^2}{h^2} dz \right] dt \qquad (2.23)$$

The instantaneous water surface elevation, η, for cnoidal waves is (e.g., Svendsen 1974)

$$\eta = \frac{H}{m} \left[\left(1 - m - \frac{E}{K}\right) + m\, cn^2(2K(\frac{t}{T} - \frac{x}{L}), m) \right] \qquad (2.24)$$

where cn is the Jacobian elliptic function and L is the wave length. Now, substituting for η and performing the integration, we get, to the lowest order,

$$\mathcal{E}(x,t) = \rho g H^2 B \qquad (2.25)$$

where

$$B = \frac{1}{m^2} \left[\frac{1}{3} \left(3m^2 - 5m + 2 + (4m - 2)\frac{E}{K}\right) - \left(1 - m - \frac{E}{K}\right)^2 \right] \qquad (2.26)$$

B is the shape parameter which is a function of x and t and is the same as given by Svendsen (1974) in the expression for energy flux.

As a first order approximation linear theory is used for the expression for radiation stress. When the wave groups are long compared to the water depth, Longuet-Higgins (1962), gives the expression for the radiation stress as

$$S_{xx} = \mathcal{E}\left(\frac{2c_g}{c} - \frac{1}{2}\right) \tag{2.27}$$

which is correct to the second order. Since we have already assumed shallow water, where $c_g = c$, the above equation becomes

$$S_{xx} = \frac{3}{2}\mathcal{E} \tag{2.28}$$

Outside the surf zone, it is assumed that the waves propagate without loss of energy. In the surf zone, it was assumed in Section 2.2 that the broken wave resembles a propagating bore. The total energy dissipation in a hydraulic jump given by 2.11, per unit time, can therefore be written as (e.g., Henderson 1966)

$$\Delta E = \rho g Q d_t \frac{(\xi - 1)^3}{4\xi} \tag{2.29}$$

where Q is the mass flux. At any particular location, the mass flux due to waves traveling with speed c_s as in (2.17) has mass flux

$$Q = c_s h \tag{2.30}$$

This means that in a wave, (2.29) can be written as

$$\Delta E = \rho g c_s h \frac{H^3}{4 d_t d_c} \tag{2.31}$$

Therefore, the dissipation in the surf zone, which is mainly turbulent dissipation, per wave is

$$\mathcal{D} = -\frac{\Delta E}{L} \quad \Rightarrow \quad \mathcal{D} = -\frac{\rho g H^3}{4hT} \frac{h^2}{d_t d_c} \tag{2.32}$$

where we have used the relation $c_w = \frac{L}{T}$, L is the wave length and T is the wave period. Expressed in terms of δ as defined in (2.19) and $\frac{H}{h}$, the dissipation inside the surf zone can be written as

$$\mathcal{D} = -\frac{\rho g H^3}{4hT} \frac{1}{\left(1 + \delta\frac{H}{h}\right)\left(1 + \frac{H}{h}(\delta - 1)\right)} \tag{2.33}$$

where ρ is the density of water, g is the gravitational acceleration, T is the wave period and h_b is the water depth at the break point.

Therefore, in the entire domain we have the energy dissipation as

$$\mathcal{D} = \begin{cases} 0 & \text{for } h > h_b \\ -\frac{\rho g H^3}{4hT} \frac{1}{\left(1+\delta\frac{H}{h}\right)\left(1+\frac{H}{h}(\delta-1)\right)} & \text{for } h \leq h_b \end{cases} \qquad (2.34)$$

Substituting (2.28) in (2.21), we have

$$\frac{\partial \mathcal{E}}{\partial t} + \frac{\partial \mathcal{E}\left[u_l + c_g\right]}{\partial x} + \frac{3}{2}\mathcal{E}\frac{\partial u_l}{\partial x} = \mathcal{D} \qquad (2.35)$$

as the energy conservation equation with $\mathcal{E}$ and $\mathcal{D}$ defined as in (2.25) and (2.34) respectively.

2.4 The numerical scheme.

Equations 2.9 and 2.35 along with the dispersion relation given by (2.20) form the equations governing the variation of wave height, wavelength and wave frequency. The equations are solved in conservation form using a finite difference scheme, which is a generalized form of the Crank-Nicholson scheme, centered in space and time (Anderson et al., 1984). The finite difference forms of the governing equations are

$$\begin{aligned} \frac{k_i^{n+1} - k_i^n}{\Delta t} \quad + \quad & \beta \left[\frac{(c_s + u_l)_{i+1}^{n+1} k_{i+1}^{n+1} - (c_s + u_l)_{i-1}^{n+1} k_{i-1}^{n+1}}{2\Delta x} \right] \\ + \quad & (1-\beta) \left[\frac{(c_s + u_l)_{i+1}^n k_{i+1}^n - (c_s + u_l)_{i-1}^n k_{i-1}^n}{2\Delta x} \right] \\ = \quad & \bigcirc\left(\Delta x^2, \Delta t^2\right) \end{aligned} \qquad (2.36)$$

and

$$\frac{\mathcal{E}_i^{n+1} - \mathcal{E}_i^n}{\Delta t} \quad + \quad \beta \left[\frac{(c_g + u_l)_{i+1}^{n+1} \mathcal{E}_{i+1}^{n+1} - (c_g + u_l)_{i-1}^{n+1} \mathcal{E}_{i-1}^{n+1}}{2\Delta x} \right]$$

$$+ \quad (1 - \beta) \left[\frac{(c_g + u_l)_{i+1}^n \mathcal{E}_{i+1}^n - (c_g + u_l)_{i-1}^n \mathcal{E}_{i-1}^n}{2\Delta x} \right]$$

$$+ \quad \frac{3}{2}\beta \mathcal{E}_i^{n+1} \left[\frac{u_{l_{i+1}}^{n+1} - u_{l_{i-1}}^{n+1}}{2\Delta x} \right] + \frac{3}{2}(1 - \beta) \mathcal{E}_i^n \left[\frac{u_{l_{i+1}}^n - u_{l_{i-1}}^n}{2\Delta x} \right]$$

$$= \quad \beta \mathcal{D}_i^{n+1} + (1 - \beta)\mathcal{D}_i^n + \bigcirc \left(\Delta x^2, \Delta t^2 \right) \tag{2.37}$$

where the superscript denotes the time step, the subscript denotes the spatial location and the parameter β is the weighting factor which governs the implicitness in the scheme. After some rearrangement of terms, the above equations can be written as

$$- \beta r_{i-1}^{n+1} k_{i-1}^{n+1} + k_i^{n+1} + \beta r_{i+1}^{n+1} k_{i+1}^{n+1} = (1 - \beta)r_{i-1}^n k_{i-1}^n + k_i^n - (1 - \beta)r_{i+1}^n k_{i+1}^n \tag{2.38}$$

and

$$-\beta p_{i-1}^{n+1} \mathcal{E}_{i-1}^{n+1} \quad + \quad \left(1 + q_i^{n+1} \right) \mathcal{E}_i^{n+1} + \beta p_{i+1}^{n+1} \mathcal{E}_{i+1}^{n+1}$$

$$= \quad \beta \mathcal{D}_i^{n+1} + (1 - \beta)\mathcal{D}_i^n + (1 - \beta)p_{i-1}^n \mathcal{E}_{i-1}^n$$

$$+ \quad \left(1 - q_i^{n+1} \right) \mathcal{E}_i^n - (1 - \beta)p_{i+1}^n \mathcal{E}_{i+1}^n \tag{2.39}$$

where

$$r_i^n = \frac{(c + u_l)_i^n \Delta t}{2\Delta x},$$

$$p_i^n = \frac{(c_g + u_l)_i^n \Delta t}{2\Delta x},$$

$$q_i^n = \frac{3}{2}\Delta t \left(\frac{\partial u_l}{\partial x} \right)_i^n.$$

The value of $\beta = 0$ corresponds to a fully explicit scheme, $\beta = 1$ corresponds to a fully implicit scheme and $\beta = 0.5$ corresponds to Crank-Nicholson scheme. The Crank-Nicholson scheme has the highest accuracy of $O(\Delta t^2, \Delta x^2)$ and is unconditionally stable for linear problems. The explicit schemes ($\beta < 0.5$) are unstable if either r_i^n or p_i^n is greater than one. The implicit schemes ($\beta > 0.5$) are unconditionally stable, again for linear problems, but are increasingly inaccurate with

larger values of β. These two equations are solved using a tridiagonal matrix solver.

Due to the breaking process, the wave undergoes a transformation. Organized energy is converted to turbulent energy, which is in turn dissipated from the system as heat. Significant changes occur in the wave speed and the wave height starts decreasing abruptly. The wave break point is therefore a point of singularity in the domain. This singularity introduces numerical instability which evolves over time. The Crank-Nicholson scheme, although very accurate, is non-dissipative, which implies that any instability, real or numerical, generated during the integration will not be damped. Since it is desirable to damp the numerical instabilities while retaining any real instability, the value of $\beta = 0.51$ is used. This value was chosen after the model was run using different values of β in the range 0.5-1.0 and comparing the results of the model with each other. This value of β is in the region of numerical stability of the finite difference scheme and is close to value corresponding to the Crank-Nicholson scheme.

Since c, B and $\mathcal{D}$ are functions of x and t, the equations have to be solved iteratively. In the first iteration, c_i^n, B_i^n and $\mathcal{D}_i^n$ are used as approximations to c_i^{n+1}, B_i^{n+1} and $\mathcal{D}_i^{n+1}$. The finite difference equations are then solved to obtain a first approximation to k_i^{n+1} and H_i^{n+1}. In the subsequent iterations, the values of c_i^{n+1}, B_i^{n+1} and $\mathcal{D}_i^{n+1}$ are calculated using (2.20), (2.26) and (2.34) respectively. These values are then used to obtain better approximations to k_i^{n+1} and H_i^{n+1}.

2.5 The boundary conditions.

The model equations are first order in space and time. One boundary condition each in space and time have to be specified for solving the equations. The bathymetry, i.e., the variation of h with respect to x, is assumed to be known.

At the shoreline, the water depth is zero. In reality, we do not have a fixed shoreline; rather, the waterline moves up and down the beach. However, it is assumed that the shoreline is fixed which allows the simplification of the shoreline boundary condition. On the other hand, the presence of the long waves introduce a finite wave height at the fixed shoreline and hence the wave speed goes to infinity as the shoreline is approached.

There are two ways to circumvent this problem. The first is to force the wave height to be zero at the shoreline. The second is to stop the computations just short of the shoreline and allow the waves to propagate out of the nearshore boundary. Here, the second option is chosen. Initially, there are no waves in the system and the values of k and H at time $t = 0$ is zero. The values of k and H are specified at the left (offshore) boundary at each time step, which is the spatial boundary condition.

At the wave break point, there is a change in wave characteristics. The wave form is assumed to transform into a bore form immediately after breaking. This implies that the wave speed is different on either side of the breaking point as per (2.20). Continuity of the short wave period is used as the matching criterion for the waves on either side of the break point. This is justified by the fact that a discontinuity in frequency would imply a discontinuity in time. The matching of wave period implies that the wave number is different across the breaking point, as per (2.5). The continuity across the break point is therefore given as

$$\frac{\partial\left(\omega - k_s u_l\right)}{\partial x}\bigg|_b = 0 \qquad (2.40)$$

At the right (onshore) boundary, the physical boundary condition is that the wave propagates out of the domain. This can be implemented numerically by writing the conservation equations in characteristic form. The characteristic

equations for hyperbolic equations have been derived as in Whitham (1974). Following the derivation given in Whitham, we get the characteristic form for the kinematic equation as

$$\frac{dk}{dt} = -k\frac{\partial(c + u_l)}{\partial x} \quad \textbf{on} \quad \frac{dx}{dt} = c + u_l \qquad (2.41)$$

and for the energy equation we get

$$\frac{d\mathcal{E}}{dt} = \mathcal{D} - \mathcal{E}\frac{\partial(c_g + u_l)}{\partial x} - S_{xx}\frac{\partial u_l}{\partial x} \quad \textbf{on} \quad \frac{dx}{dt} = c_g + u_l \qquad (2.42)$$

The two equations have different characteristic curves. In the interior of the computational domain, the finite difference solution (2.38, 2.39) is accurate up to a maximum of $O(\Delta x^2)$ in space. Consistent with this accuracy, the characteristic equations are solved at the boundary using a second order Runge-Kutta method. The resulting finite difference approximation for the above equations are

$$k_M^{n+1} = k_C^n - \frac{\Delta t}{2}\left[k_C^n\left(\frac{\partial(c + u_l)}{\partial x}\right)_C^n + k_M^{n+1}\left(\frac{\partial(c + u_l)}{\partial x}\right)_M^{n+1}\right] \qquad (2.43)$$

on

$$x_M - x_C = \Delta t\,[c + u_l]_C^n \qquad (2.44)$$

and

$$\mathcal{E}_M^{n+1} = \mathcal{E}_C^n \quad - \quad \frac{\Delta t}{2}\left[\mathcal{E}_C^n\left(\frac{\partial(c_g + u_l)}{\partial x}\right)_C^n + \mathcal{E}_M^{n+1}\left(\frac{\partial(c_g + u_l)}{\partial x}\right)_M^{n+1}\right]$$
$$\quad - \quad \frac{3\Delta t}{4}\left[\mathcal{E}_C^n\left(\frac{\partial u_l}{\partial x}\right)_C^n + \mathcal{E}_M^{n+1}\left(\frac{\partial u_l}{\partial x}\right)_M^{n+1}\right] \qquad (2.45)$$

on

$$x_M - x_C = \Delta t\,[c_g + u_l]_C^n \qquad (2.46)$$

where x_C is the point of intersection between the characteristic and the x-axis at the nth time step and x_M is the boundary. The point x_C is unknown and $c_{gC}{}^n$, c_C^n and $u_{lC}{}^n$ are functions of x_C. Therefore, the point x_C is obtained by solving

(2.44) and (2.46) iteratively. The values of k and $\mathcal{E}$ at x_C are found by linear interpolation between the adjacent grid points. Using the values of c_g, u_l, k and $\mathcal{E}$ at x_C, the values of k and $\mathcal{E}$ at x_M are calculated using equations (2.43) and (2.45). Again, these equations are implicit in k and $\mathcal{E}$ and are therefore solved by successive iteration.

Chapter 3

EXPERIMENTAL SETUP AND DATA ACQUISITION

The experimental study of wave groups was performed in the Precision Wave Tank (henceforth called the PWT) at the Ocean Engineering Laboratory at the University of Delaware. This chapter describes the laboratory equipment used in the experiments, the wave generation and the data acquisition systems.

3.1 The wave tank.

The PWT is 30.0 m long, 0.6 m wide and 1.0 m deep. A plane beach, made of CORION©, which is a smooth and impermeable material, was installed. The setup is shown in Figure 3.1. The start of the beach was 11.85 m from the wave maker. The mean slope of the beach was calculated by locating the position of the shoreline, which was at 25.93 m from the wavemaker for a water depth of 0.4 m. The mean slope of the beach, calculated as

$$m = \frac{x_s - x_0}{h_0} \qquad (3.1)$$

where 1:m is the slope, x_s is the location of the shoreline, x_0 is the location of the toe of the beach and h_0 is the depth at the constant depth section, was found to be 1:35.2. Different locations of the beach, however, had slopes varying between 1:32.5 and 1:38.5. The uniformity in the slope of the beach was affected by two

17

factors. One factor was the irregularity in the bottom of the wave flume, made of marine plywood, on which the frame of the beach rested. The second factor was that the sections forming the beach was fixed on a supporting frame at discreet points by a nut and bolt arrangement, which was tightened manually. The water depth was measured along the center of the width of the tank. Where possible, the depth measurements were taken at the joint between two adjacent plates of the beach. Figure 3.2 shows the depth variation of the beach along the tank, x is the distance from the wavemaker. Table 3.1 gives the measured slopes along with the location of measurement form the wave maker.
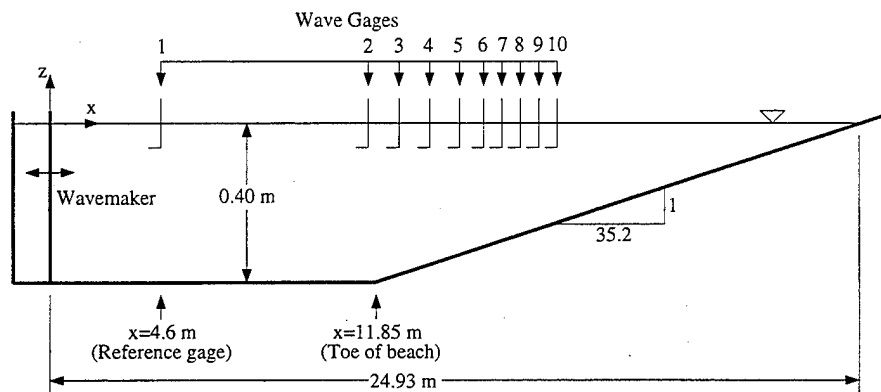
Figure 3.1: Definition sketch of the experimental setup.

Waves were generated in the PWT using a piston type wave paddle. The paddle was connected to a servo-controlled hydraulic pump. The motion of the wave maker was controlled by an IBM PS/2 computer through which the voltages corresponding to paddle displacement were specified.

Wave gages, used to measure the free surface elevation, were mounted on carriages supported on THOMPSON© roller bearings on one side and ordinary
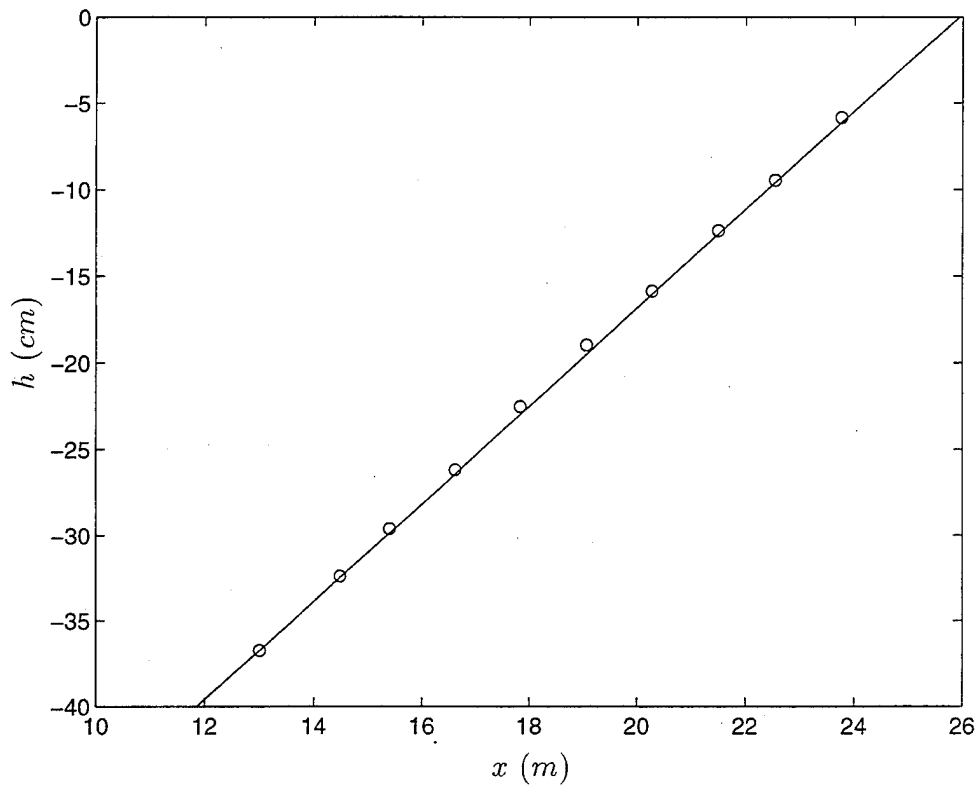
Figure 3.2: Slope of the beach calculated using the depth at the constant section and the distance between the toe of the beach and the shoreline (———) and the water depths at different locations, measured using a depth gage (○).

roller bearings on the other side of the PWT. The carriages could move the entire length of the PWT.

3.2 The wave gages.

Ten capacitance wave gages were used to measure the free surface variations. Each wave gage consisted of an insulated wire probe mounted rigidly on a stainless steel frame. The probe was connected to an electronic circuit, which consisted of two oscillators, one fixed and the other variable by means of the

x (m)	h (cm) (measured)	h (cm) (computed)
13.00	36.32	36.33
14.50	31.98	32.07
15.41	29.20	29.49
16.62	25.77	26.05
17.84	22.09	22.58
19.06	18.54	19.12
20.28	15.44	15.65
21.50	11.99	12.18
22.55	9.04	9.20
23.77	5.43	5.74

Table 3.1: Measured and computed depth in the tank. The computed depths use the slope of the beach calculated as in Equation (3.1).

changing capacitance of the probe. The capacitance of the probe changed according to the change in surface area of the probe covered by water which, in turn, corresponded to the free surface elevation. The difference in frequency was transmitted to a frequency-to-voltage converter which operated in the 0-10 voltage range. The resulting voltage was a linear function of the frequency. The voltages were then recorded in digital form by an IBM PC-AT computer expanded with a Data Translation, Inc. DT2801 circuit board.

The gages were calibrated to determine the voltages corresponding to different water surface elevations. Each gage was mounted on threaded vertical rods which could be moved up and down by a stepper motor. All motors were centrally controlled. This arrangement made it possible to calibrate all gages at the same time. The calibration was done before and after each experiment.

The calibration data for the gages were obtained by raising and lowering the gages at increments of 1 cm and recording the output voltage corresponding

to the displacement of the gage. The gage readings were taken twice, once as the gages moved up and once as they moved down. It was found that the meniscus at the probe slightly affected the calibration data and the error in the voltage reading due to this corresponded to ± 0.05 *cm*. Averaging the two readings at each point eliminated some of this effect and the average was taken as the calibration data for that position. Calibration data points were fit linearly with a least squares fit. A typical calibration curve for a wave gage is shown in Figure 3.3. The linearity of the calibration curves was found to be consistent throughout the experiments.
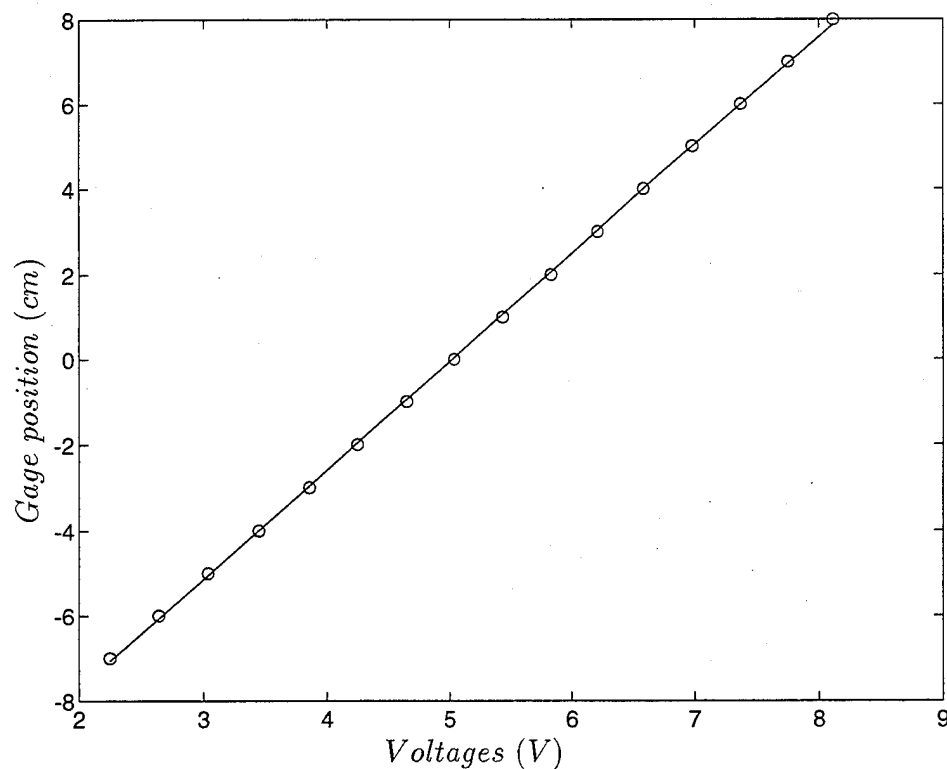
Figure 3.3: A typical calibration curve showing the data (o) and the linear fit (————).

3.3 The interface device.

Two Data Translation, Inc. DT2801 circuit boards were used as the hardware interface devices, one between the PS/2 for wave generation and the servo-control and the other between the frequency to voltage converter and the PC-AT. Each board was equipped with two D/A channels for converting digital signals to analog form. The board was also equipped with two different settings for analog to digital conversions. The setting used in the data collection gave 16 A/D channels with a voltage range of 0-10 V.

One D/A channel, on the DT2801 board connected to the PS/2, was used to transmit the paddle displacement voltage to the servo-control. An A/D channel on the same board was used to obtain the feedback from the servo-control. Ten of the 16 A/D channels on the DT2801 board connected to the PC-AT were used to collect data from the gages. A real-time software package, PCLAB, developed by Data Translation, Inc., for use with the DT2801 board, was used as the software interface.

3.4 The wave generation.

To study the effect that time varying waves have on the wave break point as well as on the propagation in the surf zone, wave groups were generated in the Precision Wave Tank. The study of wave propagation in the surf zone requires a wide surf zone so that measurements can be obtained from a large number of locations. Since higher waves break at larger depths, large wave heights were desired. However, sine waves are unstable when the wave heights are large. Hence, cnoidal wave theory was used to generate the individual waves in the group.

Each wave group was formed by joining the time series of cnoidal waves of

varying height, but with the same wave period. The time series of each cnoidal wave in the group was calculated using the method developed by Goring (1976). This method determines the trajectory of a piston wave maker for the generation of permanent form long waves. For such a wave, with zero net mass flux as in a wave tank, the velocity averaged over depth is given by

$$\bar{u}(t) = \frac{c\eta(t)}{h + \eta(t)} \tag{3.2}$$

where c is the wave speed, h is the still water level, and η is the instantaneous water surface elevation. If the instantaneous displacement of the wavemaker is denoted by $\xi(t)$, then

$$\frac{d\xi(t)}{dt} = \bar{u}(t) = \frac{c\eta(\xi, t)}{h + \eta(\xi, t)} \tag{3.3}$$

where $\frac{d}{dt}$ is the Lagrangian derivative. This equation is integrated over time to obtain $\xi(t)$. For cnoidal waves, the instantaneous water surface elevation is given by

$$\eta(\xi, t) = \eta_t + H cn^2(\theta, m) \tag{3.4}$$

where $\theta = 2K\left(\frac{t}{T} - \frac{\xi}{L}\right)$, η_t is the depth of the wave trough from the still water level, H is the wave height, T is the wave period, cn is the Jacobian elliptic function, m is the elliptic parameter, and K is the complete elliptic integral of the first kind.

The envelope of the wave height was generated with a sinusoidal variation. For this, the wave heights within each group is calculated as

$$H(i) = H_m(1 + \frac{\delta}{2}\sin\frac{2\pi i}{n}); \quad i = 1, \ldots, n \tag{3.5}$$

where $H(i)$ represents the height of the ith wave in the group, H_m is the mean wave height of the group, δ is the percentage variation of the wave height in the group and n is the total number of waves in a group. This definition of the wave heights in the group, where the argument of the sine is from $\frac{2\pi}{n}$ to 2π, gives all

different wave heights when n is odd; that is, there is a lack of symmetry in the wave group structure. The time series of each of the i waves was calculated using Equation 3.4.

The waves were joined at the mean water line of the time series for each of the waves in the group. Thus, discontinuities in η, due to the small difference in shape of the neighboring waves with different heights, are avoided. There were, however, small differences in η_t where the wave signals were joined. The resulting time series for the group is shown in Figure 3.4. It is emphasized that the wave groups thus generated by the heuristic method described above do not constitute a permanent form solution to the Boussinesq equations for a wave group and therefore cannot be expected to propagate without change in form, as the results will show. This issue will be discussed further in the next chapter.

3.5   The data acquisition.

Initially, when the wavemaker is started from rest, the waves generated are not fully developed, i.e., the initial waves are not of the specified height and period. A 30 minute time lag was given between the start of wave generation in the tank and the start of data acquisition to allow the full development of the waves and thus achieve a steady state. It was verified that this time lag was sufficient to achieve a steady state wave field in the tank for all practical purposes. Further discussion on the steadiness wave field is given in Section 4.2, where the repeatability of the generated waves are discussed.

Subroutines for data acquisition were developed and written in Fortran utilizing the PCLAB routines. There are two features of the system that limit the duration of data acquisition. For one, the DT2801 board was equipped to handle only $32K$ data values at one time. This limitation was overcome by making
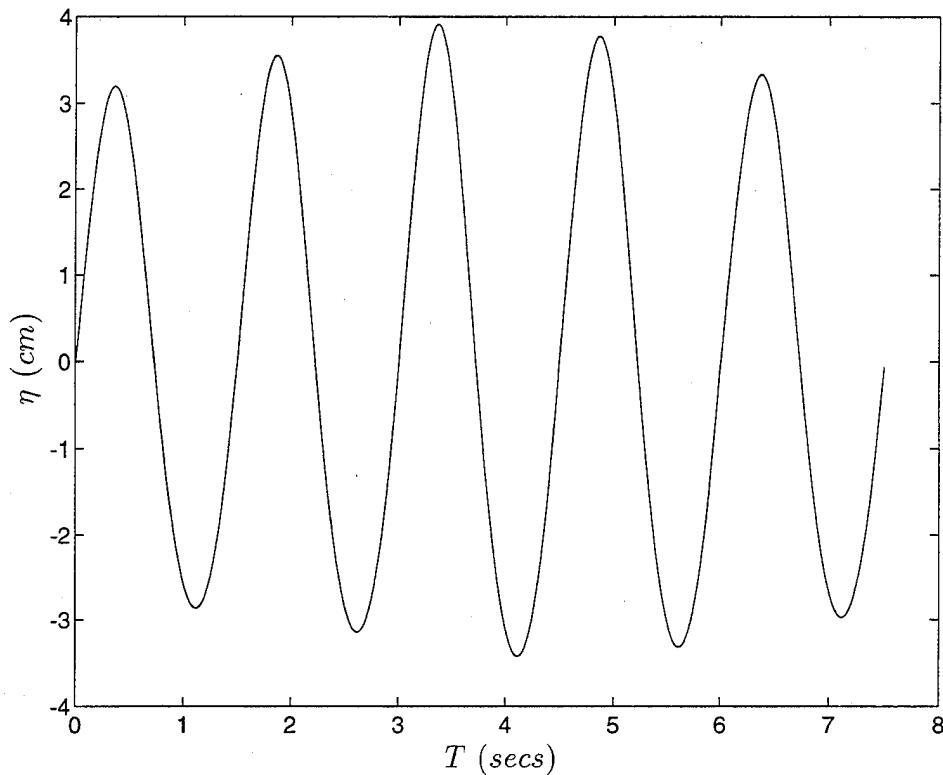
Figure 3.4: Computed time series, linked at the mean, for Experiment W01.

repeated calls to the PCLAB routines. Secondly, the Fortran compiler had a limitation of $64K$ bytes, which implies that the PCLAB routines could be run at most twice during one run of an experiment. Therefore, no more than $64K$ data values could be collected in a single run.

Data were collected from each gage with a sampling frequency of 50 Hz for a duration of 120 seconds. Ten gages were used to measure the free surface elevation at different locations in the PWT for each run of an experiment. This meant that a total of $60,000$ data points were recorded each time, which was well within the limit of $64K$ data points.

The data from each gage was collected as voltages. Calibration data for

each gage was used to calculate the free surface elevation at the corresponding location. The data was then analyzed as will be discussed in the next chapter.

Chapter 4

DATA ANALYSIS

The collected data is presented and analyzed in this chapter. Five sets of experiments were performed and analyzed. The experimental parameters are described in Section 4.1 . The repeatability of the experiments is discussed in Section 4.2. The wave heights, wave periods and the phase speeds are the inputs to the numerical model presented in Chapter 2. Upcrossing analysis, used to obtain these quantities from the experimental data, is discussed in Section 4.3. The results of the analysis are presented in Sections 4.4 - 4.5. The long waves in the tank are analyzed in Sections 4.6 and 4.7. The groupiness of the short waves, inside and outside the surf zone, is discussed in Section 4.8.

4.1 The experimental parameters.

Five sets of experiments were performed in the PWT with different wave heights, periods and groupiness factor, as listed in Table 4.1. The water depth at the constant-depth section was kept at 40 cm for all experiments. The groupiness factor is defined here as

$$\delta = 100\frac{\Delta a}{H_m} \tag{4.1}$$

where Δa is the difference between the maximum amplitude and the minimum amplitude in the group.

Experiment number	Mean wave height H_m (cm)	Wave period T_m (sec)	Groupiness factor δ
W01	6.7	1.5	20%
W02	9.5	2.5	20%
W03	9.5	2.5	40%
W04	11.9	2.5	20%
W05	11.9	2.5	40%

Table 4.1: Wave parameters.

In spite of all efforts, there were small variations in the wave surface elevation from one group to the next. This was particularly the case inside the surf zone. The discussion on this is given in Section 4.2 where the repeatability of the groups are discussed. The results presented in the following represent statistical average over as many wave groups as possible.

Two conflicting constraints were instrumental in the choice of the number of waves in a group. On one hand was the limit on sampling time mentioned in Section 3.5. Data were collected for 120 seconds in each run of an experiment. Two different wave periods, 1.5 seconds and 2.5 seconds, were used in the experiments. Thus, data for 80 waves and 48 waves were collected in the respective cases. Since the capability of ensemble averaging over several wave groups was necessary, the number of waves in a group had to be small.

On the other hand, the study of time varying wave heights was desired. For this, it was desirable to have a large number of waves in a group. The lack of symmetry of the waves in the wave groups, as mentioned in Section 3.4, generated in the tank helped increase the number of different waves in the group. The choice of five waves in a group gave 16 and 9 complete groups respectively for wave periods of 1.5 and 2.5 seconds. The wave heights of the waves in each experiment

are listed in Table 4.2.

Experiment number	Wave heights (cm)				
W01	7.34	7.09	6.31	6.06	6.70
W02	10.40	10.06	8.94	8.60	9.50
W03	11.31	10.62	8.38	7.69	9.50
W04	13.03	12.60	11.20	10.77	11.90
W05	14.16	13.30	10.50	9.64	11.90

Table 4.2: Wave heights in the groups.

Ten gages were available for acquiring data at any particular time. The gage nearest the wavemaker was used as a reference gage. The reference gage was located 4.6m from the wavemaker so as to allow the evanescent modes to die out before the waves reached that gage. Each experiment was repeated a number of times with the remaining nine gages at different locations in order to get enough measuring points to accurately describe the variations before and after breaking. The different gage locations chosen for each run of an experiment are tabulated in Appendix A.

4.2   The repeatability of wave groups.

As mentioned in Section 4.1, all the final results are formed as the ensemble average of the data from each of the wave groups in a sample. However, as each experiment was repeated a number of times with different gage positions for each run, the wave motion had to be repeatable. The repeatability of the incoming waves from one run of an experiment to another was checked using the ensemble averaged data from the gage at the reference location.

Due to the variation of the wave height, long waves are generated in the tank both at the wave maker and at wave breaking. The long wave motion is also influenced by the reflection from the slope. In general, the long waves thus generated in the tank are a combination of free and bound long waves with the group frequency. Additionally, disturbances due to the sudden initiation of wave motion in the tank will be present during the early stages of wave generation. This wave motion is composed of a combination of the natural modes of the oscillation for the tank. Due to friction and interaction with the breaking process, this part of the motion will die out after a while.

To allow the long waves to reach a steady state and to allow the initial disturbances to die out, 30 minutes was allowed to elapse between the start of the wave generation and the data collection. As mentioned earlier, each experiment was repeated a number of times with different gage positions. Data collection for each run took approximately 10 minutes. Data from each experiment were collected without stopping the wave generation process between each run. In figure 4.1, the ensemble averaged wave group from each run of Experiment W02, at the reference location, is plotted one on top of the other. It is found that the difference between the maximum value and the minimum value of the different groups is atmost 5% of the mean wave height of the group. This validates the assumption that the wave field has attained steady state, within acceptable limits, at the time of data acquisition.

Figures 4.2 and 4.3 show the variability in water surface elevation from group to group at a particular location. Large variations between the groups would imply that the number of groups would have to be larger for any reliable statistical averaging. Figure 4.2 shows typical results from a point outside the surf zone and Figure 4.3 shows typical results from inside the surf zone. It is

seen that outside the surf zone, there is very little variation between groups. The maximum deviation of the water surface elevation of the individual groups from that of the phase-averaged group was found to be approximately 5%. Inside the surf zone, some variability is observed due to turbulence. In addition, due to sharp changes in the wave profile, data may not be read at the exact time when the wave crest passes through the gage location, even with a sampling rate of 50 Hz, which contributes to the variability. The maximum deviation from the phase averaged group inside the surf zone is found to be approximately 15%.
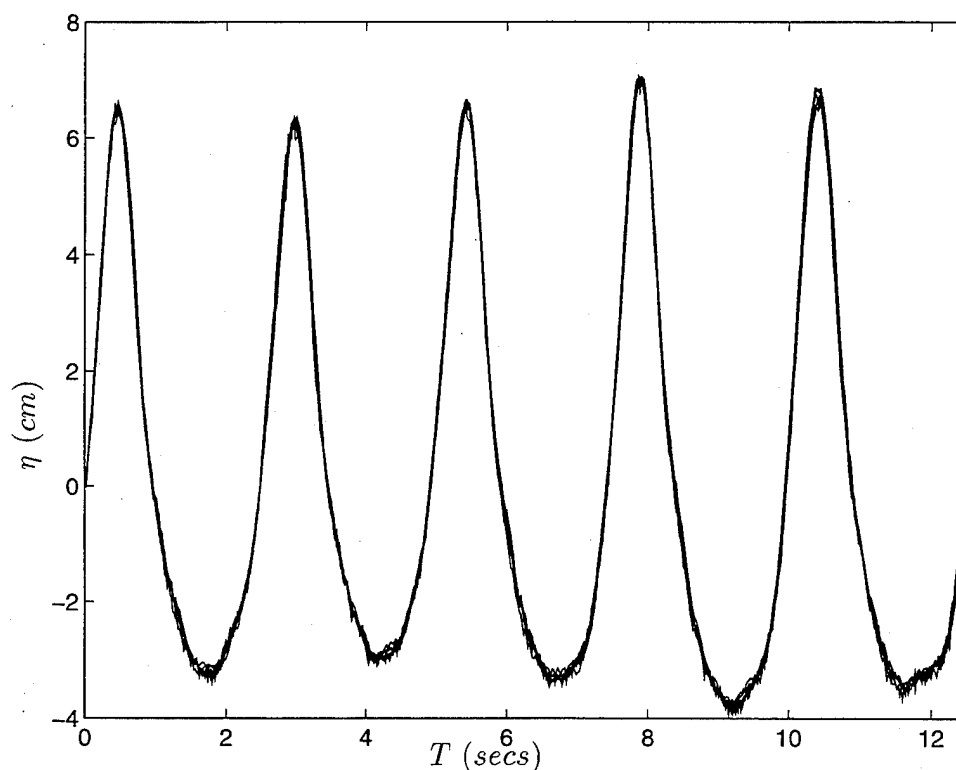
Figure 4.1: Ensemble averaged wave groups at the reference gage ($x = 4.6\ m$, $h = 0.4\ m$) for each run in Experiment W02.
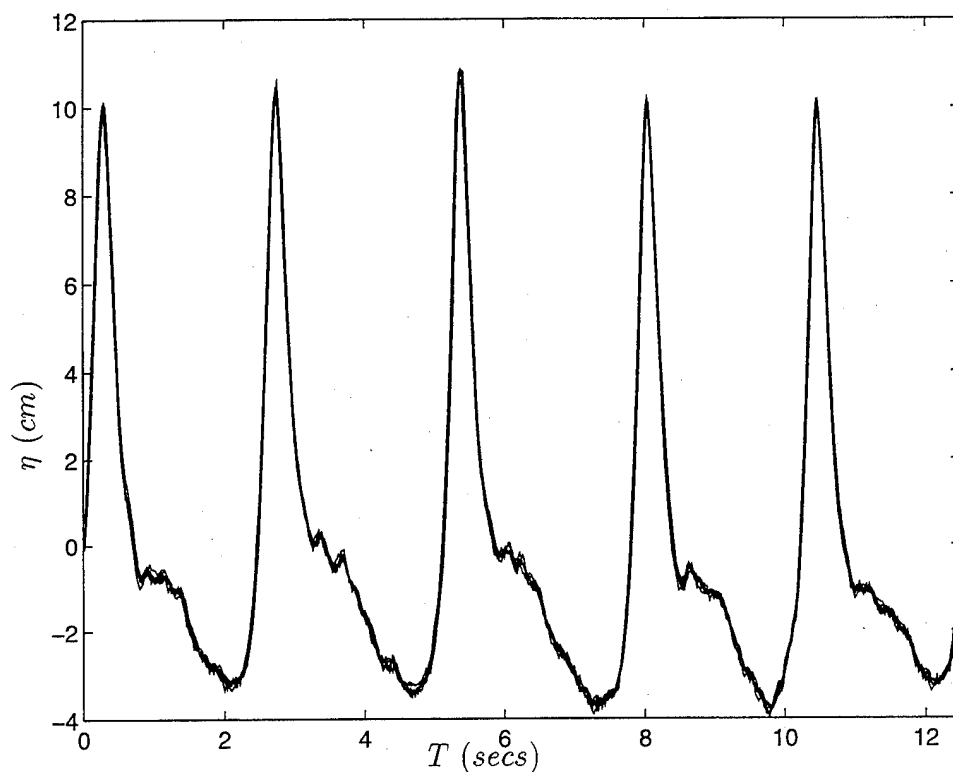
Figure 4.2: Incident wave groups in the shoaling region at $x = 18.1\ m$ ($h = 0.219$ m) for experiment W02.

4.3 The upcrossing analysis.

The start of a wave, the upcrossing point, was defined as the point where the water surface elevation became higher than a reference water level. The wave period was the difference between successive upcrossing points. The wave height was the difference between the maximum and minimum surface elevation between successive upcrossing points. Upcrossing analysis was used to determine the wave period, wave height and the phase speed of the individual waves in the groups.

The mean water level, defined as the mean of the time series, was chosen as the reference level for a zero-upcrossing analysis. Pronounced secondary crests
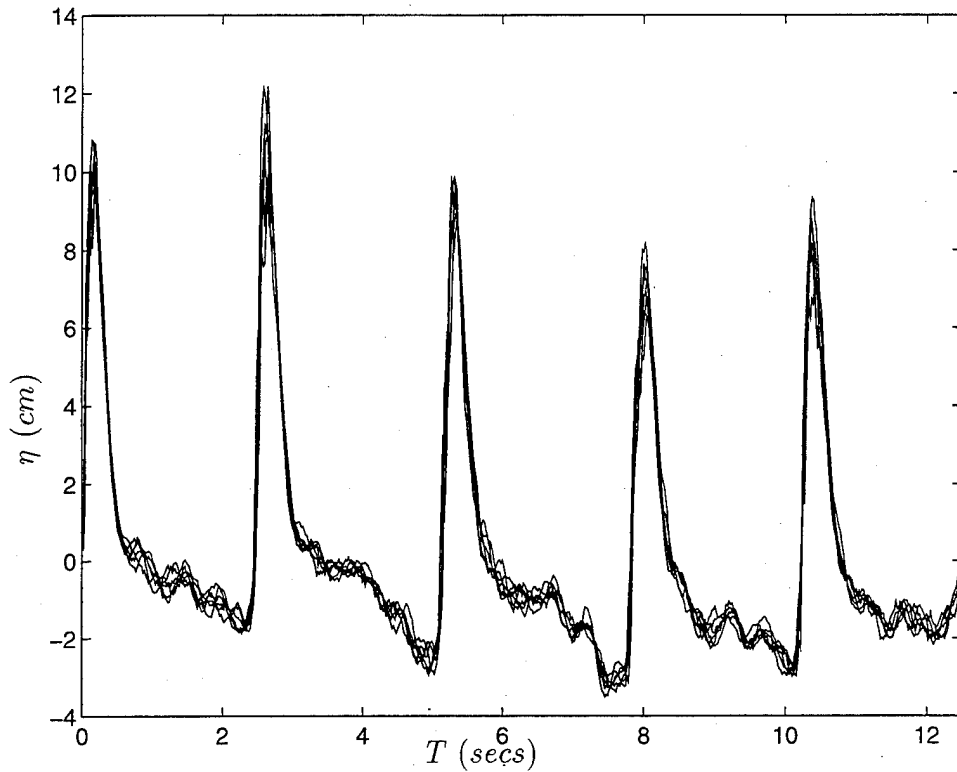
Figure 4.3: Incident wave groups in the surf zone at $x = 20.5 \ m$, $h = 0.184 \ m$ for experiment W02. Breaking is between $x = 19.40 \ m$ and $x = 19.80$ m using (4.2) and between $x = 19.45 \ m$ and $x = 20.10 \ m$ using (4.4).

were present at the wave troughs, especially close to wave breaking point. This could be due to at least three different inaccuracies associated with the way the waves are generated. The first reason is that even for ordinary cnoidal waves satisfying the requirement that the Ursell parameter $\frac{HL^2}{h^3}$ be $O(1)$, the velocity variation over depth is not uniform as imposed by the piston wave maker. Secondly, the waves generated actually have a much larger amplitude than assumed by the cnoidal wave theory, so that second or higher order effects are non-negligible. Finally, the wave group is approximated by a series of slightly different cnoidal

waves added together as described in section 3.4. This is not known to be a permanent form solution to the Boussinesq equations, so, even if the waves had been generated perfectly correctly, they would probably interact within the groups and hence modify as they propagate down the tank. For all these reasons, we would expect the wave motion generated to show high frequency irregularities. Comparison between the spectra of the measured wave at the reference location and that of the input signal to the wave maker (Figure 4.4) shows higher energy for the measured waves at higher frequencies. Figure 4.1 shows more clearly the existence of moderate high frequency motion at the reference location.
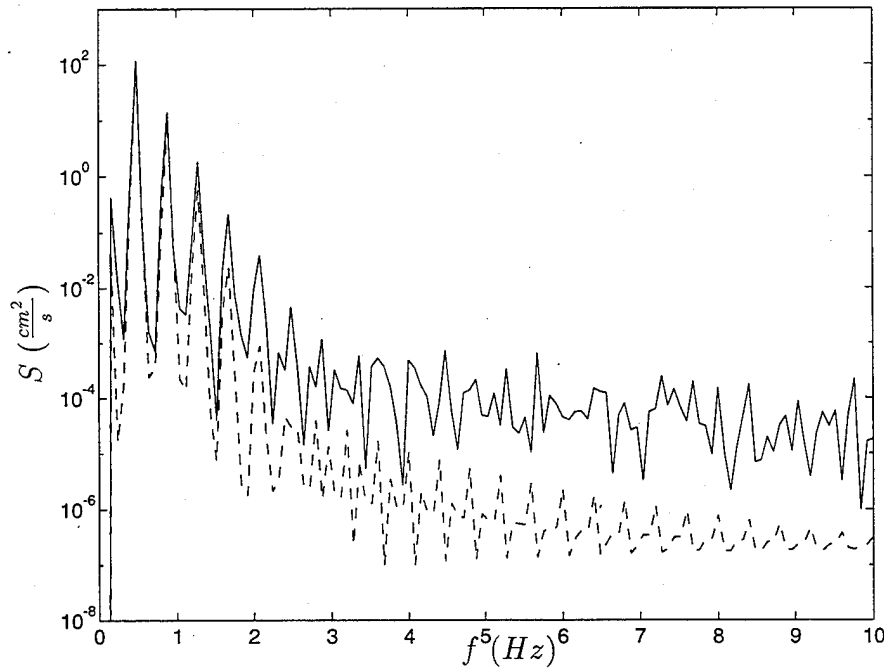
Figure 4.4: Comparison of the powerspectra at the reference location (———) and the input signal to the wave maker (– – –).

In Figure 4.2 ($x = 18.1m, h = 0.219m$), these irregularities have clearly

grown substantially, though it is obvious that they still are repeated very accurately from group to group within the experiment shown. Using a zero-upcrossing definition of waves, the crests of the high frequency wavelets would show up as separate waves if the crest height was above the mean water level. For a consistent count of the waves at each position, the results from upcrossing analysis using different reference levels were compared to each other and the spurious waves were eliminated from the analysis.

As mentioned in Section 3.5, the data was collected in digital form at a fixed rate of 50Hz. Therefore, the data points were not necessarily available for the upcrossing of a wave or at the wave crest or trough. To obtain a better estimate of the upcrossing times as well as the maximum and minimum of the surface elevation of a wave, the data points were interpolated. Linear interpolation was used for estimation of the upcrossing point. Parabolic interpolation was used for the estimation of the extrema.

4.4 The tracking of individual waves.

To determine the variation of the heights, periods and the phase speeds of the individual waves in a group, waves are tracked using the the upcrossing time at each location. The waves were tracked for each run of an experiment. The number of runs in each experiment was different with six runs (numbered R01-R06) for Experiment W01, seven (R01-R07) for Experiment W02, nine (R01-R09) for Experiment W03, W04 and W05. For each run, the gages are numbered from 01-10 for convenience in identification of their location. Gage 01, which was $4.6m$ from the wavemaker, is the reference gage. Gages 02-10 are used in tracking the waves. The first wave recorded by Gage 02 is the first wave which can be tracked all the way through the gage array. For a particular wave, the upcrossing time at

a gage farther from the wave maker would be later in time.

The distances between adjacent wave gages are known. Data points were obtained simultaneously from all ten gages. The time taken by a wave to travel between two gages is taken as the difference between its upcrossing times at the two gages. The average speed of the wave between the two gage locations was calculated. It is assumed that the phase speed of the wave does not vary significantly between two gages, given that the distance between two gages is small compared to the wavelengths and also given that the slope of the beach was small.

Figures B.1 to B.25 gives a brief overview of the results for the wave heights, the wave periods and the phase velocities of the individual waves along the length of the domain for all the experiments. The individual waves are tracked all the way to the surf zone using data from gages from different runs which are close to each other.

4.4.1 Variation of the wave height H

The waves input to the wave maker has sinusoidal variation in wave heights and constant period. Barring some experimental variability, the variation in wave heights of the different waves in the group along the beach is seen to be regular, in the sense that the shoaling outside the surf zone as well as the wave height decay inside the surf zone is monotonous. As mentioned in the previous section, to obtain a better estimate of the wave heights, parabolic interpolation was used at the extrema. Even so, the rapid variation of the surface elevation close to breaking point as well as inside the surf zone is a cause for some error in the determination of the wave height if the gage was not sampled close to when the wave crest passes by. From the figures, it is seen that the wave height decay, and therefore the energy dissipation, is higher near the breaking region than that

observed further into the surf zone.

4.4.2 Variation of the wave period T

It is seen from the figures that the individual wave periods remain fairly constant outside the surf zone. However, it also appears that higher waves have larger periods after the wave group propagates some distance from the wave maker, although, for continuity reasons, the wave period of the group is equal to the wave period input to the wavemaker. As mentioned in the previous section, existence of secondary wave crests close to the wave fronts could lead to errors in the estimation of the wave period. This is avoided by using different upcrossing levels to obtain a reliable estimate of the wave periods. Inside the surf zone, the wave periods show marked deviations from that of outside the surf zone. A look at a time series from a gage inside the surf zone, as in Figure 4.5, provides an insight into this phenomenon. The solid line in the figure is the water surface elevation at $23.2\ m$ from the wave maker and the dashed line is the long wave at that location. By comparing the time lapse between the individual crests in the figure, we see that the waves which are on the trough of the long wave, which corresponds to offshore mass flux, show an increase in wave period, whereas the waves on the the crest of the long wave, which corresponds to onshore mass flux, show decreased wave periods. A more detailed discussion and comparison with the numerical model and the experimental results is given in section 5.2.

4.4.3 Variation of the phase velocities c

The phase velocities are calculated using the wave periods obtained from the upcrossing analysis and the distance between the gages. The phase velocities of the waves are seen to decrease until breaking as one would expect due to the
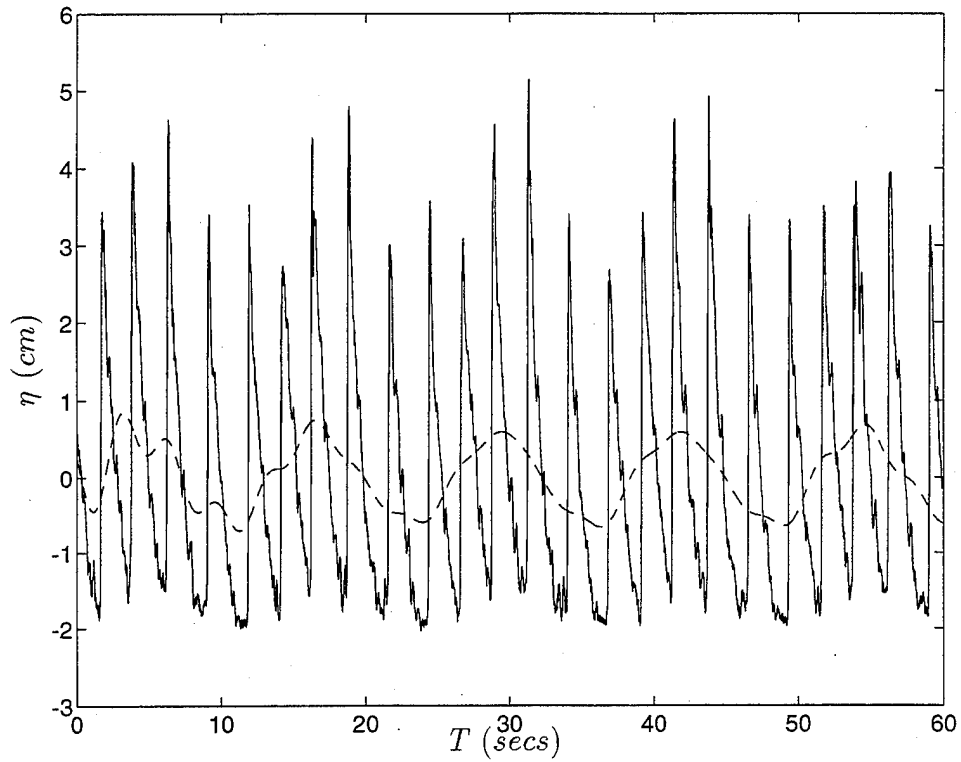
Figure 4.5: Water surface elevation (———) and long wave (— — —) at $x = 23.2$ m ($h = .076$ m).

decreasing water depth. After breaking, the phase velocities increase for sometime before reaching a maximum value and then starts decreasing again. Error in estimating the phase velocity comes from two main sources. One, as mentioned before, is the error in estimating the wave period. The other is the error in positioning the gages. Care was taken to ensure the accuracy of the gage positions, although, as the positioning was done manually, accuracy greater than ± 2 mm, cannot be claimed. However, it can easily be verified that this error will not greatly influence the value of the phase velocity calculated.

4.5 The identification of wave break point.

The wave break points were identified using two methods. The first method was to define the position of the maximum height of each wave as the breaking point of that particular wave,

$$H_b \equiv H_{max} \tag{4.2}$$

which corresponded to

$$\left(\frac{H}{h}\right)_b \equiv \left(\frac{H_{max}}{h_{H_{max}}}\right) \tag{4.3}$$

where the subscript b corresponds to the wave breaking point, H_{max} is the maximum wave height, $h_{H_{max}}$ is the still water depth at H_{max}.

The second method was to define the position of the maximum ratio between wave height and water depth as the breaking point, which corresponded to

$$\left(\frac{H}{h}\right)_b \equiv \left(\frac{H}{h}\right)_{max} \tag{4.4}$$

Both these definitions could represent different breaking positions for each of the five waves in the group. The wave heights, phase speed and the wave period obtained from the data using the up-crossing method was used to find the parameters at breaking. The location of the break point, values of wave height, still water depth, the ratio between wave height and water depth, the wave period, and the phase speed for each wave within a group for all of the experiments are tabulated in Table 4.3 and 4.4. Table 4.3 lists this information at the breaking point defined by Equation 4.2. Table 4.4 lists the information at breaker point as defined in Equation 4.4.

The value of $(\frac{H}{h})_b$ is found to range from 0.833 to 1.028 when Equation 4.2 is used, and from 0.835 to 1.094 when Equation 4.4 is used. For the 1.5 second waves, we see that the larger waves break in deeper water. However, the values

Position x (m)	Wave height H_{max} (cm)	Water depth $h_{H_{max}}$ (cm)	$\frac{H_{max}}{h_{H_{max}}}$	Wave period $T_{H_{max}}$ (secs)	Phase-speed c (m/s)
Experiment W01					
22.40	9.833	9.561	1.028	1.445	1.114
22.10	9.957	10.427	0.955	1.526	1.097
21.90	10.032	11.004	0.912	1.569	1.194
21.90	9.868	10.427	0.946	1.520	1.258
21.90	9.459	10.427	0.907	1.446	1.136
Experiment W02					
19.80	15.882	17.063	0.931	2.454	1.532
19.55	16.819	17.784	0.946	2.682	1.472
19.55	17.749	17.784	0.998	2.712	1.472
19.40	16.862	18.217	0.926	2.403	1.502
19.55	16.027	17.784	0.901	2.256	1.472
Experiment W03					
20.20	14.991	15.909	0.942	2.488	1.469
19.65	17.941	17.496	1.025	2.856	1.499
19.15	18.364	18.938	0.970	2.793	1.426
19.10	17.495	19.660	0.890	2.786	1.308
19.60	16.138	19.660	0.821	2.292	1.414
Experiment W04					
18.95	18.333	19.515	0.934	2.451	1.551
18.75	19.446	20.092	0.968	2.702	1.587
18.15	20.149	21.823	0.923	2.695	1.477
18.15	19.242	21.823	0.882	2.377	1.367
18.30	18.541	21.391	0.867	2.287	1.504
Experiment W05					
19.50	17.570	17.928	0.980	2.418	1.558
18.60	20.747	20.525	1.011	2.852	1.606
18.05	21.092	22.112	0.954	2.808	1.504
17.20	18.534	22.256	0.833	2.306	1.689
18.45	17.997	20.958	0.859	2.111	1.609

Table 4.3: Breaking point information from H_{max} criterion.

Position x (m)	Wave height $H_{(\frac{H}{h})max}$ (cm)	Water depth $h_{H_{max}}$ (cm)	$\left(\frac{H}{h}\right)_{max}$	Wave period $T_{H_{max}}$ (secs)	phase-speed c (m/s)
Experiment W01					
22.60	9.334	8.984	1.039	1.517	1.053
22.50	9.305	9.273	1.003	1.550	0.983
22.20	9.804	10.138	0.967	1.522	1.089
22.30	9.724	9.850	0.987	1.450	1.102
22.70	9.155	8.696	1.053	1.513	1.072
Experiment W02					
20.10	15.130	16.197	0.934	2.464	1.456
19.90	16.423	16.774	0.979	2.700	1.539
19.55	17.749	17.784	0.998	2.712	1.472
19.45	16.862	18.217	0.926	2.403	1.502
19.55	16.027	17.784	0.901	2.256	1.472
Experiment W03					
20.45	14.883	15.188	0.980	2.501	1.464
20.15	17.554	16.053	1.094	2.797	1.489
19.55	17.585	17.784	0.989	2.782	1.481
19.10	17.495	19.660	0.890	2.786	1.308
19.70	14.704	17.351	0.847	2.108	1.482
Experiment W04					
18.95	18.333	19.515	0.939	2.451	1.551
18.80	19.393	19.948	0.972	2.692	1.576
18.30	20.107	21.391	0.940	2.700	1.504
18.15	19.242	21.823	0.882	2.377	1.367
18.50	18.253	20.814	0.877	2.276	1.629
Experiment W05					
19.50	17.570	17.928	0.980	2.418	1.558
19.15	19.775	18.938	1.044	2.790	1.531
18.25	20.673	21.535	0.960	2.788	1.483
18.05	18.470	22.112	0.835	2.301	1.388
18.45	17.997	20.958	0.859	2.111	1.609

Table 4.4: Breaking point information from $\left(\frac{H}{h}\right)_{max}$ criterion.

of $(\frac{H}{h})_b$ do not seem to have a specific trend. Except for Experiment W02, in the case of the 2.5 second waves, we see that the largest breaking depth is for the wave which comes after the largest wave, regardless of which definition is used to identify the breaking point. However, the value of $(\frac{H}{h})_b$ is the largest for the wave coming after the largest wave. A possible reason for this phenomenon is that the larger wave would have smaller depth at the trough and hence the wave immediately behind the larger wave would be approaching shallower water sooner and the wave height to water depth ratio would be much larger.

Numerous attempts have been made to predict the wave breaking point. Southgate (1993) reviews some of these attempts. All methods of prediction are based on empirical formulations using available experimental data.

Svendsen and Hansen (1976) conducted experiments with regular waves and observed that the parameter S, which describes the relative change of water depth over a wave length, given by

$$S = h_x \frac{L}{h} \tag{4.5}$$

where h_x is the slope of the bottom, is a reliable representation of the breaker point. Svendsen (1987) came up with an empirical formula to predict the breaking points for the experiments conducted by Svendsen and Hansen (1976) as

$$\left(\frac{H}{h}\right)_b = 1.9 \left(\frac{S_b}{1 - 2S_b}\right)^{\frac{1}{2}} \tag{4.6}$$

where S_b is the value of S at the breaking point. Hansen (1990) gives a simpler approximation to the data for the range $0.25 < S < 1$ as

$$\left(\frac{H}{h}\right)_b = 1.05 S^{0.20} \tag{4.7}$$

The values at the breaking point from the present experiments are compared with the formula 4.6 in Figure 4.6. The wave length at the breaking point is calculated using

$$L_b = c_b T_b \qquad (4.8)$$

where c_b and T_b are the wave speed and wave period measured at breaking. The comparison shows that the predicted value of the breaking point is higher than obtained from our experimental data. The empirical formula was a best fit for the breaking point of regular waves. However, the present experiments were conducted with time varying wave heights which influences the wave breaking. Based on this observation, it can be concluded that the effect of the group is to make the waves break at larger depths.
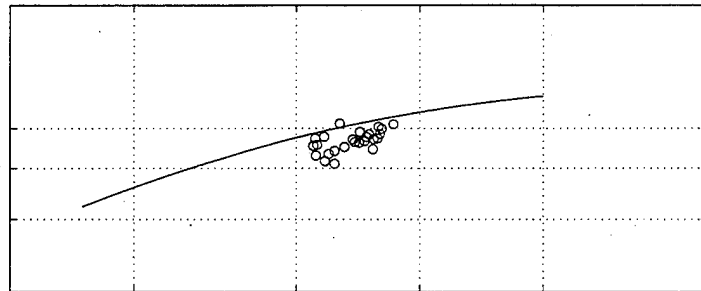

Figure 4.6: Comparison of breaking between regular waves and waves in a group. The plot shows the empirical formula given by Svendsen (1987) (— — —), the values from the present experiment (o) and the data from Svendsen and Hansen 1976 (⊙).

4.6   The long waves in the PWT.

Comparison of the spectra of the wave field at the reference location to the spectra of the input signal to the wave maker, as illustrated in Figure 4.4, shows higher energy at the group frequency. This indicates the generation and existence of long waves in the tank.

To study the long wave amplitude variation across the wave tank, the gage data was first low-pass filtered. This was done by taking the Fourier Transform of the gage data and discarding all components above a third of the peak frequency. The Inverse-Fourier Transform of the filtered data then gave the long wave amplitudes.

A fourier decomposition method was used to determine the amplitudes of the standing waves and that of the propagating waves in the tank. The water surface elevation measured at the gage location was assumed to be composed of an incident wave, a free reflected wave and a standing wave. The three-gage array method as developed by Mansard and Funke (1980) was used to separate the waves. The aim was to obtain the amplitudes of the different waves in such a way that the error in computing the amplitudes was minimized. The standing wave on a sloping bottom is known to resemble a zeroth order Bessel function. The gages used for the separation were located on the sloping bottom. The expression for the water surface elevation at any gage location x_j is

$$\eta(x_j, t) = a \left(\frac{h_0}{h_j}\right)^{\frac{1}{4}} e^{i(kx_j - \omega t)} + b J_0 \left(\frac{2\omega}{\sqrt{gh}}(l - x_j)\right) e^{-i\omega t} + c \left(\frac{h_0}{h_j}\right)^{\frac{1}{4}} e^{i(-kx_j - \omega t)}$$

(4.9)

where a, b and c are the amplitudes of the different components and $\left(\frac{h_0}{h_j}\right)^{\frac{1}{4}}$ is the shoaling coefficient. Taking the Fourier Transform of (4.9), we get

$$\hat{\eta}(x_j, \omega) = a \left(\frac{h_0}{h_j}\right)^{\frac{1}{4}} e^{ikx_j} + b J_0 \left(\frac{2\omega}{\sqrt{gh}}(l - x_j)\right) + c \left(\frac{h_0}{h_j}\right)^{\frac{1}{4}} e^{-ikx_j} + \epsilon(x_j) \quad (4.10)$$

Experiment Number	Incident wave amplitude (cm)	Reflected wave amplitude (cm)	Standing wave amplitude (cm)
W01	0.001	0.001	0.250
W02	0.002	0.001	0.975
W03	0.003	0.002	1.554
W04	0.002	0.001	1.113
W05	0.003	0.003	1.804

Table 4.5: The amplitudes of the long wave components in the tank.

where $\epsilon(x_j)$ is the error associated with each location. We can write (4.10) as

$$\epsilon^2(x_j) = \left[\hat{\eta}(x_j, \omega) - \left(a \left(\frac{h_0}{h_j} \right)^{\frac{1}{4}} e^{ikx_j} + bJ_0 \left(\frac{2\omega}{\sqrt{gh}}(l - x_j) \right) + c \left(\frac{h_0}{h_j} \right)^{\frac{1}{4}} e^{-ikx_j} \right) \right]^2$$

(4.11)

We find the amplitudes such that the sum of the square of the errors, $\varepsilon = \Sigma_j \epsilon^2(x_j)$ is a minimum. Therefore, we have

$$\frac{\partial \varepsilon}{\partial a} = \frac{\partial \varepsilon}{\partial b} = \frac{\partial \varepsilon}{\partial c} = 0$$

(4.12)

which gives three equations in the three unknowns, a, b and c. Solving these three equations, the amplitudes of the different components obtained are tabulated in Table 4.5.

The computations showed that the free wave amplitudes are small compared to the amplitude of the standing wave. The long wave amplitudes obtained from the data and the amplitudes obtained according to the three-gage array method are plotted in Figures 4.7-4.11. The wave group could be exciting the seiching modes of the wave tank and therefore most of the long wave energy could be in the seiching mode of the PWT. To verify this hypothesis, the seiching modes of the PWT were found analytically. The shallow water equations were used to obtain the seiching modes.
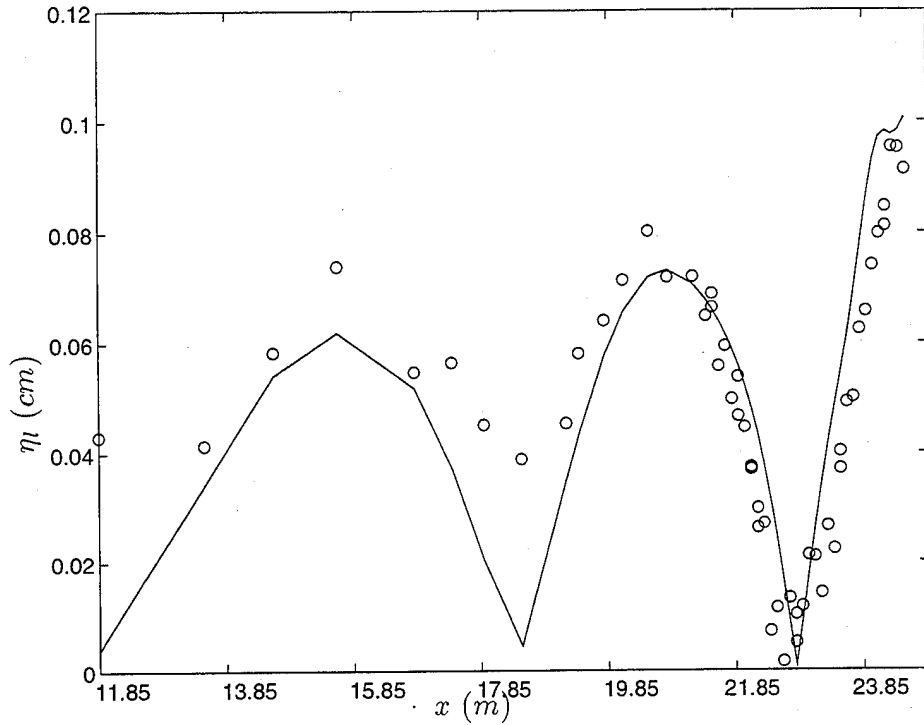
Figure 4.7: Long wave amplitudes for Experiments W01; data is (○) and three-gage array result is (———).

4.7 The seiching in the PWT.

In the previous section, we found that the long waves were mainly standing waves on the sloping bottom. We need to find out if the long waves are in resonance with the seiching modes of the tank. In this section, we try to obtain the seiching modes as an analytical function. To obtain an analytical solution, we assume the shear stresses to be negligible and that $\eta \ll h(x)$. We also assume that the tank has fixed dimensions. The analysis given below follows that of Wilson (1972). We have the wave equation as the equation governing the seiching in the tank which
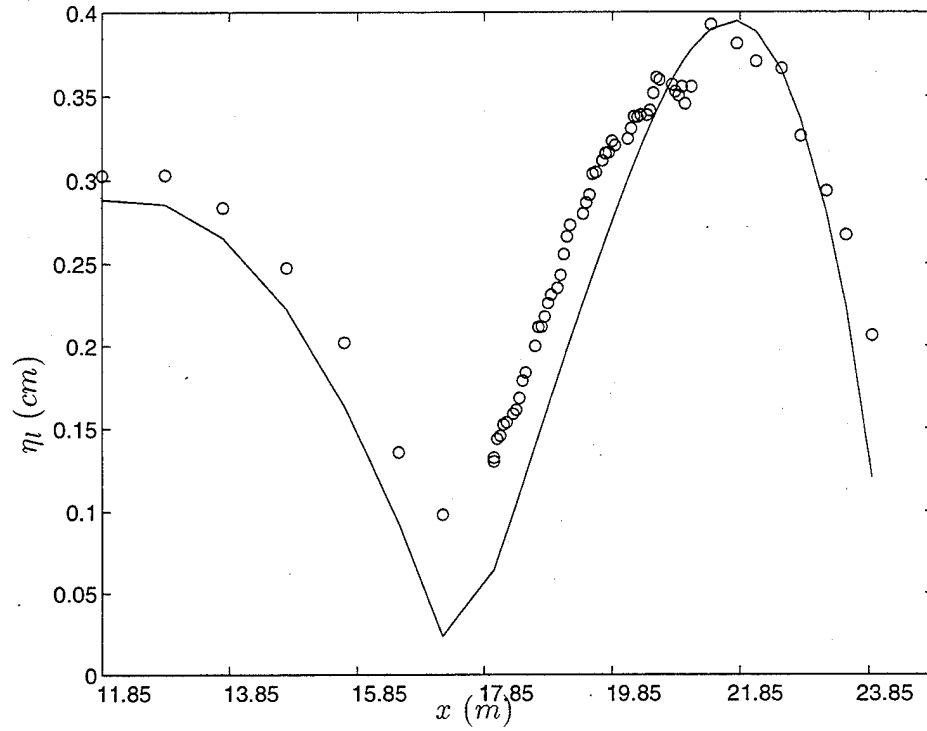
Figure 4.8: Long wave amplitudes for Experiments W02; data is (○) and three-gage array result is (———).

is

$$\frac{\partial^2 \eta}{\partial t^2} - \frac{\partial}{\partial x}\left(gh(x)\frac{\partial \eta}{\partial x}\right) = 0 \tag{4.13}$$

Assuming periodic and sinusoidal variation for η in time, we also have

$$\eta(x,t) = \zeta(x)\cos(\omega t) \tag{4.14}$$

Substituting (4.14) in (4.13), we can write

$$\frac{\partial}{\partial x}\left(gh(x)\frac{\partial \zeta}{\partial x}\right) + \omega^2 \zeta = 0 \tag{4.15}$$
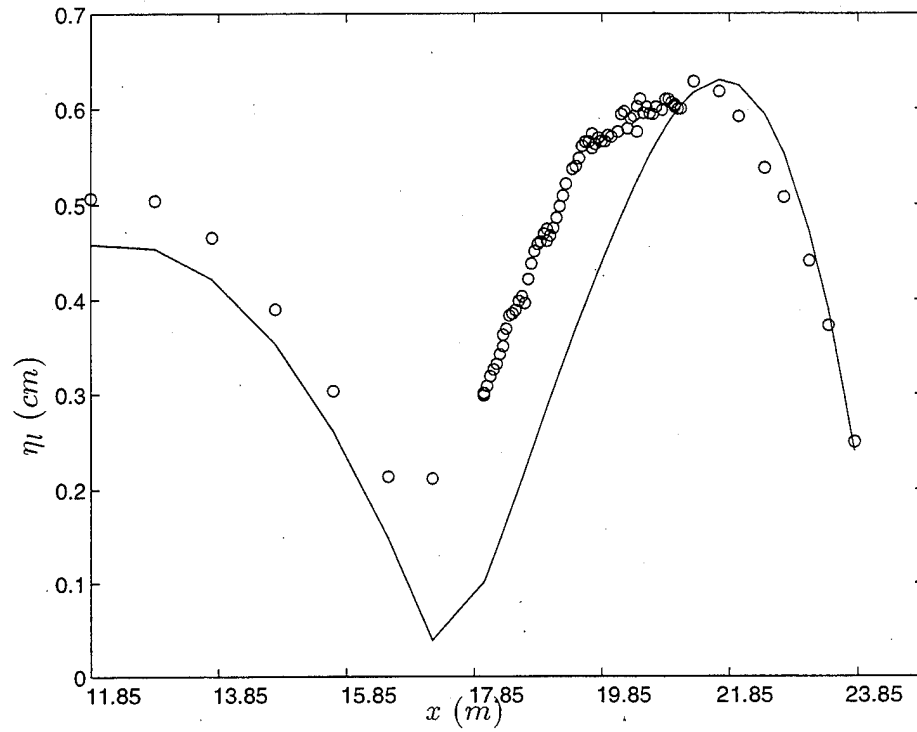
Figure 4.9: Long wave amplitudes for Experiments W03; data is (o) and three-gage array result is (————).

For the tank, the bottom is defined by

$$h(x) = \begin{cases} h_0 & x < x_0 \\ \frac{h_0(l-x)}{l-x_0} & x \geq x_0 \end{cases} \tag{4.16}$$

Equation (4.13) is solved separately for the two regions of differing bottom slopes and the resulting solutions are match at the toe of the beach, i.e. at $x = x_0$. Let us first consider the region of constant depth. In this region, (4.13) reduces to

$$g h_0 \frac{\partial^2 \zeta}{\partial x^2} + \omega^2 \zeta = 0 \tag{4.17}$$
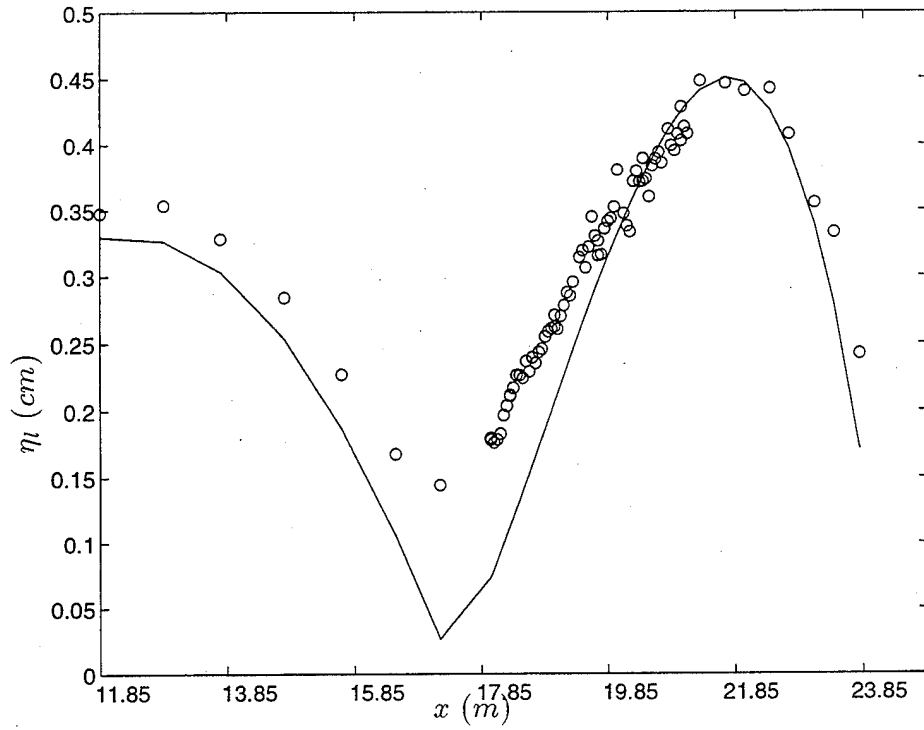
Figure 4.10: Long wave amplitudes for Experiments W04; data is (○) and three-gage array result is (———).

which has the general solution

$$\zeta = A \, \cos\left(\frac{\omega}{\sqrt{gh_0}}x\right) + B \, \sin\left(\frac{\omega}{\sqrt{gh_0}}x\right) \tag{4.18}$$

At the wave maker $(x = 0)$, the standing wave has an antinode, i.e., $\frac{\partial \zeta}{\partial x} = 0$, which implies $B = 0$. Therefore, for the constant depth section,

$$\zeta = A \, \cos\left(\frac{\omega}{\sqrt{gh}}x\right) \tag{4.19}$$

In the region of variable depth, (4.13) is

$$\frac{\partial}{\partial x}\left(\frac{gh_0(l-x)}{l-x_0}\frac{\partial \zeta}{\partial x}\right) + \omega^2 \zeta = 0 \tag{4.20}$$
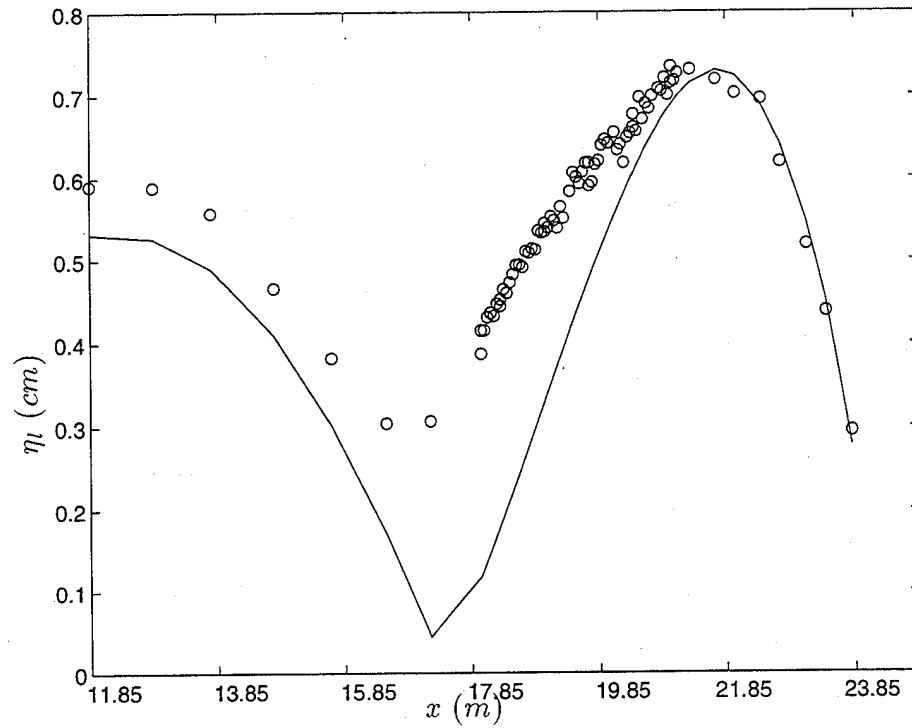
Figure 4.11: Long wave amplitudes for Experiments W05; data is (o) and three-gage array result is (————).

This is a classical Bessel Equation (e.g., Greenberg 1988) which has the solution

$$\zeta = C J_0(y) + D Y_0(y) \qquad (4.21)$$

where $y = \frac{2\omega(l-x)}{\sqrt{gh}}$. At the shoreline, we require ζ to be bounded and therefore set $D = 0$ and we get the solution in the sloping region as

$$\zeta = C J_0\left(\frac{2\omega}{\sqrt{gh}}(l - x)\right) \qquad (4.22)$$

Equation (4.19) and (4.22) together form the equation for the seiching in the tank. The coefficients A and C are obtained by matching the two solutions at the toe of the beach. Two matching conditions are required to solve for the the

two coefficients. We stipulate that there be no dicontinuity in the water surface and no discontinuity in the slope of the water surface, i.e.

$$\zeta(x_0^+) = \zeta(x_0^-)$$
$$\left.\frac{\partial \zeta}{\partial x}\right|_{x_0^+} = \left.\frac{\partial \zeta}{\partial x}\right|_{x_0^-} \tag{4.23}$$

where x_0^+ implies approaching x_0 from the wave maker and x_0^- implies approaching x_0 from the shoreline. These matching conditions give

$$A \cos\left(\frac{\omega}{\sqrt{gh_0}}x_0\right) = C J_0\left(\frac{2\omega(l - x_0)}{\sqrt{gh_0}}\right)$$
$$A \sin\left(\frac{\omega}{\sqrt{gh_0}}x_0\right) = -2C J_1\left(\frac{2\omega(l - x_0)}{\sqrt{gh_0}}\right) \tag{4.24}$$

Solving these two equations, we obtain the coefficients for the equation for seiching. To obtain the seiching frequencies, we divide one equation by the other and write

$$\tan\left(\frac{\omega}{\sqrt{gh_0}}x_0\right) + \frac{2J_1\left(\frac{2\omega(l-x_0)}{\sqrt{gh_0}}\right)}{J_0\left(\frac{2\omega(l-x_0)}{\sqrt{gh_0}}\right)} = 0 \tag{4.25}$$

The zeros of this equation give the seiching frequencies for the tank. The function on the left side of the equation is plotted in Figure 4.12. The first five seiching frequencies are tabulated in Table 4.6. The table also gives the corresponding seiching periods. It is seen that the second harmonic is very close to the group frequency in Experiments W02-W05 and the fourth harmonic is close to the group frequency in Experiment W01. This would indicate that the seiching modes in the tank are excited by the group frequency and therefore the predominant long wave component is the seiching mode. This means that the resonant interaction between the wave group and the seiching mode in the tank is not negligible. The analysis of this phenomenon is, however, beyond the scope of the present work.
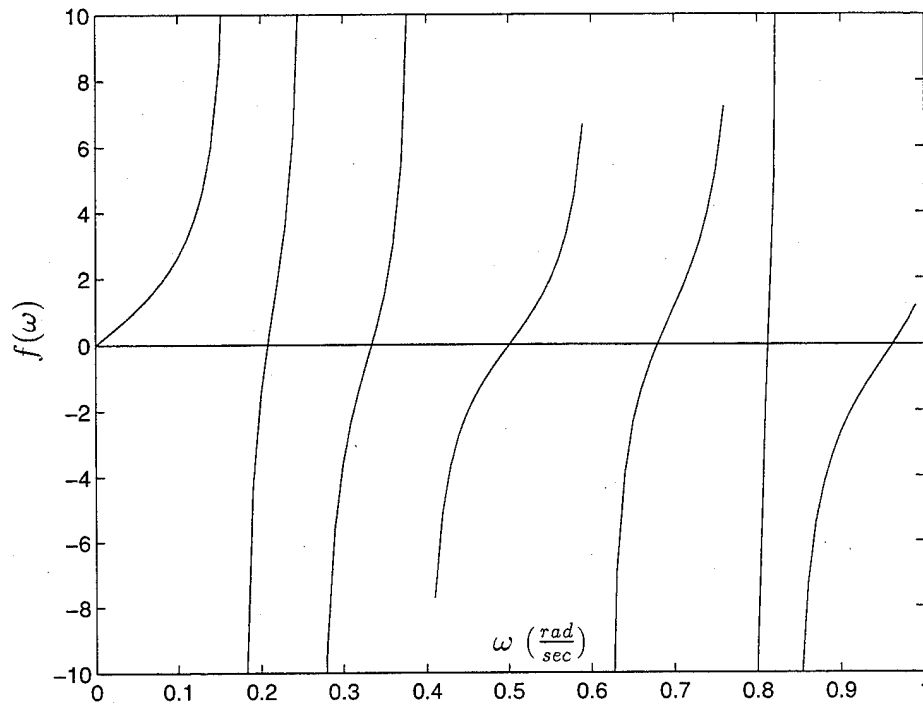
Figure 4.12: Plot showing the zeros of the function which describes the seiching mode.

4.8 · The wave groupiness in the surf zone.

The variation in wave break point and the amount of groupiness in the surf zone are used as the main mechanism in the models for the generation of long waves. Symonds et al. (1982) found analytically that long waves can be generated by variation in the breaking depth. On the other hand, Schäffer & Svendsen (1988) found that the long waves can also be generated by the presence of groupiness inside the surf zone in the absence of variation of breaking point. Schäffer & Svendsen (1988) proposed that the generation of long waves was due to a combination of the two factors. List (1991) analyzed field data and found that a substantial level of groupiness survives the breaking process. In this section we

Seiching mode	Frequency (rad/s)	Period (s)
0	0.2084	30.15
1	0.3345	18.78
2	0.5014	12.53
3	0.6795	9.25
4	0.8140	7.72

Table 4.6: Seiching frequencies and their corresponding periods in the tank.

try to analyze whether groupiness exists in the surf zone for our case and if so, attempt to quantify the groupiness.

To quantify the amount of groupiness inside the surf zone, two methods were used. The first method was the SIWEH (Smoothed Instantaneous Wave-Energy History) method as described by Funke & Mansard (1979). In this method, the SIWEH is defined as

$$E(t) = \frac{1}{T_p} \int_{-\infty}^{\infty} \eta^2(t + \tau) Q(\tau) d\tau \tag{4.26}$$

where T_p is the peak spectral period and $Q(\tau)$ represents the Bartlett filter defined by:

$$Q(\tau) = \begin{cases} 1 - \frac{|\tau|}{T_p} & |\tau| < T_p \\ 0 & |\tau| \geq T_p \end{cases} \tag{4.27}$$

The groupiness factor is defined as

$$G_s = \frac{(m_E)^{0.5}}{m_o} \tag{4.28}$$

where m_E is the variance of the SIWEH spectrum and m_o is the variance of the short wave spectrum.

List (1991) describes the inadequecies of this method in analyzing the groupiness and proposes an alternate method. In this method, the groupiness

factor is calculated using an envelope function. The envelope function is calculated in three steps:

- Find $|\eta(t)|$

- Lowpass filter $|\eta(t)|$ to remove the incident waves leaving only the low frequency signal related to the amplitude variation

- The signal is then multiplied by $\frac{\pi}{2}$ to obtain the envelope function $A(t)$

The groupiness factor is then calculated as

$$G_l = \frac{\sqrt{2}\sigma_A}{\bar{A}(t)} \tag{4.29}$$

where σ_A and $\bar{A}(t)$ are the standard deviation and mean of $A(t)$ respectively.

In calculating the envelope function, List assumes a sinusoidal wave form at the final step. Assumption of sinusoidal waves, in our case, would result in an underprediction of the mean envelope height.

Figures 4.13 to 4.17 show the groupiness factors of the incident waves in the five experiments as a function of the distance from the wave maker. Although there is considerable scatter in the groupiness factor, especially in the surf zone, List's method (Equation 4.29) gives lower values of groupiness than the SIWEH method (Equation 4.28) for all the experiments. The groupiness, according to List's method, decreases as the waves propagate into the surf zone. However, there is still significant amount of groupiness even after the waves break. The SIWEH method, on the other hand, shows that the groupiness of the waves is lesser near the breaking region and as the waves propagate into the surf zone, the groupiness is even more pronounced than that outside the surf zone. In fact, the groupiness inside the surf zone is, more often than not, higher than the groupiness input at the wavemaker during the generation of the waves.
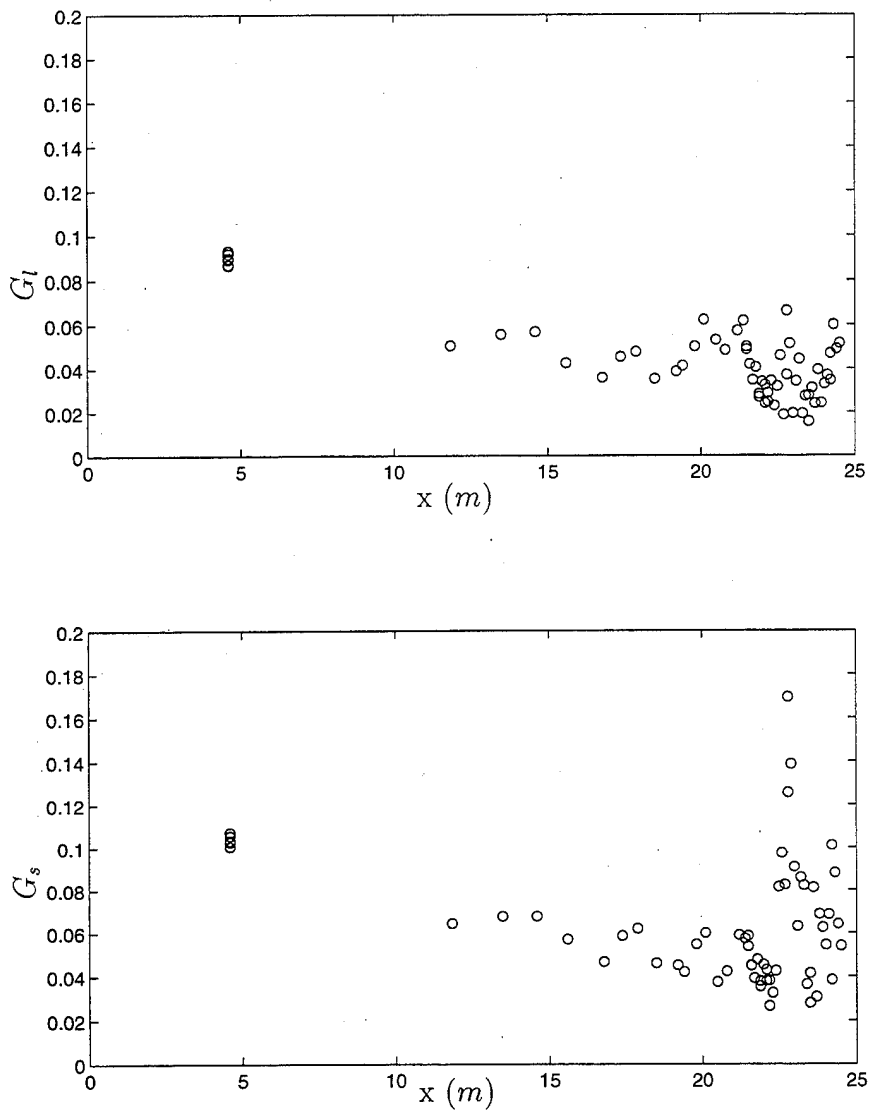
Figure 4.13: Groupiness factor computed as in Equations (4.28) and (4.29) for Experiment W01. Breaking is between $x = 21.90$ m and $x = 22.70$ m.
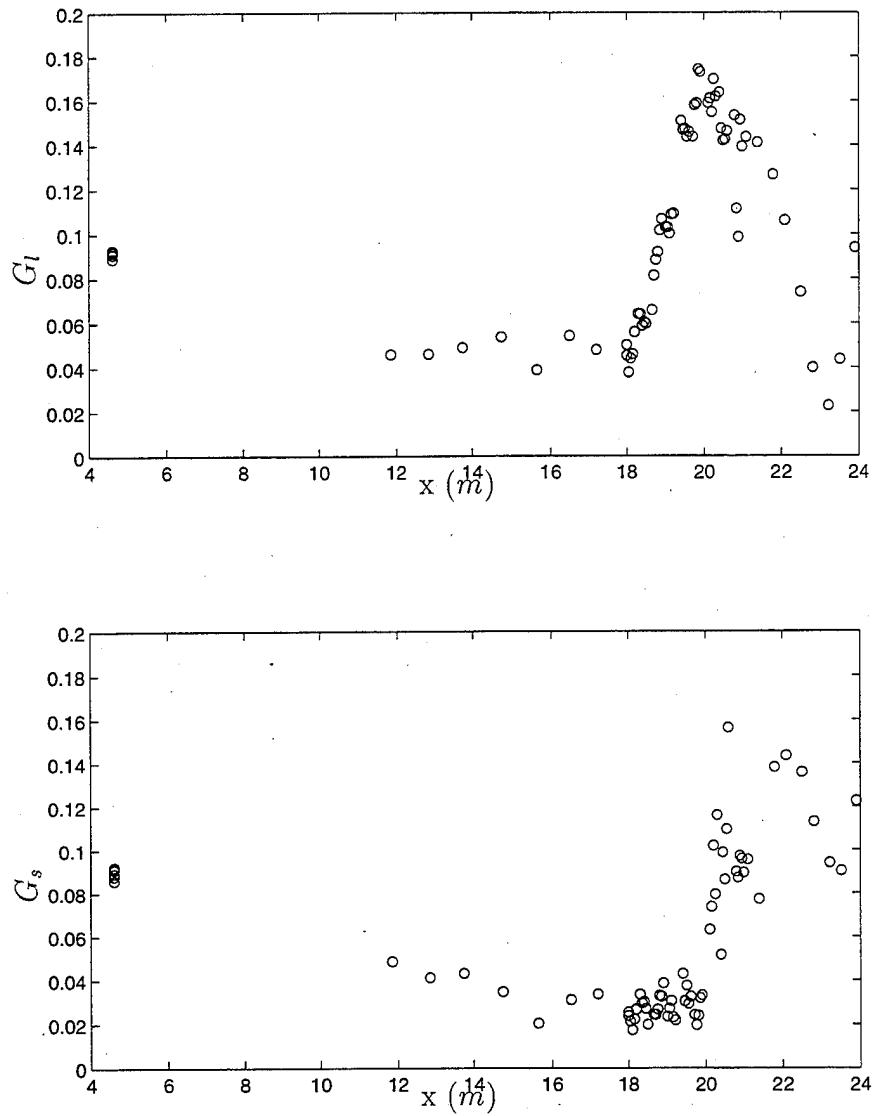
Figure 4.14: Groupiness factor computed as in Equations (4.28) and (4.29) for Experiment W02. Breaking is between $x = 19.40 \ m$ and $x = 20.10 \ m$.
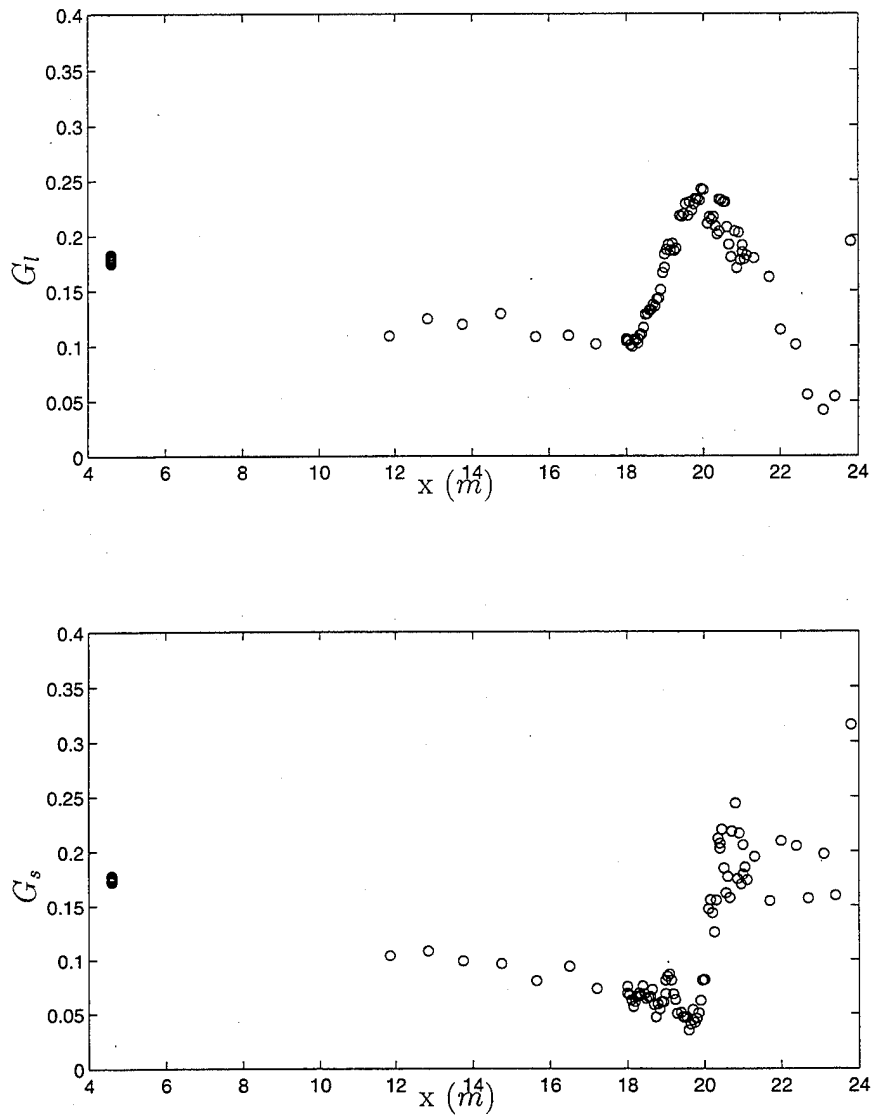
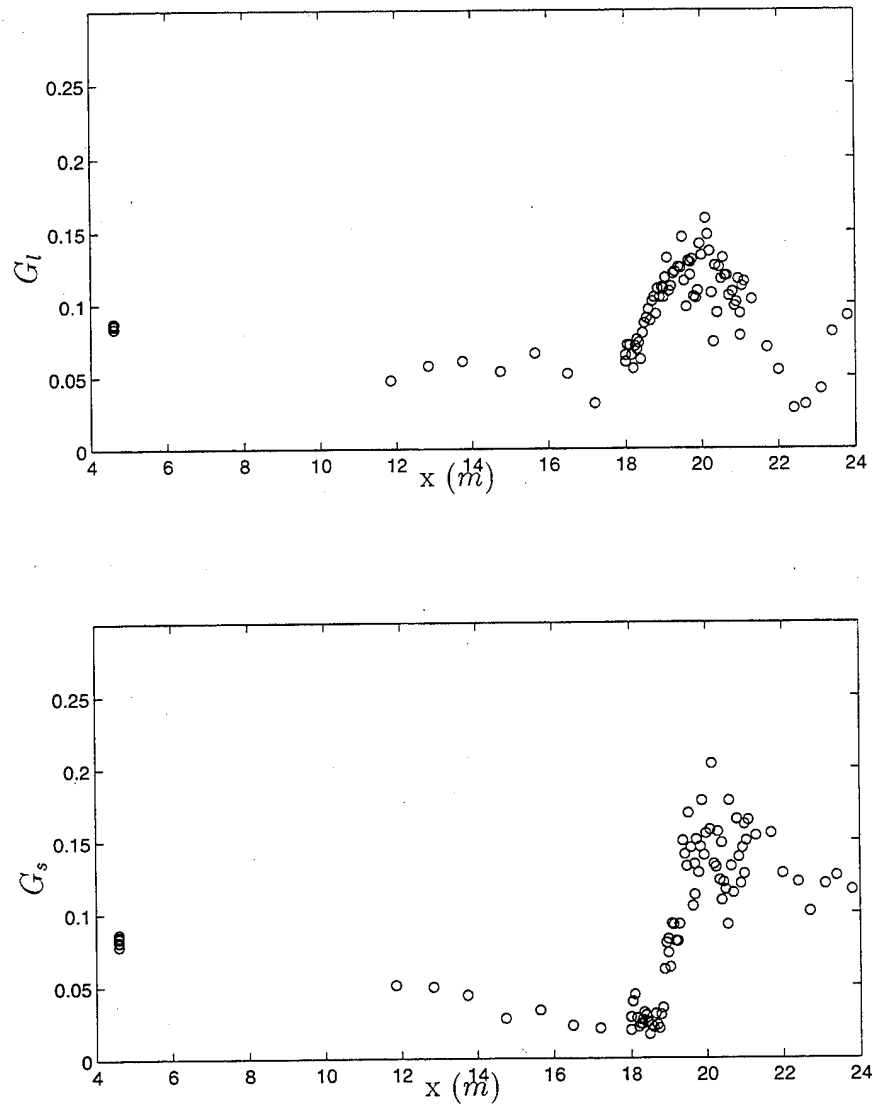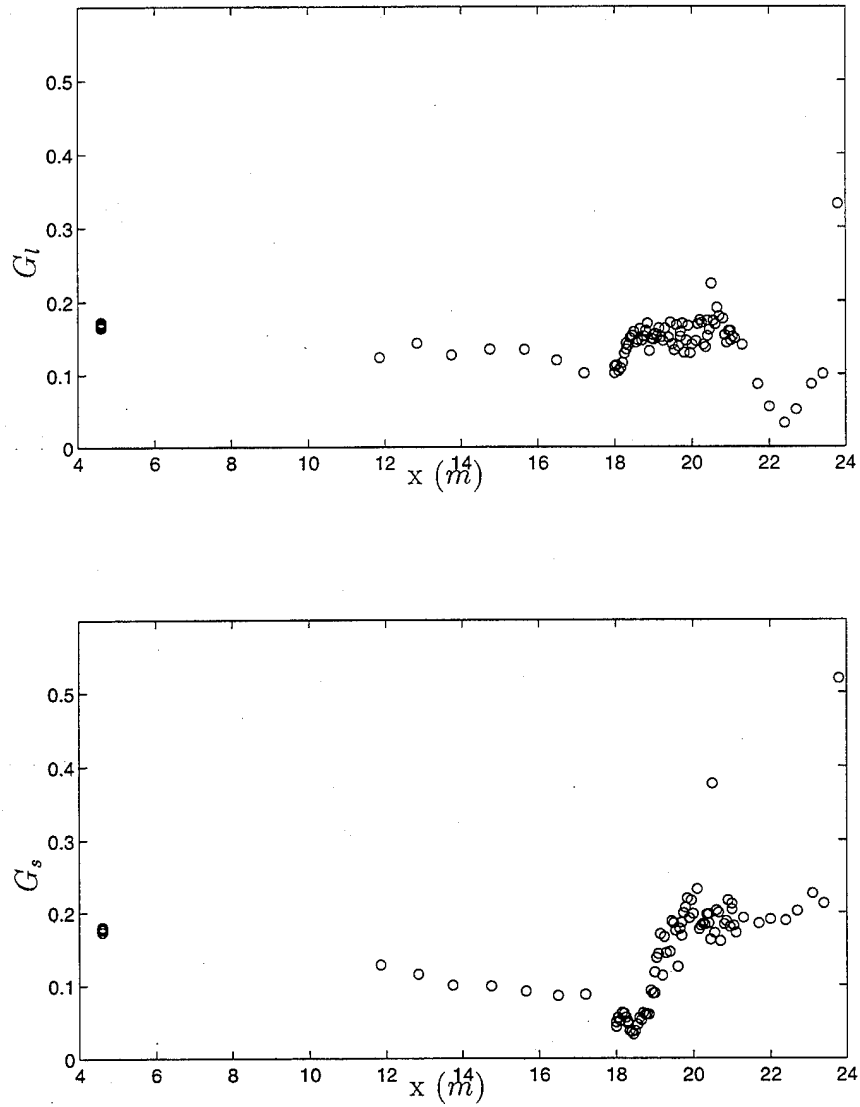**Figure 4.15:** Groupiness factor computed as in Equations (4.28) and (4.29) for Experiment W03. Breaking is between $x = 19.10\ m$ and $x = 20.45\ m$.

58

Figure 4.16: Groupiness factor computed as in Equations (4.28) and (4.29) for Experiment W04. Breaking is between $x = 18.15\ m$ and $x = 18.95\ m$.

Figure 4.17: Groupiness factor computed as in Equations (4.28) and (4.29) for Experiment W05. Breaking is between $x = 17.20\ m$ and $x = 19.50\ m$.

Chapter 5

MODEL COMPARISON AND CONCLUSIONS

In this chapter, comparisons between model and data are presented. First the model results for monochromatic wave propagation were compared to the individual wave data in a group, obtained from the experiments. The results are discussed in Section 5.1. The model results for wave group propagation were then compared to the wave data for the group and discussed in Section 5.2.

5.1 Comparision between model and data for individual waves.

Assuming that the individual waves in a group can be treated as monochromatic waves, the variation of the wave height, wave period and phase speed for each wave in a group, as obtained from the data, was used to verify the model predictions of individual wave propagation. This means that wave-wave interactions are neglected for this comparison. The results from the model are plotted along with the experimental data.

To reiterate, the model predicts the wave averaged quantities, namely, the wave height, wave period and the phase speed, at any location in the domain. The model equations are (2.38) and (2.39), which are the finite difference forms of the conservation equations, along with the dispersion relation (2.20). At the shoreline

60

boundary, the characteristic forms of the conservation equations are used. The dissipation in the domain is calculated using (2.34).

The input parameters, for this comparison, to the model are as follows. The inputs to the model at the offshore boundary are the wave height and the wave period. In addition, the long wave amplitude in the domain is also specified. The beach slope was specified as $m = 1 : 35.2$, which corresponded to the average beach slope during the experiments. The computation was started at the toe of the beach and was carried out to a depth of 1 cm. The grid spacing in the spatial domain (dx) was 0.05 m and the time step (dt) was 0.05 $secs$. The water depth at the toe of the beach was given as $h_0 = 0.4\ m$, which again corresponded to the experimental conditions.

The initial condition imposed is a cold start, i.e., there are initially no waves in the domain. The wave heights from the experiments range between 6 cm and 12 cm and wave periods range from 1.5 $secs$ to 2.5 $secs$. Specifying the actual wave period and wave height, at the offshore boundary, at the first time step would imply that there is a discontinuity in the water surface. Such discontinuities exist only at wave breaking. To avoid this discontinuity in water surface at the offshore boundary, a '$tanh$' factor was included in the offshore boundary condition, i.e., the wave height at the offshore boundary was calculated as

$$H_1^n = H_B \left[tanh \left(\frac{n\pi dt}{T} \right) \right]^2 \tag{5.1}$$

where H_B was the wave height specified at the boundary, T, the wave period and dt, the time step. The value of this factor increases from zero at the first time step of computation to one at the end of the third wave period, within the machine precision, which ensured a smooth start-up condition for the model.

No variation of the wave height or wave period, other than the startup

variation mentioned above, was specified at the offshore boundary. The long wave in the tank was found to have a period very close to that of the wave group generated in the tank (Sections 4.6 and 4.7). The group period was therefore specified as the long wave period. In view of the finding that the group period was close to the seiching period in the tank and also that the long waves have very prominent nodes and antinodes in the tank, the long wave was specified as a standing wave. Figures 5.1 to 5.15 show the results for the highest wave in the group for each experiment. In this report, comparisons are presented only for the highest wave in the group unless further illustration of the phenomena under discussion is required. Since the comparison in this section is for monochromatic waves, H, c and T are not functions of time t.

5.1.1   Prediction of wave height $H(x)$.

The wave heights predicted by the model are compared with the wave heights obtained from the data. Figures 5.1, 5.4, 5.7, 5.10 and 5.13 show the comparison for the highest wave in each of the five experiments. It can be seen from the figures that although the predictions are quite good in most of the domain, the wave heights are not predicted well near the breaking point and also that, except in Figure 5.1, the wave break point for the model is at a lower depth than observed. There are three possible reasons for these inaccuracies, the first being the neglection of the wave-wave interactions. Near the breaking region, the waves are highly nonlinear which results in non-negligible interactions. The second reason is that the model equations are based on cnoidal theory, which assumes $\frac{H}{h} \ll 1$. The theory is not accurate where the waves approach breaking. The third reason is that the prediction of breaking is based on Equation (4.6) which was based on data from monochromatic waves, for which the free second harmonics were

removed at the wavemaker by modifying the motion of the wavemaker. Furthermore, the slope of the beach in the wave tank is not uniform, which may have some influence on the measured wave heights. Although the prediction of H is not accurate near the breaking point, it can be seen from the figures that further into the surf zone, the predictions improve again.The energy dissipation in the surf zone, calculated in the model assuming bore theory, is proportional to H^3. This means that for a higher wave height, the dissipation is considerably larger. Once the wave height predicted by the model comes close to that observed from experiments, the prediction and observation match closely.

5.1.2 Prediction of wave speed $c(x)$.

Figures 5.2, 5.5, 5.8, 5.11 and 5.14 show the comparison between the predicted and the observed wave speeds. In the figures, the wave speed is normalized by $\sqrt{gh}$. The model predicts the wave speed based on cnoidal theory. However, it can be seen from the figures that the wave speed observed, before breaking, is very close to $\sqrt{gh}$. Therefore, in addition to obtaining the model results for wave speed defined as in (2.20), which is

$$
\frac{c_s^2}{gh} = \begin{cases} 1 + \frac{H}{mh}\left(2 - m - 3\frac{E(m)}{K(m)}\right) & \text{for } h > h_b \\ \\ 1 + \left(-\frac{3}{2} + 3\delta\right)\frac{H}{h} + \left(\frac{1}{2} - 3\delta + 3\delta^2\right)\left(\frac{H}{h}\right)^2 \\ + \left(\frac{1}{2}\delta - \frac{3}{2}\delta^2 + \delta^3\right)\left(\frac{H}{h}\right)^3 & \text{for } h \leq h_b \end{cases}
\tag{5.2}
$$

the model results are also obtained for wave speed defined as

$$
\frac{c_s^2}{gh} = \begin{cases} 1 & \text{for } h > h_b \\ \\ 1 + \left(-\frac{3}{2} + 3\delta\right)\frac{H}{h} + \left(\frac{1}{2} - 3\delta + 3\delta^2\right)\left(\frac{H}{h}\right)^2 \\ + \left(\frac{1}{2}\delta - \frac{3}{2}\delta^2 + \delta^3\right)\left(\frac{H}{h}\right)^3 & \text{for } h \leq h_b \end{cases}
\tag{5.3}
$$

Using $\sqrt{gh}$ as the wave speed before breaking gives a better prediction of the observed wave speed.

Inside the surf zone, the wave speed in the model is assumed to be that of a bore. In addition, the model assumes that the wave is transformed into a bore immediately after breaking, i.e., there is no effective transition zone to allow the waves to transform from wave to bore. Furthermore, it can be observed that the wave speeds observed in the surf zone reaches a value close to $1.5\sqrt{gh}$, whereas the bore formulation predicts a wave speed of close to $1.2\sqrt{gh}$ for the value of $\frac{\eta_c}{H} = 0.7$ which was observed from the experiments. All these reasons contribute to the overprediction of the wave speed immediately after breaking and the underprediction of the same further into the surf zone.

5.1.3 Prediction of wave period $T(x)$.

Figures 5.3, 5.6, 5.9, 5.12 and 5.15 show the comparison between the predicted and the observed wave periods. It is seen that the trends in the variation of the wave period is predicted well by the model. However, the wave periods themselves are underpredicted in the surf zone. It is illustrative to consider the wave period predicted for the waves with lower H. For maximum contrast, the prediction of T for the lowest wave in Experiment W02 is shown in Figure 5.16. Is can be seen from this figure that the wave period predicted is higher than that observed. One possible reason for this could be that the wave-wave interactions between the short waves in a group are considerable and therefore, the values of the wave period are not predicted accurately. In addition, it was also assumed that the effect of the long wave can be approximated to that of a current (Section 2.1), which implies that the frequency of the long wave is assumed to
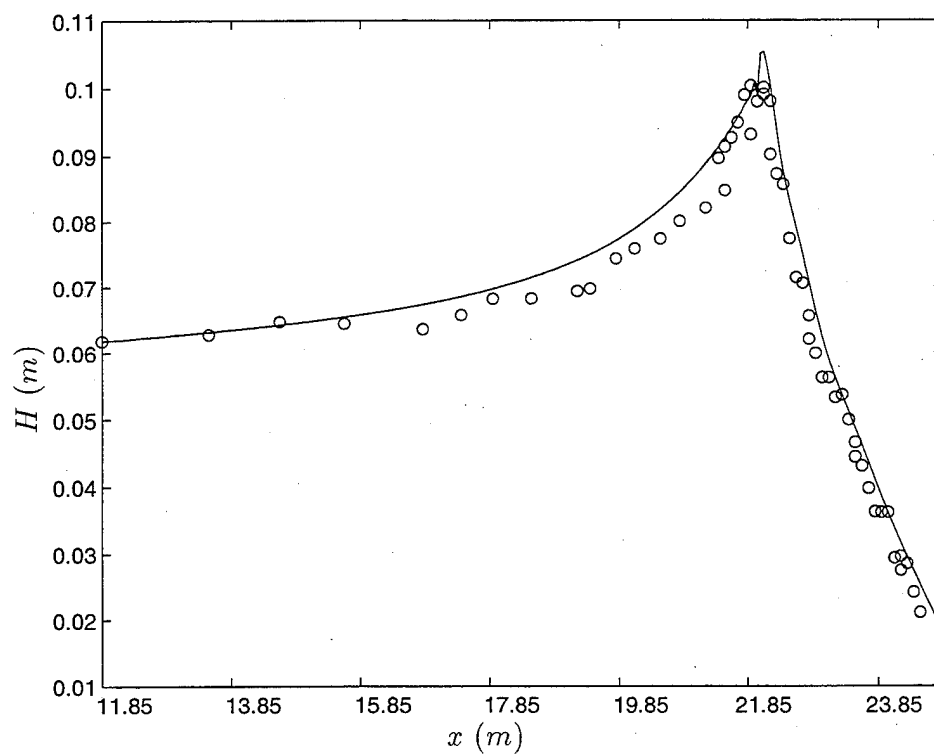
Figure 5.1: Comparison between model prediction of wave height (———) and data (○) for the highest wave in Experiment W01.
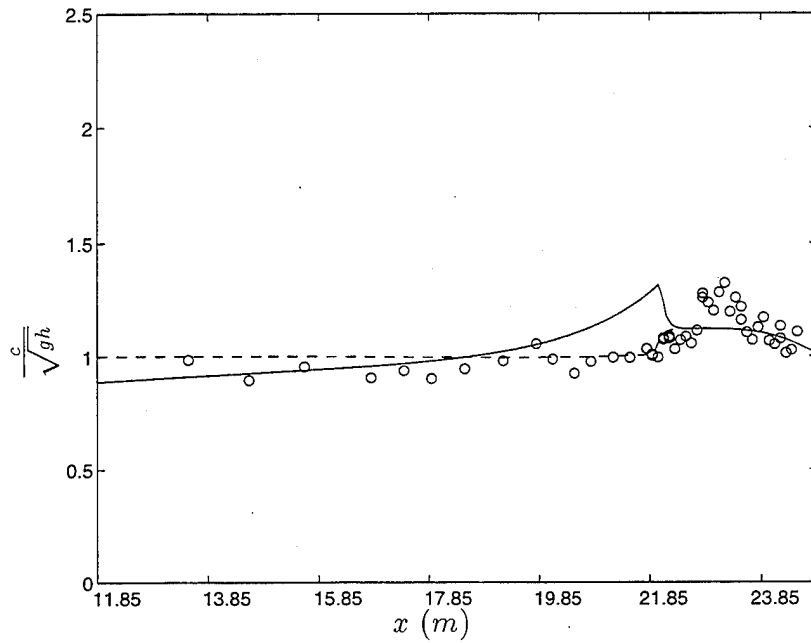
Figure 5.2: Comparison between model prediction of wave speed using Equation 5.2 (——), model prediction of wave speed using Equation 5.3 (— —) and data (o) for the highest wave in Experiment W01.
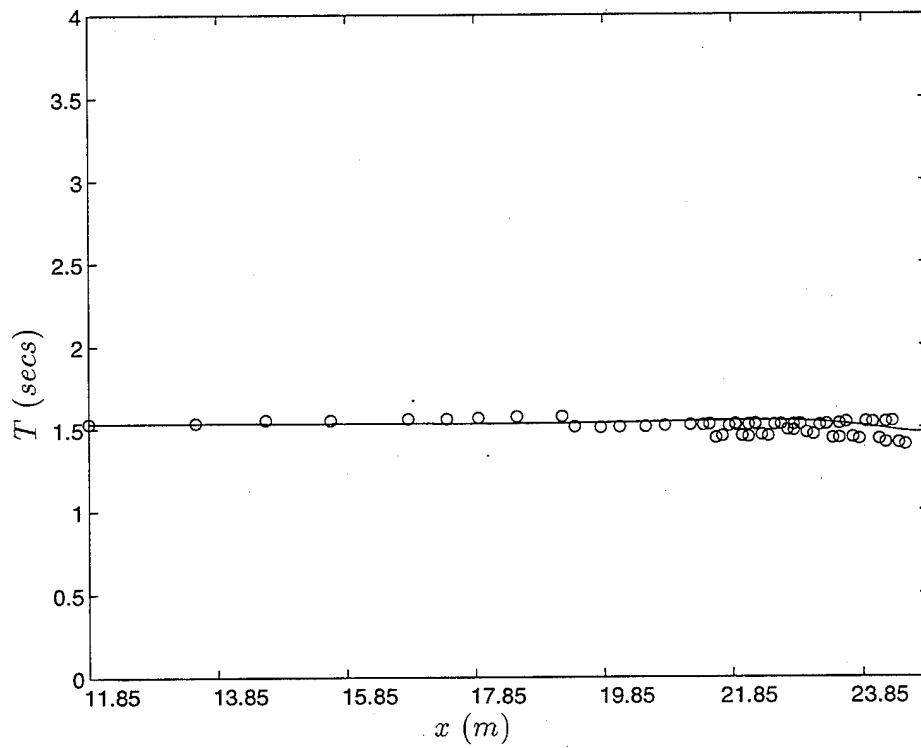
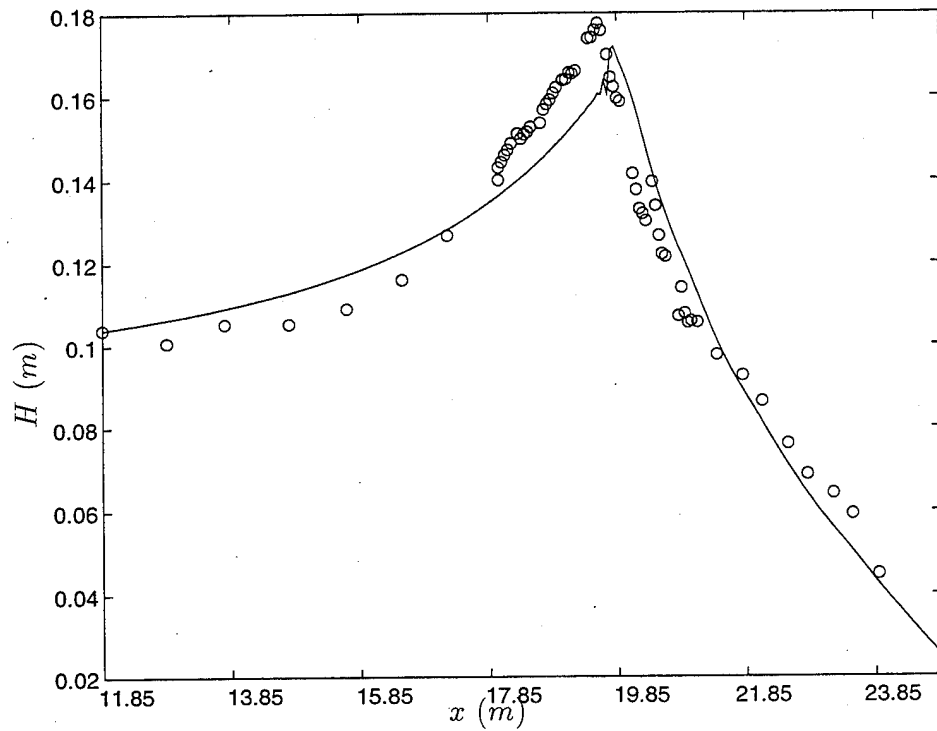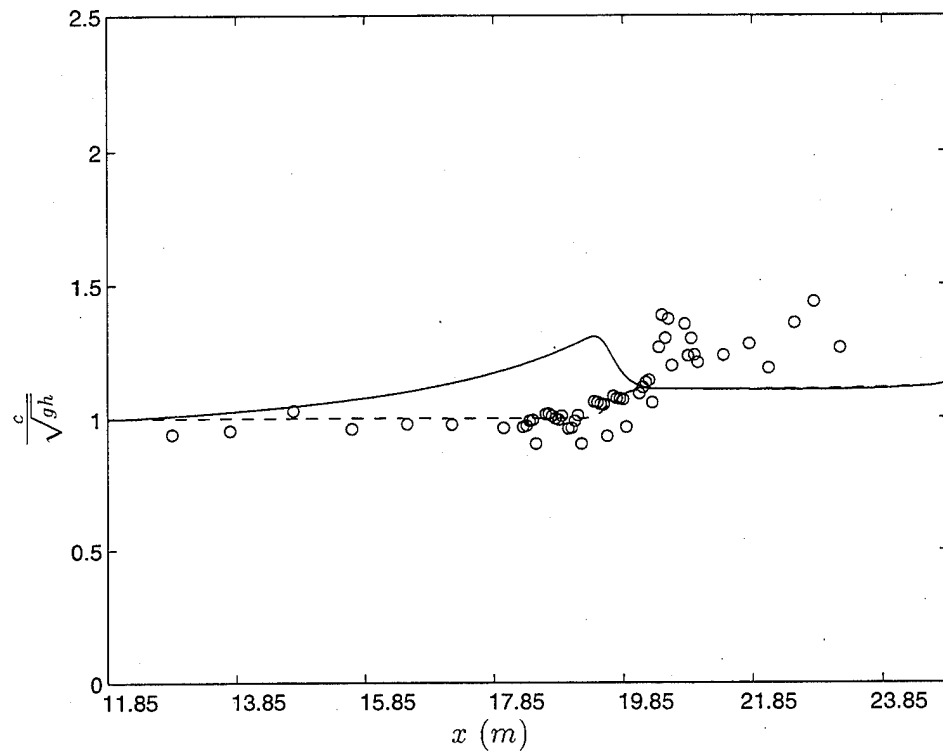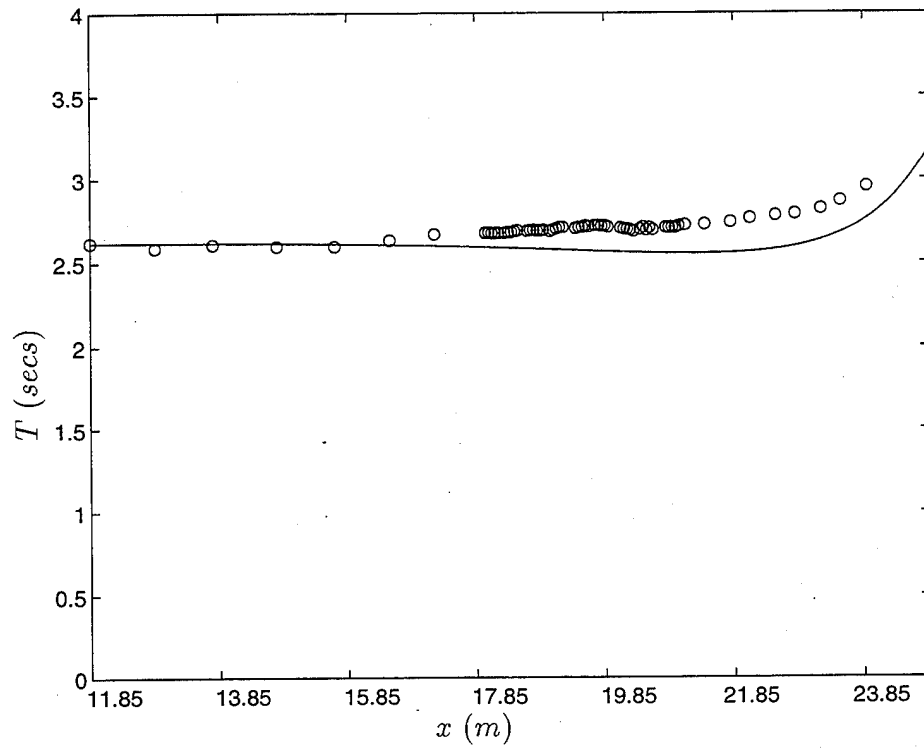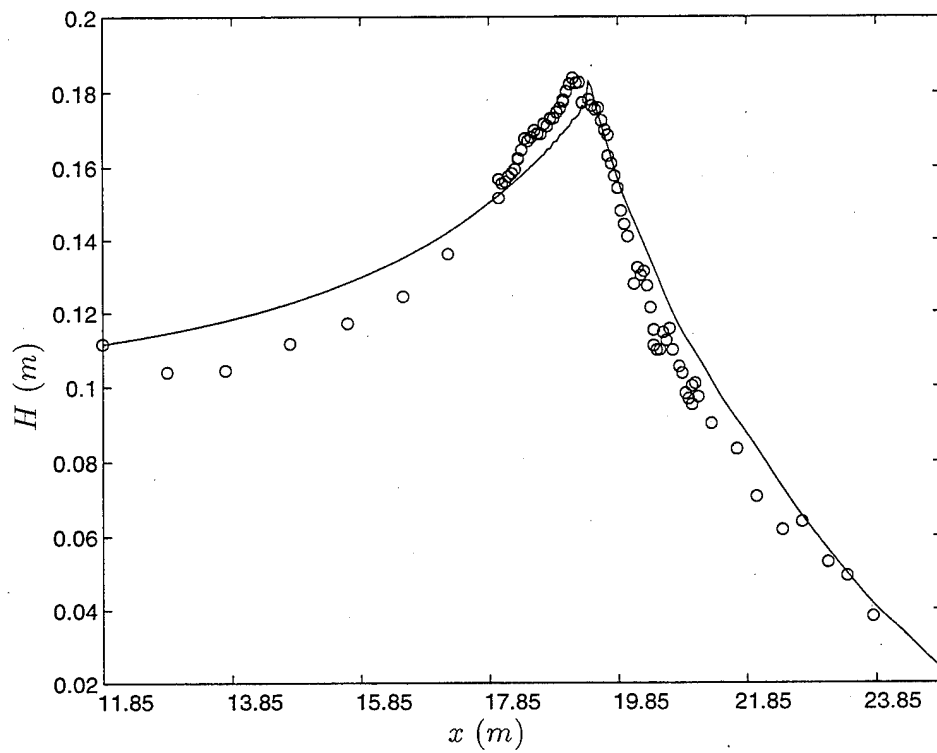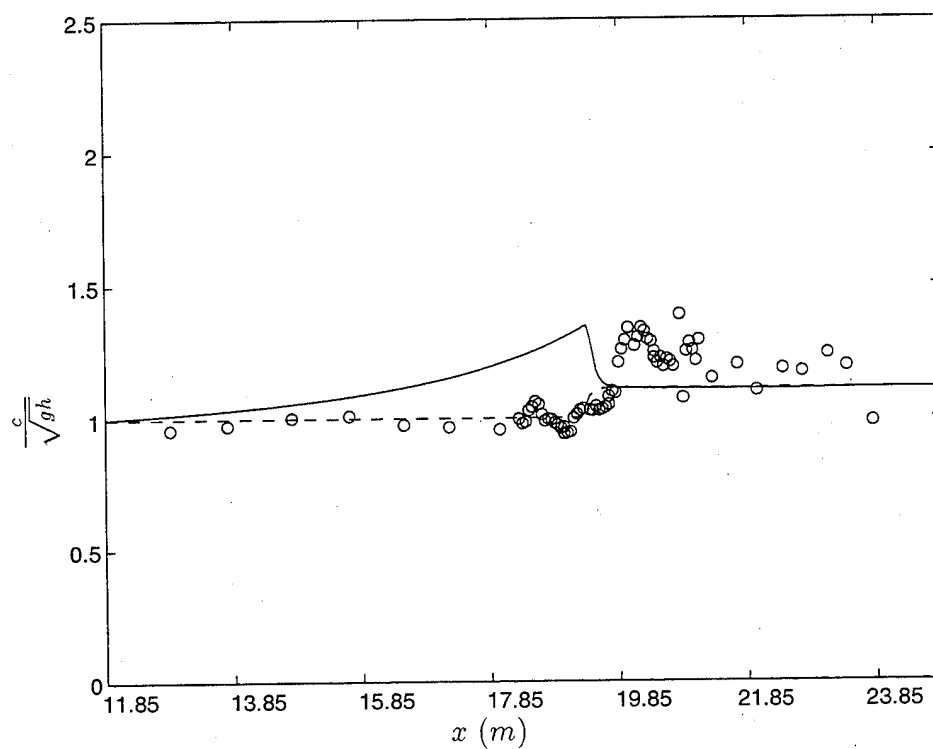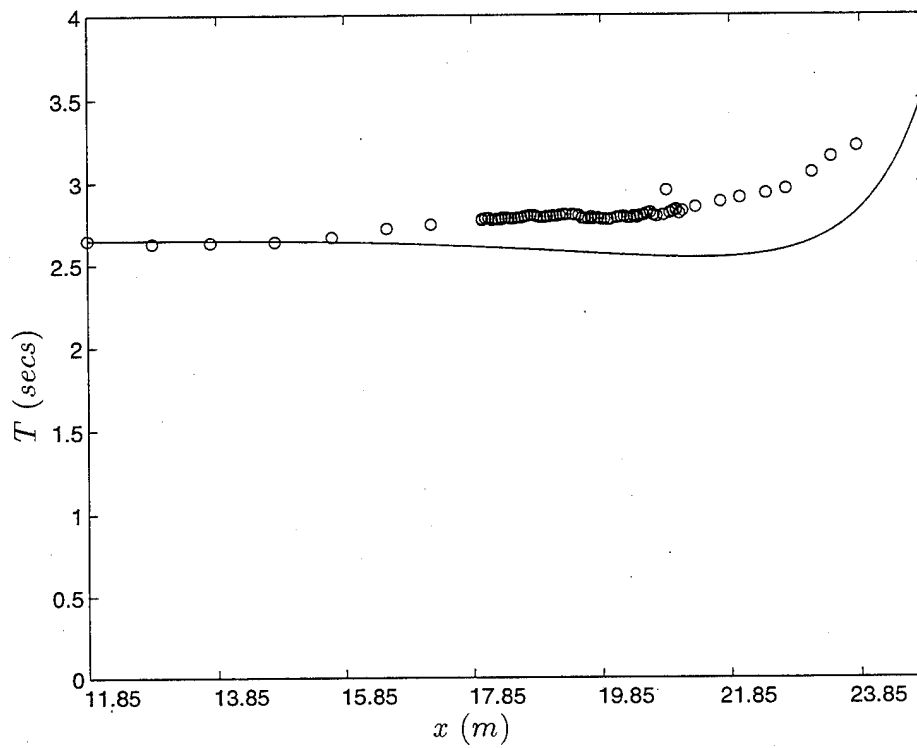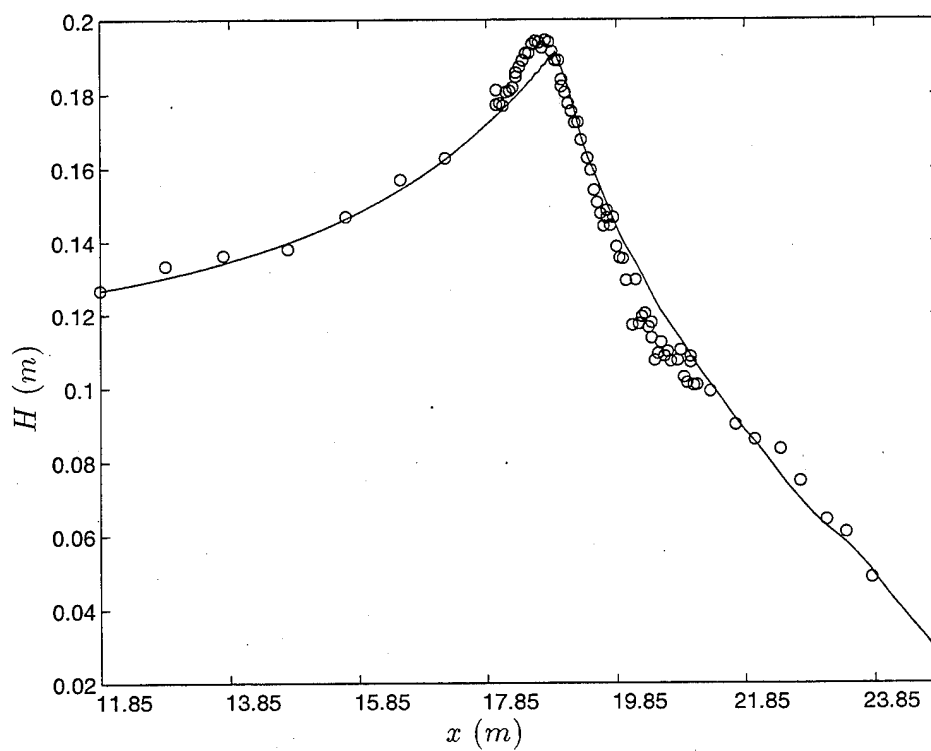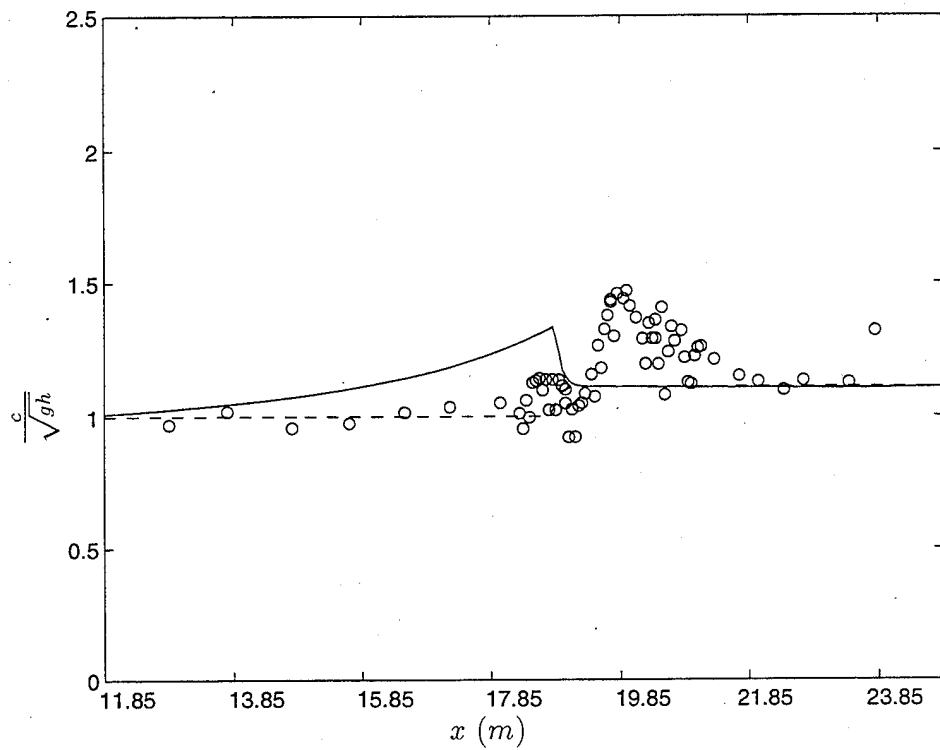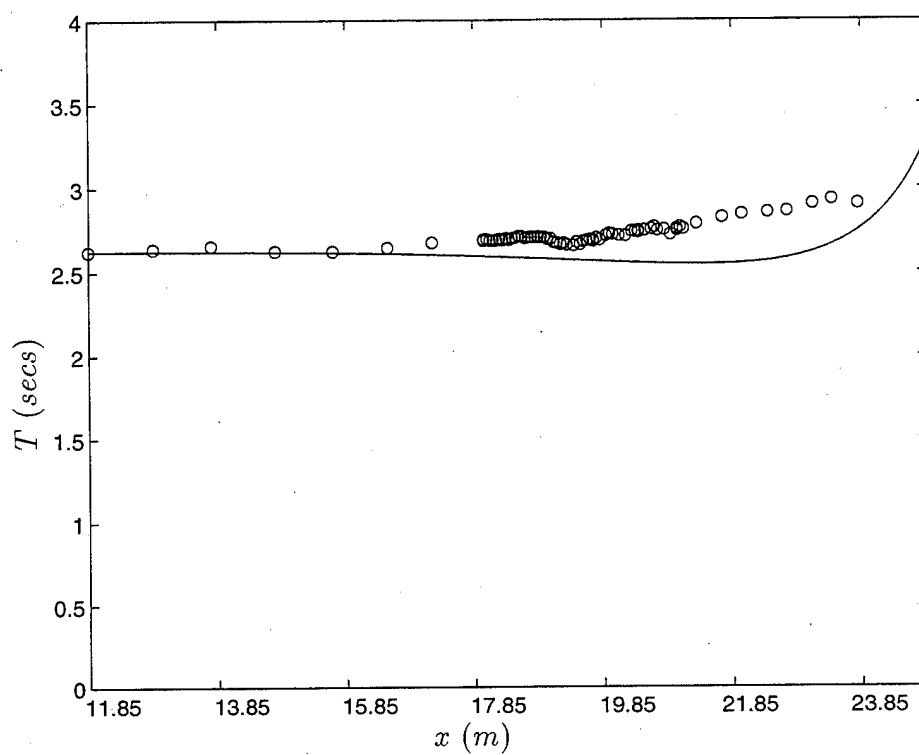**Figure 5.3:** Comparison between model prediction of wave period (———) and data (o) for the highest wave in Experiment W01.

Figure 5.4: Comparison between model prediction of wave height (————) and data (o) for the highest wave in Experiment W02.

Figure 5.5: Comparison between model prediction of wave speed using Equation 5.2 (———), model prediction of wave speed using Equation 5.3 (− − −) and data (○) for the highest wave in Experiment W02.

Figure 5.6: Comparison between model prediction of wave period (———) and data (o) for the highest wave in Experiment W02.
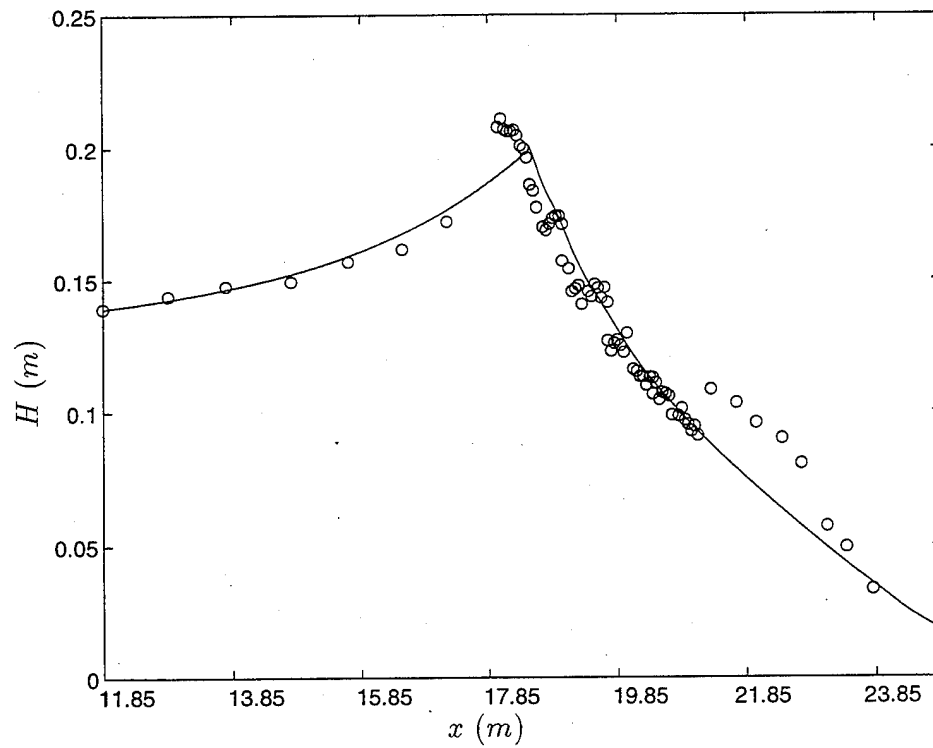
Figure 5.7: Comparison between model prediction of wave height (———) and data (○) for the highest wave in Experiment W03.
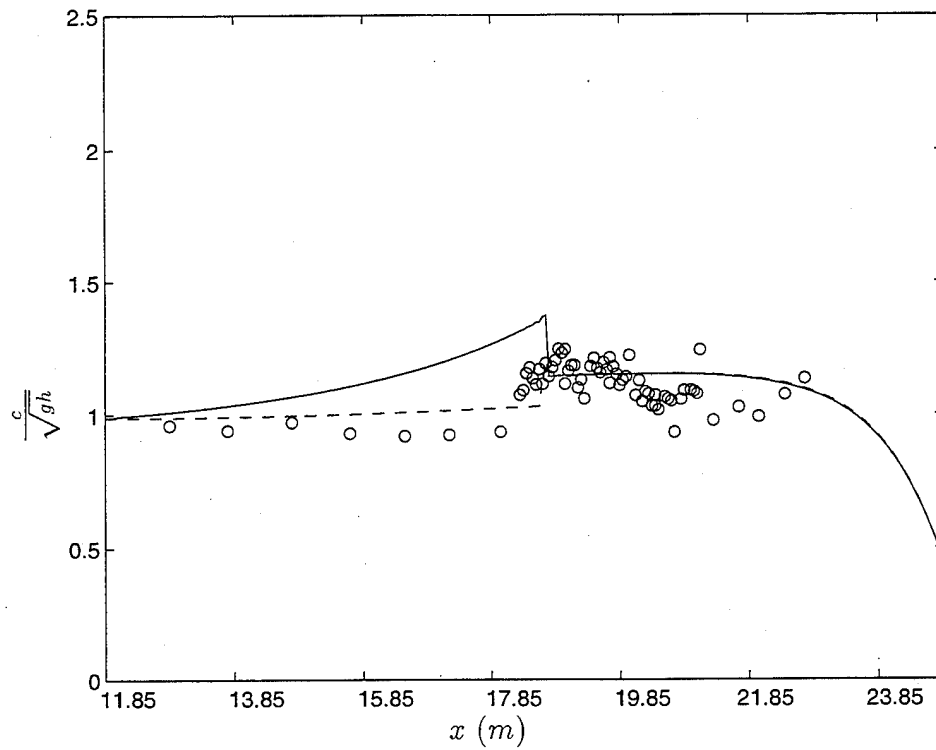
Figure 5.8: Comparison between model prediction of wave speed using Equation 5.2 (———), model prediction of wave speed using Equation 5.3 (— — —) and data (o) for the highest wave in Experiment W03.
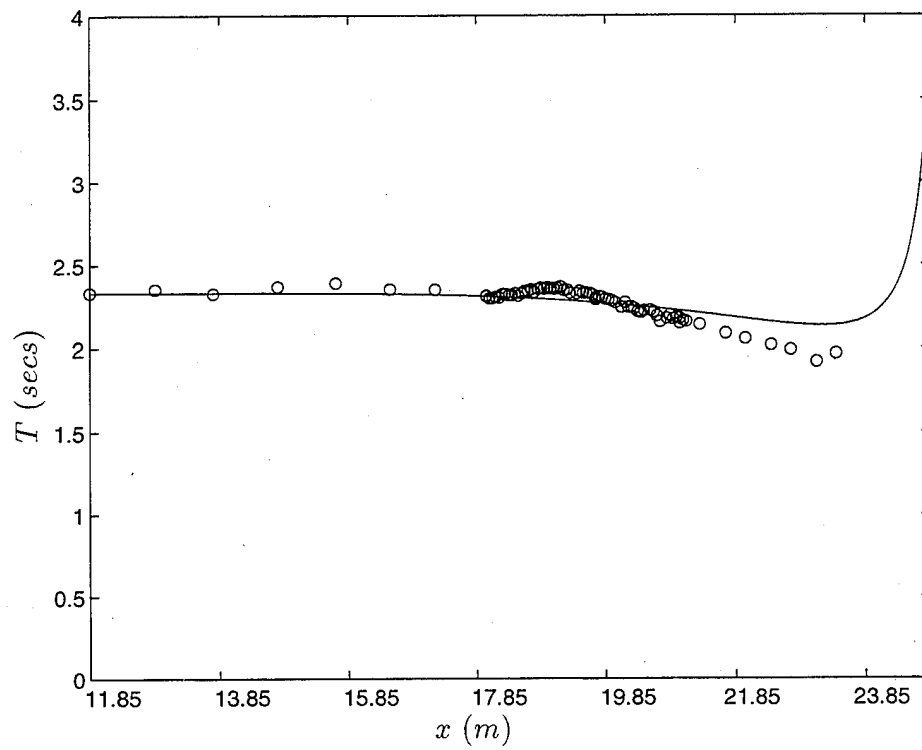
Figure 5.9: Comparison between model prediction of wave period (————) and data (o) for the highest wave in Experiment W03.
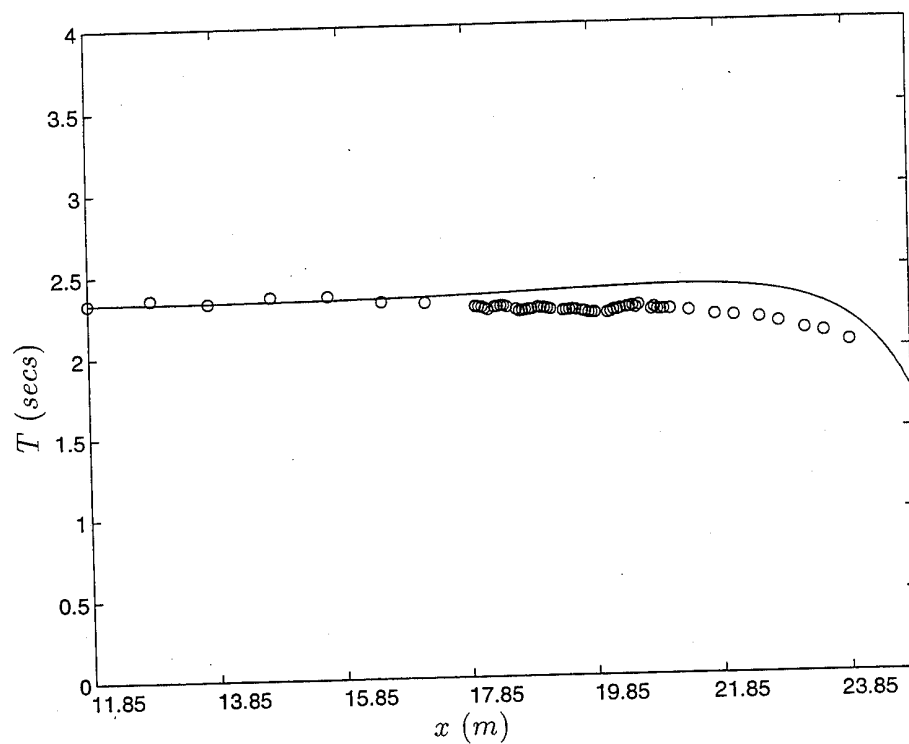
Figure 5.10: Comparison between model prediction of wave height (————) and data (o) for the highest wave in Experiment W04.

Figure 5.11: Comparison between model prediction of wave speed using Equation 5.2 (———), model prediction of wave speed using Equation 5.3 (— — —) and data (o) for the highest wave in Experiment W04.

Figure 5.12: Comparison between model prediction of wave period (———) and data (o) for the highest wave in Experiment W04.

Figure 5.13: Comparison between model prediction of wave height (———) and data (o) for the highest wave in Experiment W05.

Figure 5.14: Comparison between model prediction of wave speed using Equation 5.2 (———), model prediction of wave speed using Equation 5.3 (— — —) and data (○) for the highest wave in Experiment W05.

Figure 5.15: Comparison between model prediction of wave period (———) and data (o) for the highest wave in Experiment W05.

Figure 5.16: Comparison between model prediction of wave period (———) and data (o) for the lowest wave in Experiment W02.

5.2 Comparison between model and data for the groups.

In this section, the model results for the prediction of the wave group propagation is compared with the data obtained from the experiments.

The model parameters are the same as in the previous section, i.e., $h_0 = 0.4m$, $dx = 0.05m$ and $dt = 0.05secs$. In the previous section, it was found that Equation 5.3 predicts the wave speed better than Equation 5.2. Therefore, for the comparisons in this section, Equation (5.3) is the dispersion relation in the model.

The envelope variation is obtained by approximating the wave heights and frequencies by a continuous function through the data points. These two quantities are provided as input to the model at the left boundary. The '$tanh$' factor as in (5.1) is included to prempt the onset of instabilities in the startup of the model.

Comparisons are shown for the locations given in Table 5.1. Figures 5.17 to 5.41 illustrate the group profiles at each of these locations. For each experiment, the first two locations given in the table are in the shoaling region, the third location is in the breaking region and the last two locations are in the surf zone.

Experiment number	Comparison at x (m)					Breaking region x (m) - x (m)
W01	13.50	20.10	22.00	23.00	24.50	21.90 - 22.70
W02	12.85	18.00	19.55	20.85	22.80	19.40 - 20.10
W03	12.85	18.60	19.60	20.90	23.40	19.10 - 20.45
W04	12.85	18.60	19.60	20.90	22.70	18.15 - 18.95
W05	12.85	18.60	19.40	20.90	22.70	17.20 - 19.50

Table 5.1: Positions at which comparisons are presented for each experiment and the corresponding breaking region.

It is found that the model predicts the wave height variation upto the surf zone considerably well. Inside the surf zone, the model prediction depends on the energy dissipation as given by Equation 2.34. The energy dissipation in the surf zone is calculated assuming that it is equivalent to the dissipation in a hydraulic jump, which is proportional to the cube of the wave height. Therefore, the higher wave decays at a much faster rate than the lower waves. This tends to reduce the groupiness in the surf zone as seen from Figures 5.20, 5.21, 5.25, 5.26, 5.30, 5.31, 5.35, 5.36, 5.40 and 5.41. In the Figures 5.20 and 5.21, which is for Experiment W01, the prediction is reasonably accurate. As the wave height and the groupiness increases, the predictions deteriorate.

The model prediction of the wave speed, calculated as in (5.3), is quite good outside the surf zone. In the transition region, the wave speed is over predicted. The reason for this is, in the model, the waves are assumed to transform into bore form as soon as they break. Inside the surf zone, the model prediction of the wave speed is less than that observed from the experiments. As mentioned in Section 5.1.2, the bore speed is less than the wave speed observed in the surf zone, which is the cause for this underprediction. However, the variation of the wave speed in the surf zone is realized in the model.

The wave periods obtained from the model are very close to that observed in the experiments. The variation of the wave period is also predicted very well by the model, except in a few cases as in Figures 5.30, 5.31, 5.35, 5.36, 5.39, 5.40 and 5.41. The higher the groupiness, the worse the prediction. The reason for this could be the neglect of the nonlinear interactions between the short waves as well as between the short and long waves.

Overall, the model predictions are quite accurate, although the inclusion of the wave-wave interactions and a better model for the surf zone wave speed
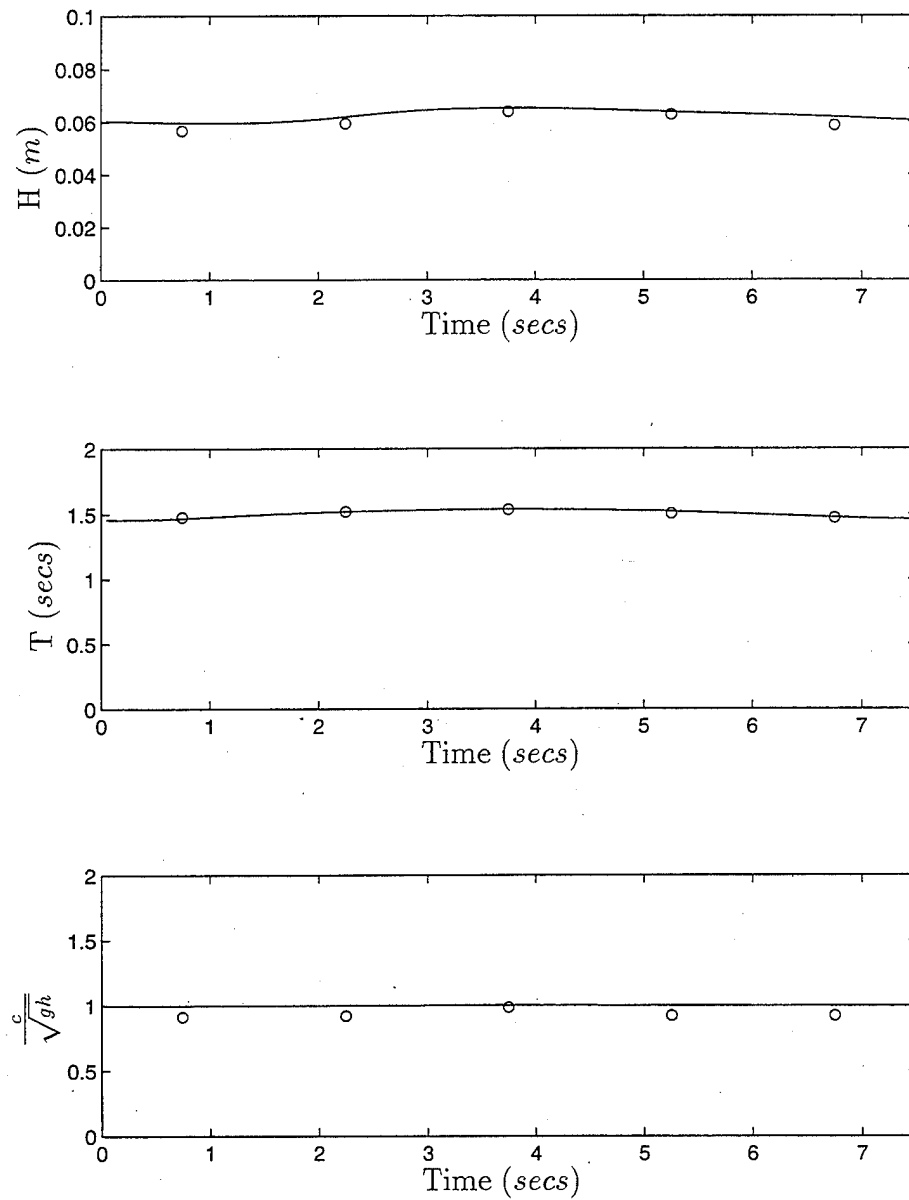
would improve the performance of the model.

Figure 5.17: Comparison between model prediction of wave group profile (————) and data (∘) for Experiment W01 at $x = 13.50\ m$ ($h = 0.3531\ m$). From the top, the figures are for wave height, wave period and normalized wave speed.
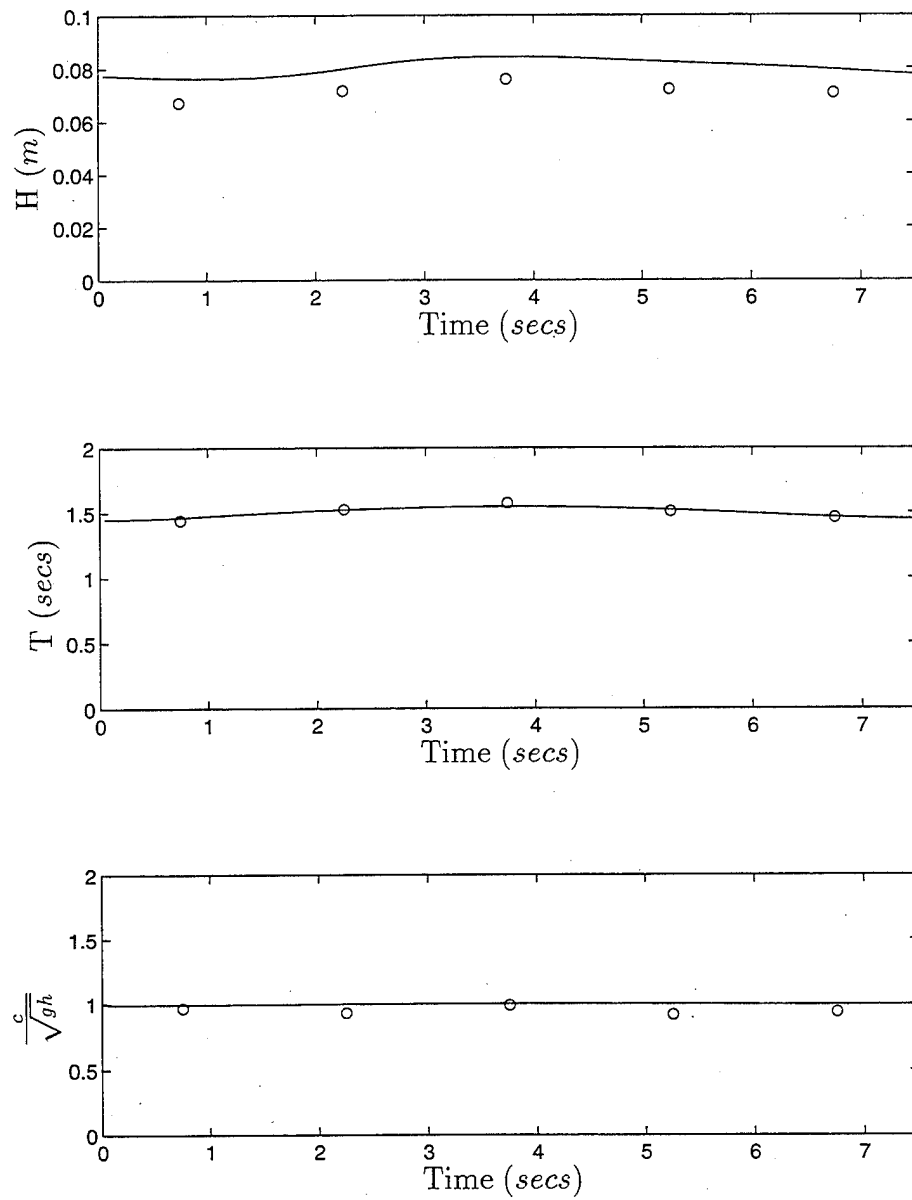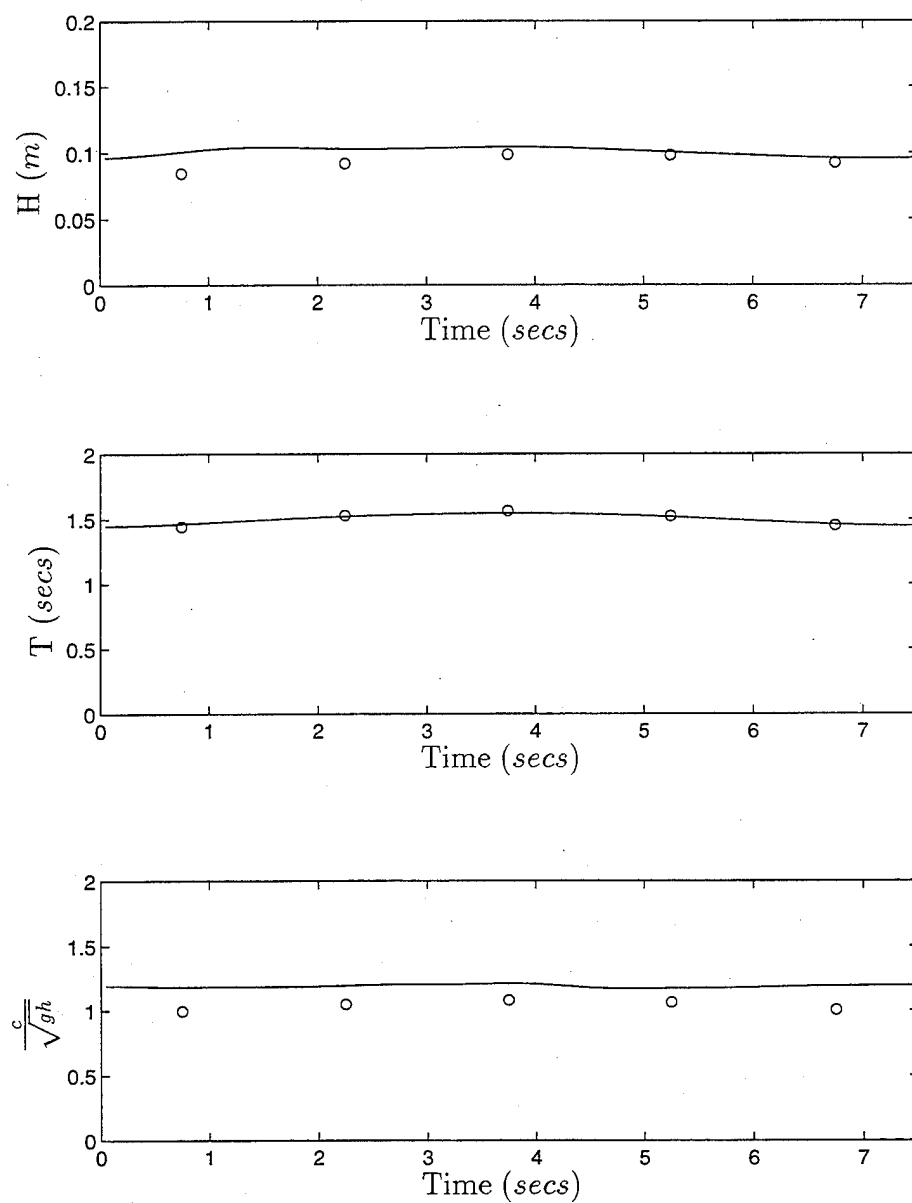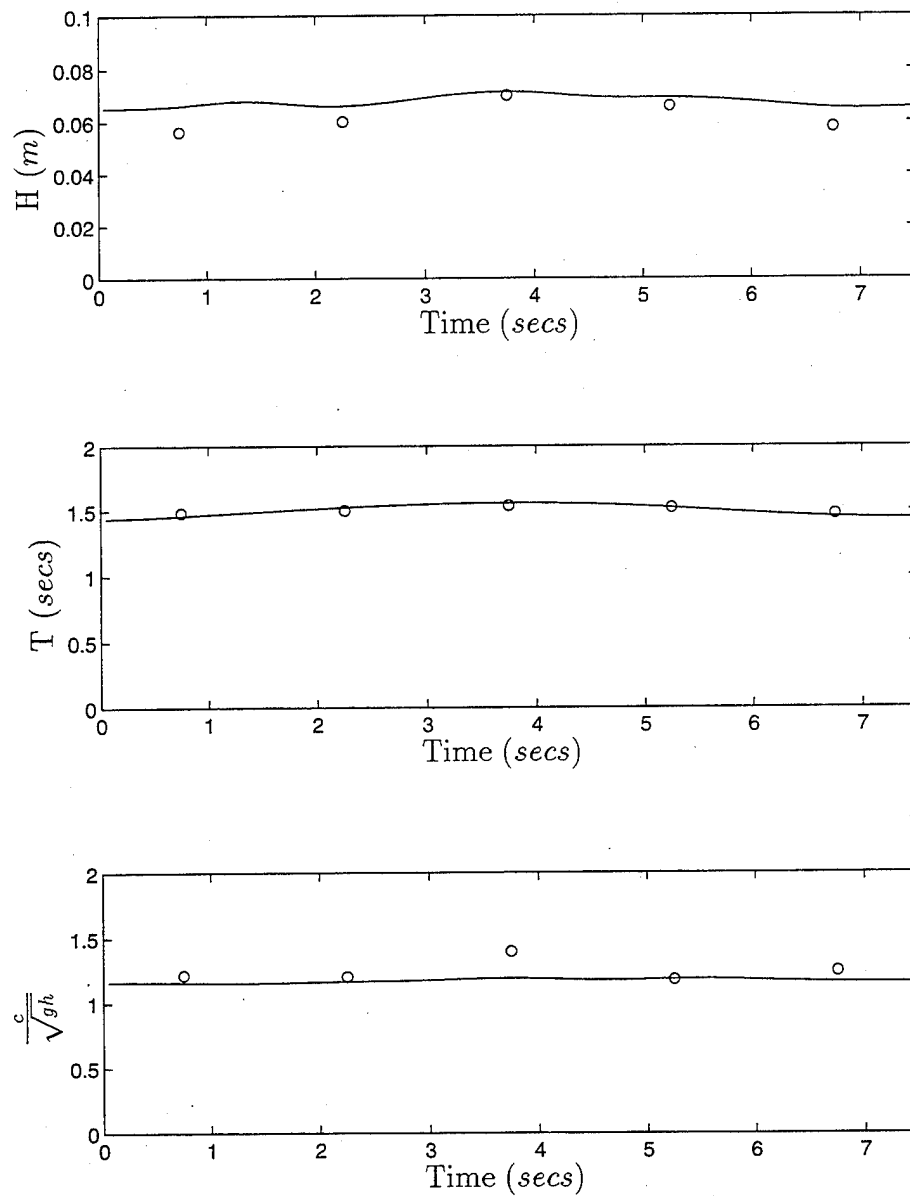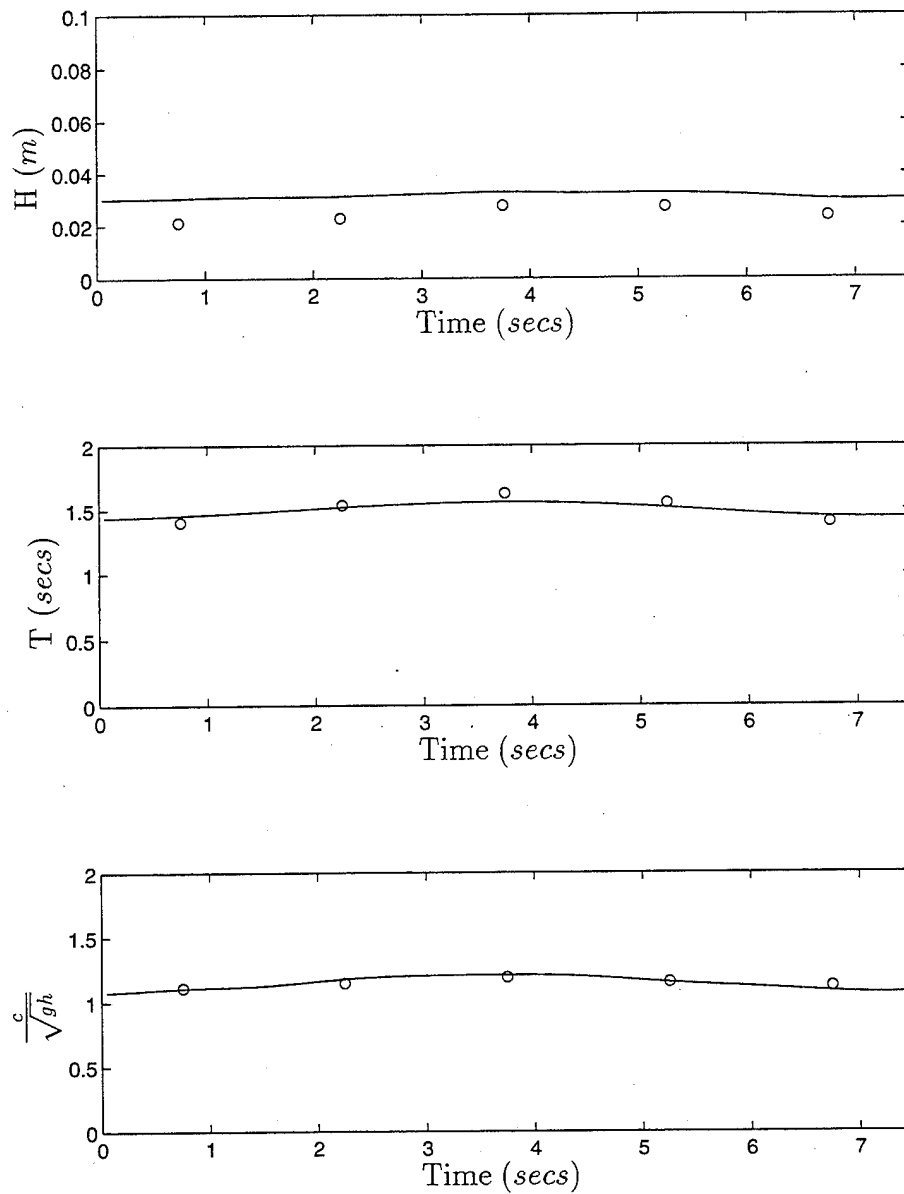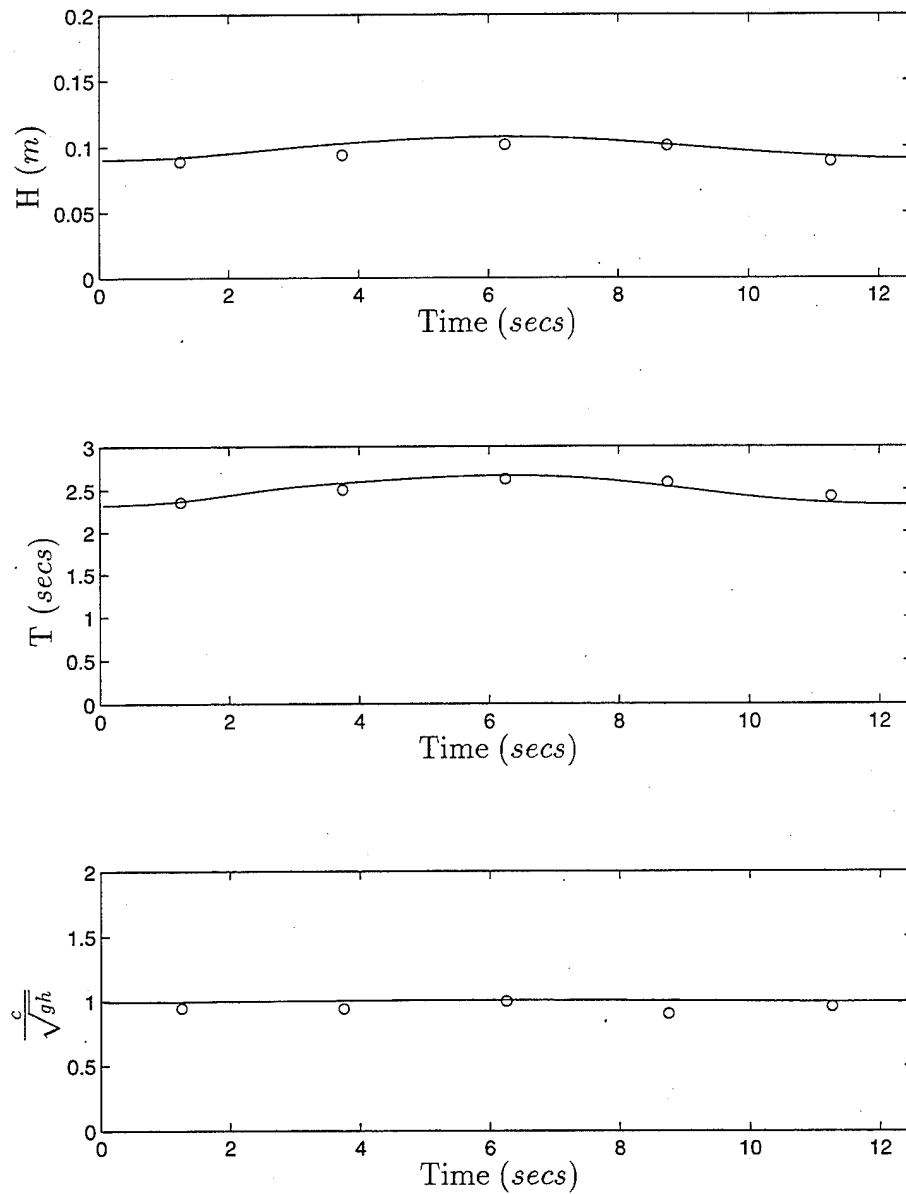
Figure 5.18: Comparison between model prediction of wave group profile (————) and data (o) for Experiment W01 at $x = 20.10$ m ($h = 0.1656$ m). From the top, the figures are for wave height, wave period and normalized wave speed.
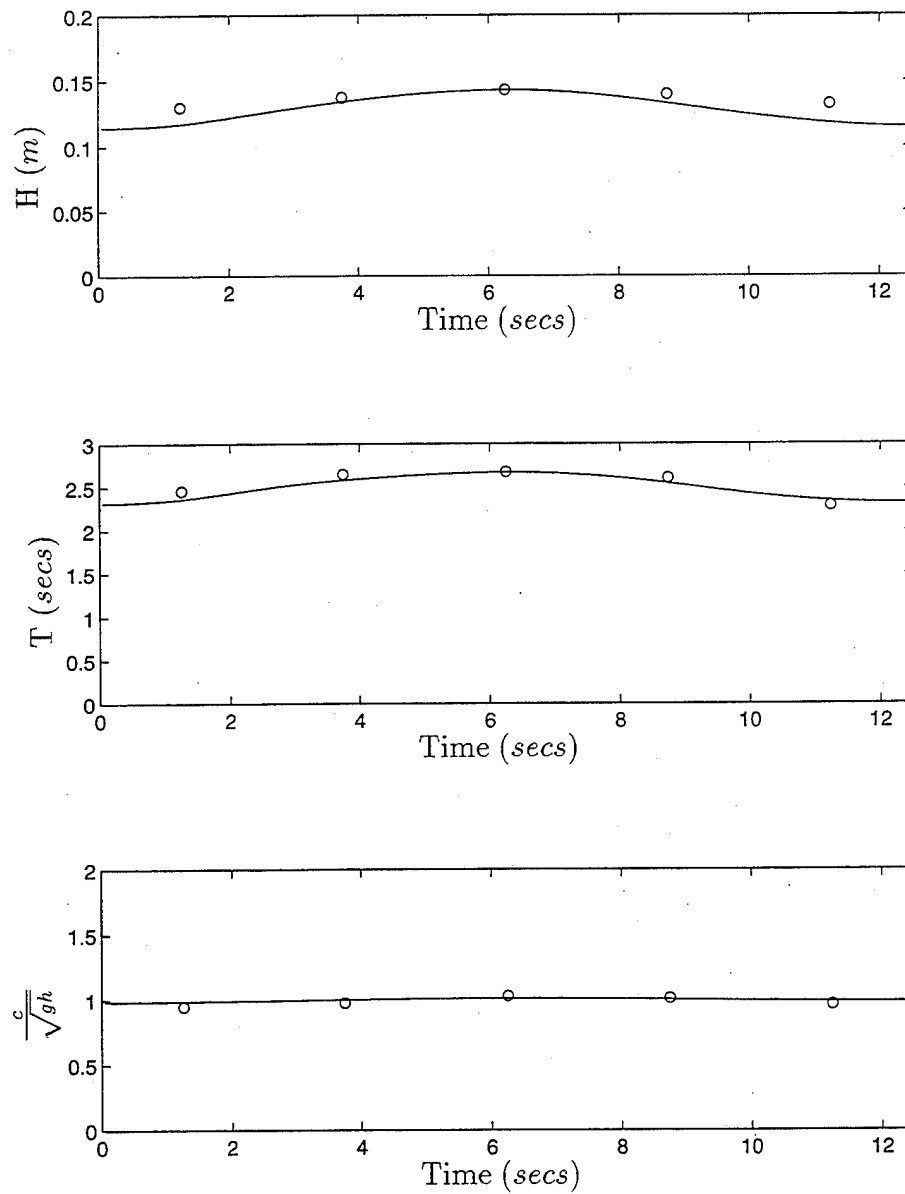
Figure 5.19: Comparison between model prediction of wave group profile (————) and data (○) for Experiment W01 at $x = 22.00$ m ($h = 0.1116$ m). From the top, the figures are for wave height, wave period and normalized wave speed.
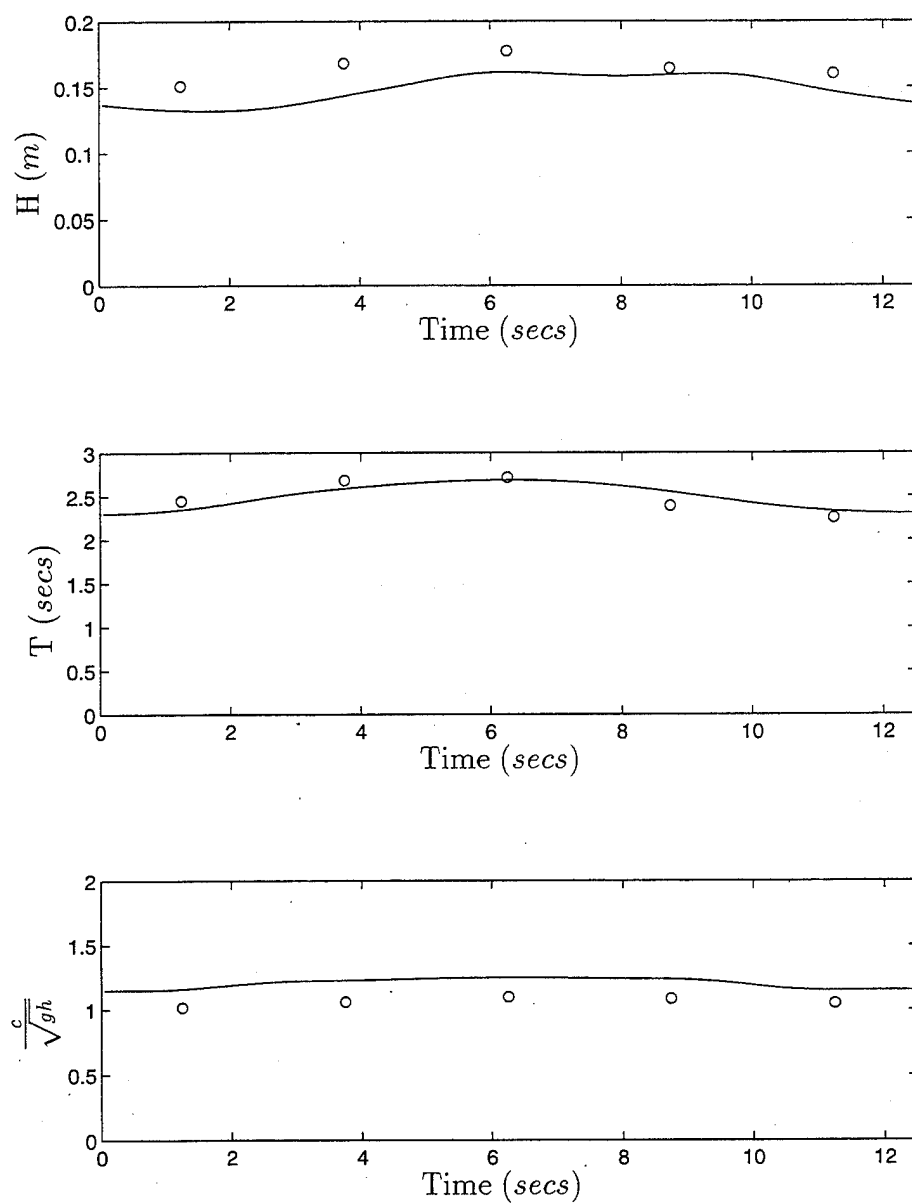
Figure 5.20: Comparison between model prediction of wave group profile (————) and data (○) for Experiment W01 at $x = 23.00$ m ($h = 0.0832$ m). From the top, the figures are for wave height, wave period and normalized wave speed.
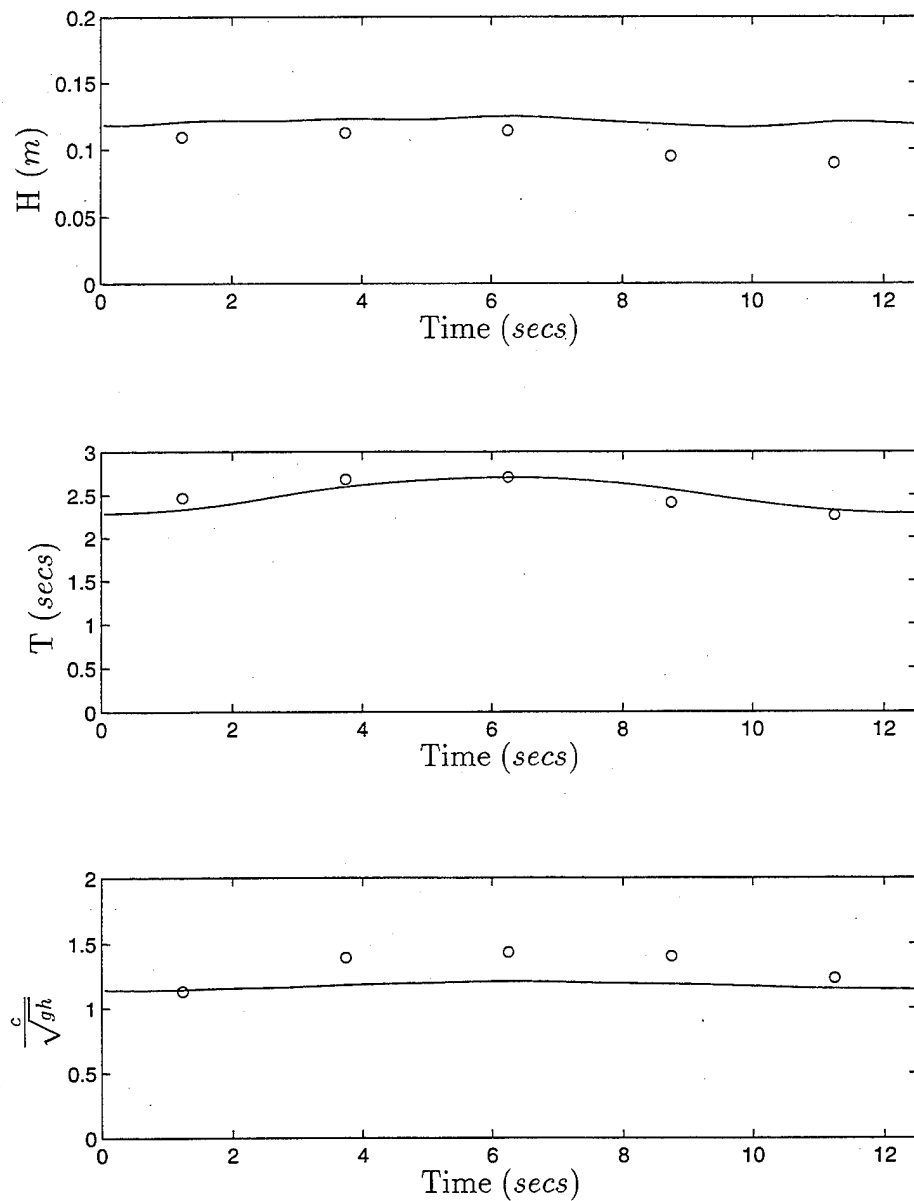
Figure 5.21: Comparison between model prediction of wave group profile (————) and data (o) for Experiment W01 at $x = 24.50\ m$ ($h = 0.0406\ m$). From the top, the figures are for wave height, wave period and normalized wave speed.

Figure 5.22: Comparison between model prediction of wave group profile (————) and data (○) for Experiment W02 at $x = 12.85\ m$ ($h = 0.3716\ m$). From the top, the figures are for wave height, wave period and normalized wave speed.
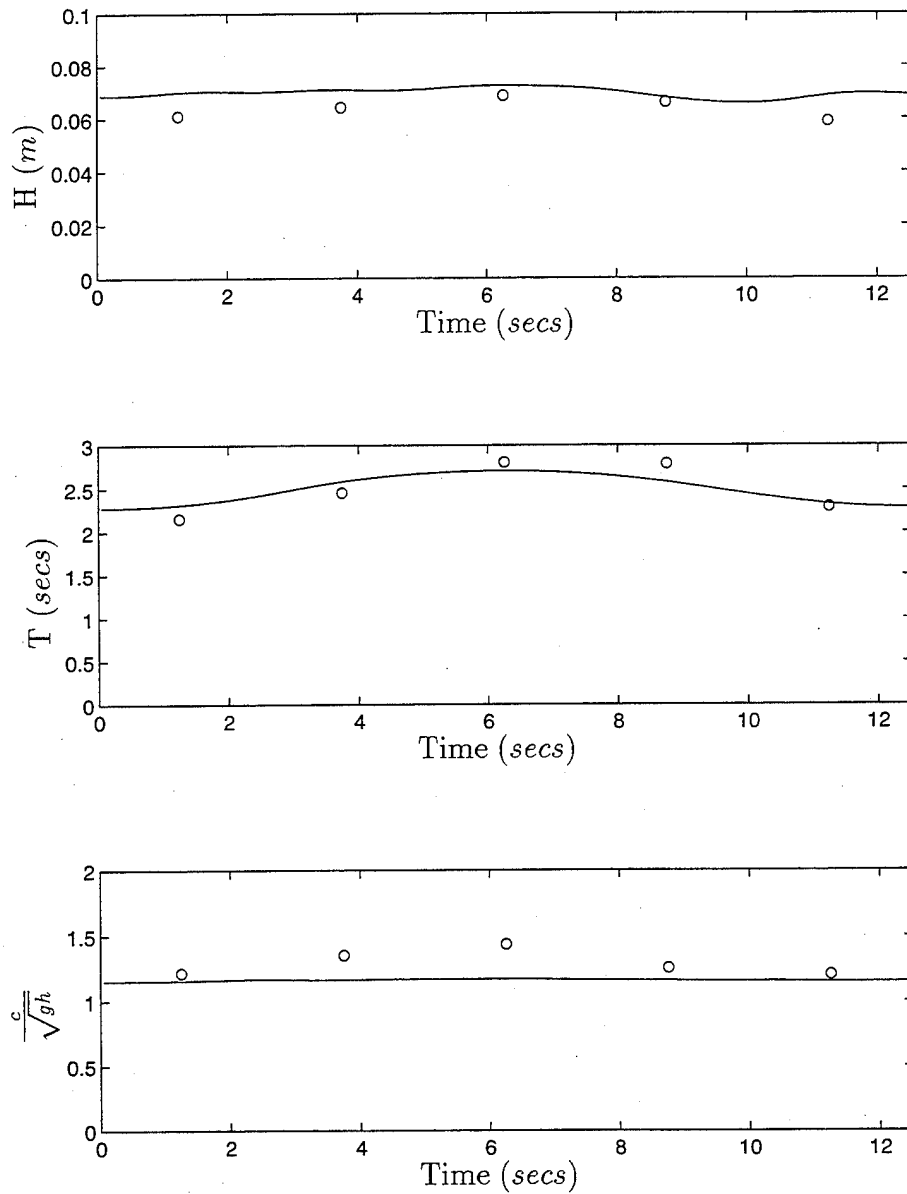
Figure 5.23: Comparison between model prediction of wave group profile (————) and data (○) for Experiment W02 at $x = 18.00\ m$ ($h = 0.2253\ m$). From the top, the figures are for wave height, wave period and normalized wave speed.
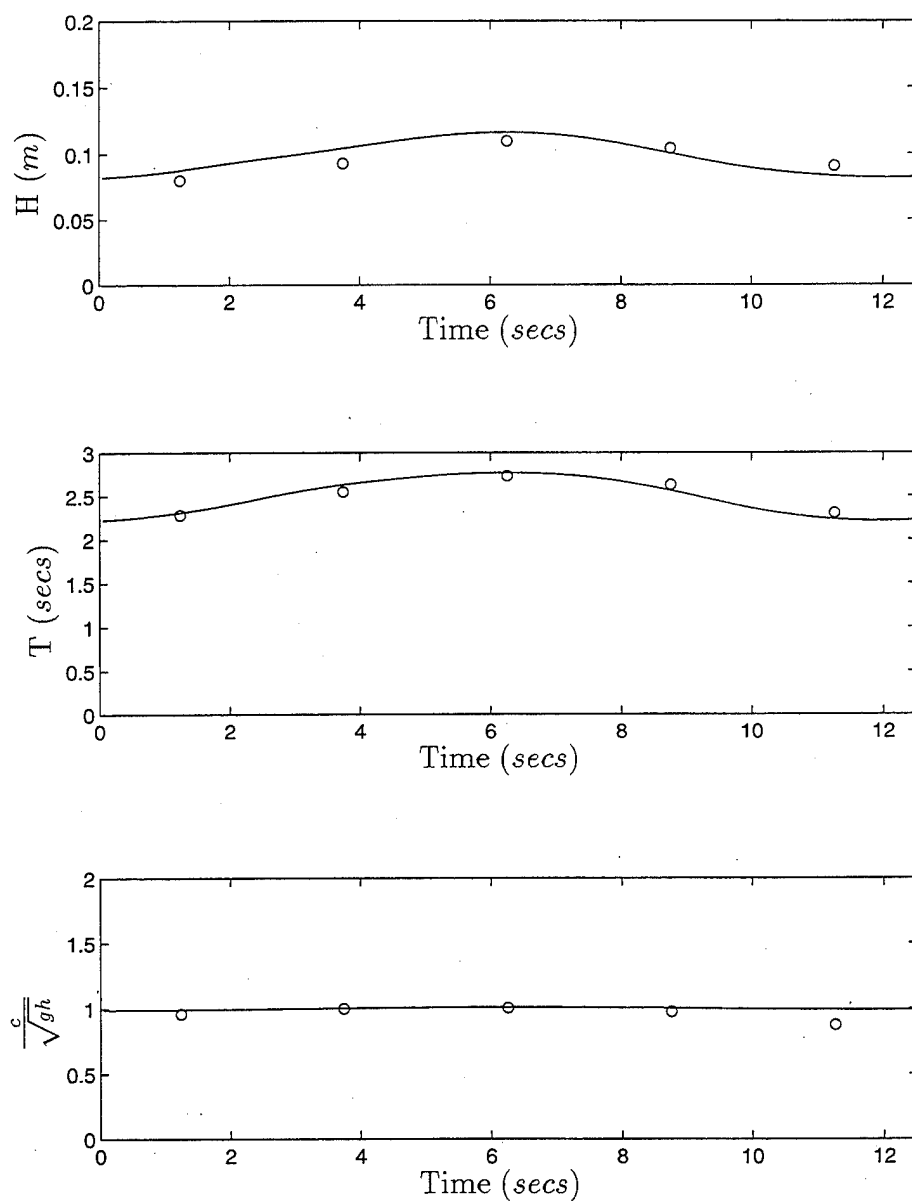
Figure 5.24: Comparison between model prediction of wave group profile (———) and data (○) for Experiment W02 at $x = 19.55\ m$ ($h = 0.1813\ m$). From the top, the figures are for wave height, wave period and normalized wave speed.

Figure 5.25: Comparison between model prediction of wave group profile (———) and data (○) for Experiment W02 at $x = 20.85\ m$ ($h = 0.1443\ m$). From the top, the figures are for wave height, wave period and normalized wave speed.
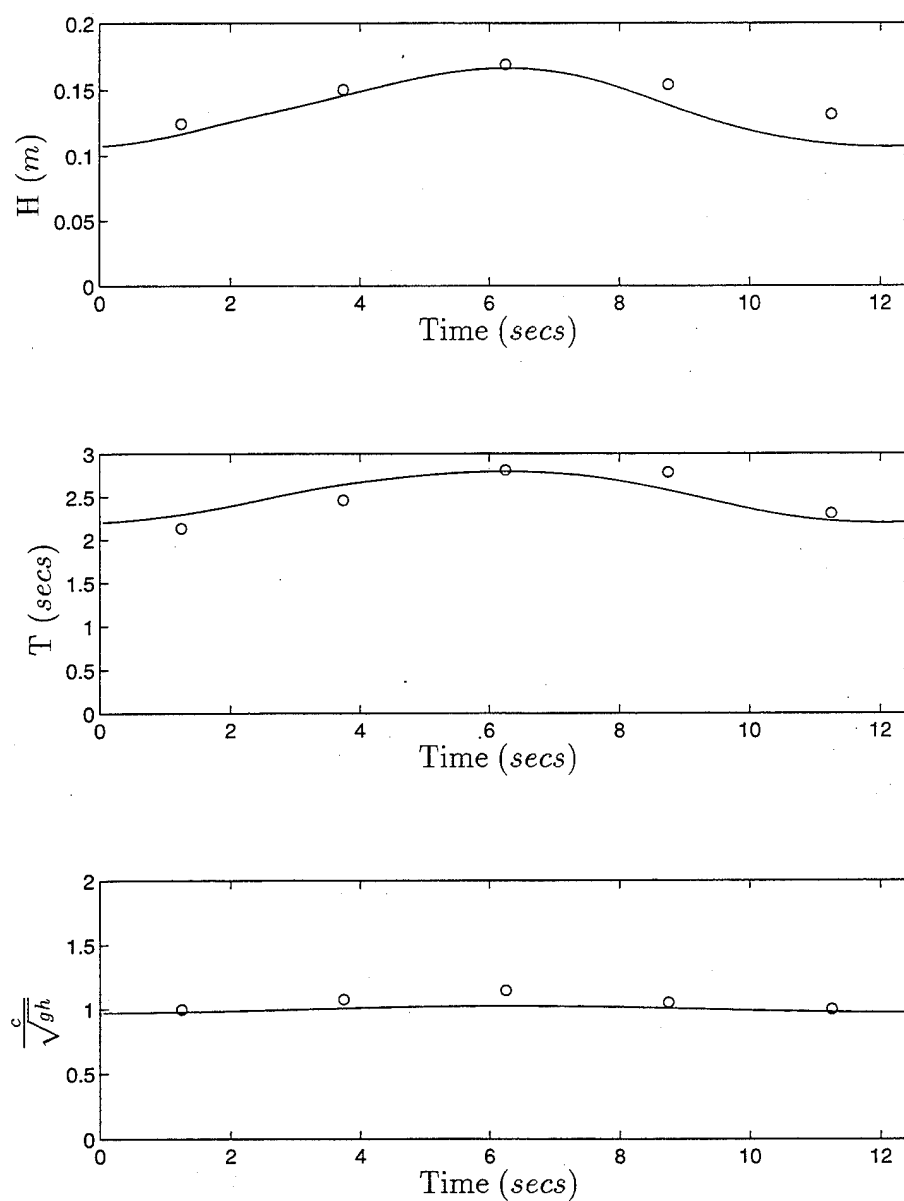
Figure 5.26: Comparison between model prediction of wave group profile (————) and data (○) for Experiment W02 at $x = 22.80$ m ($h = 0.0889$ m). From the top, the figures are for wave height, wave period and normalized wave speed.
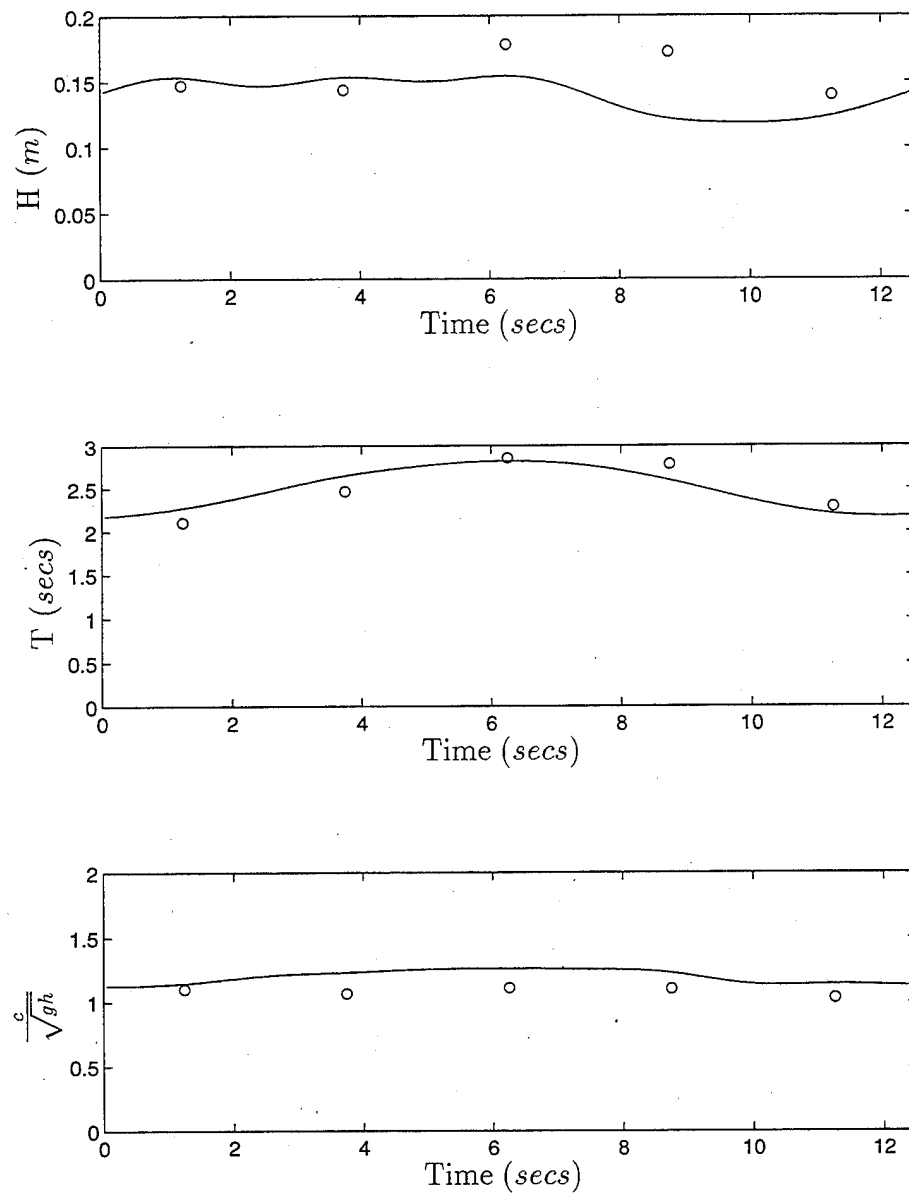
Figure 5.27: Comparison between model prediction of wave group profile (————) and data (○) for Experiment W03 at $x = 12.85\ m$ ($h = 0.3716\ m$). From the top, the figures are for wave height, wave period and normalized wave speed.
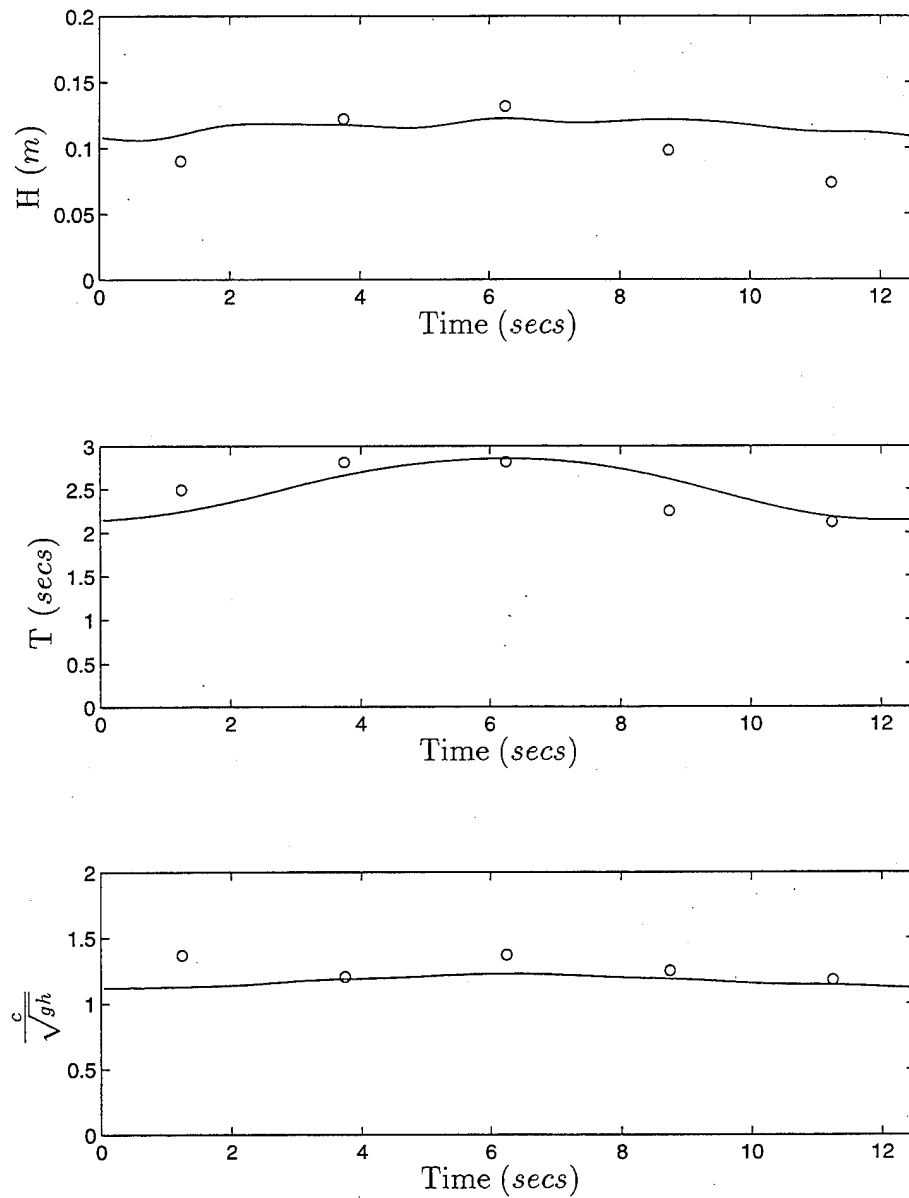
Figure 5.28: Comparison between model prediction of wave group profile
(———) and data (○) for Experiment W03 at $x = 18.60$ m
($h = 0.2082$ m). From the top, the figures are for wave height,
wave period and normalized wave speed.

Figure 5.29: Comparison between model prediction of wave group profile (————) and data (○) for Experiment W03 at $x = 19.60$ m ($h = 0.1798$ m). From the top, the figures are for wave height, wave period and normalized wave speed.
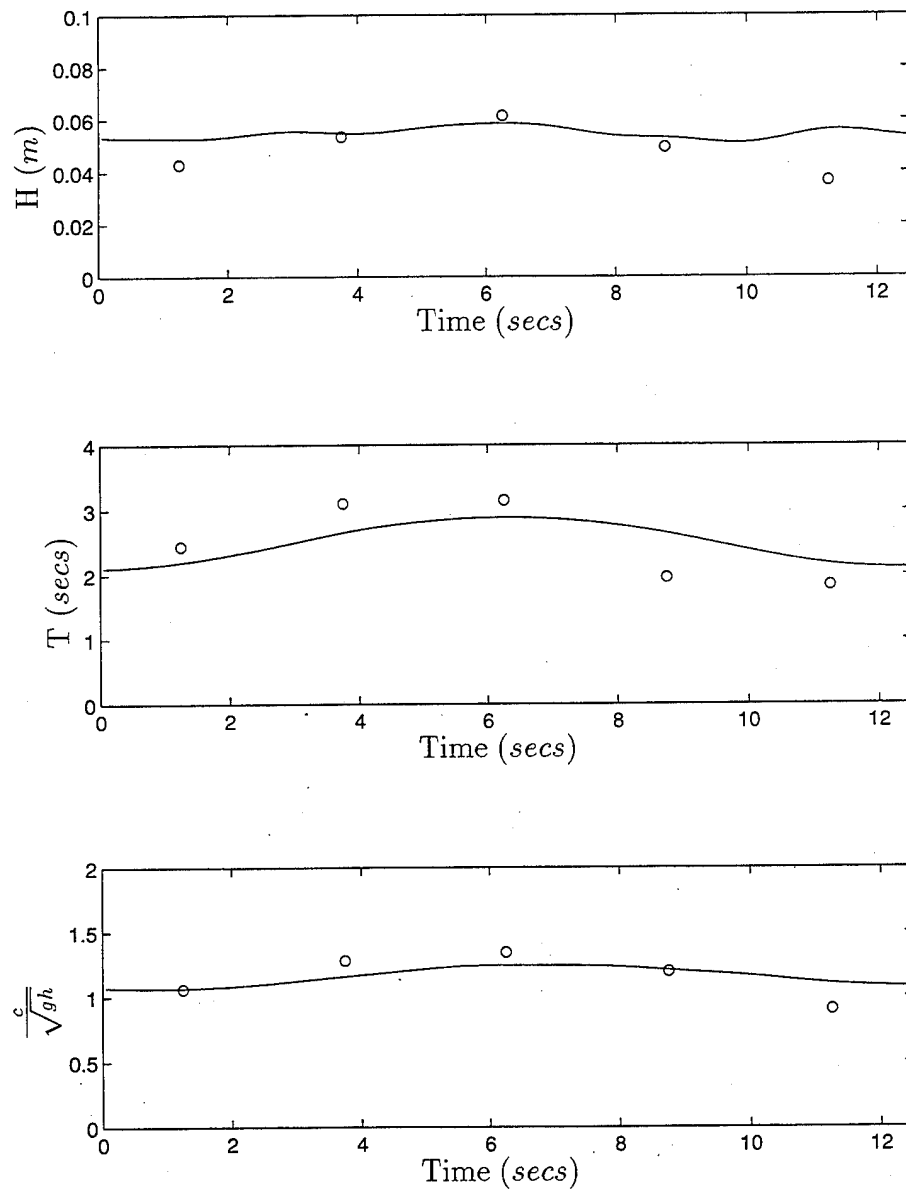
Figure 5.30: Comparison between model prediction of wave group profile (———) and data (○) for Experiment W03 at $x = 20.90 \ m$ ($h = 0.1429 \ m$). From the top, the figures are for wave height, wave period and normalized wave speed.

Figure 5.31: Comparison between model prediction of wave group profile (————) and data (o) for Experiment W03 at $x = 23.40\ m$ ($h = 0.0719\ m$). From the top, the figures are for wave height, wave period and normalized wave speed.
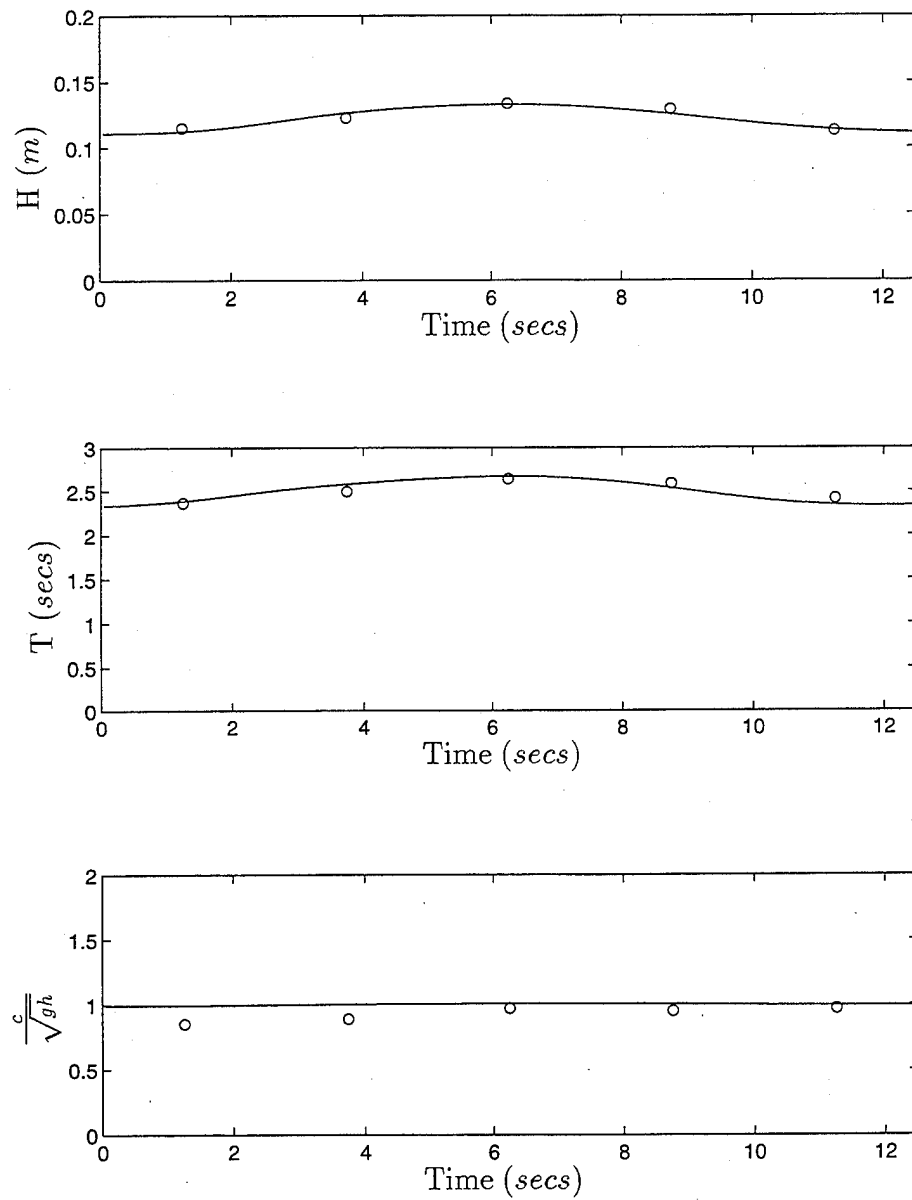
Figure 5.32: Comparison between model prediction of wave group profile (———) and data (o) for Experiment W04 at $x = 12.85\ m$ ($h = 0.3716\ m$). From the top, the figures are for wave height, wave period and normalized wave speed.
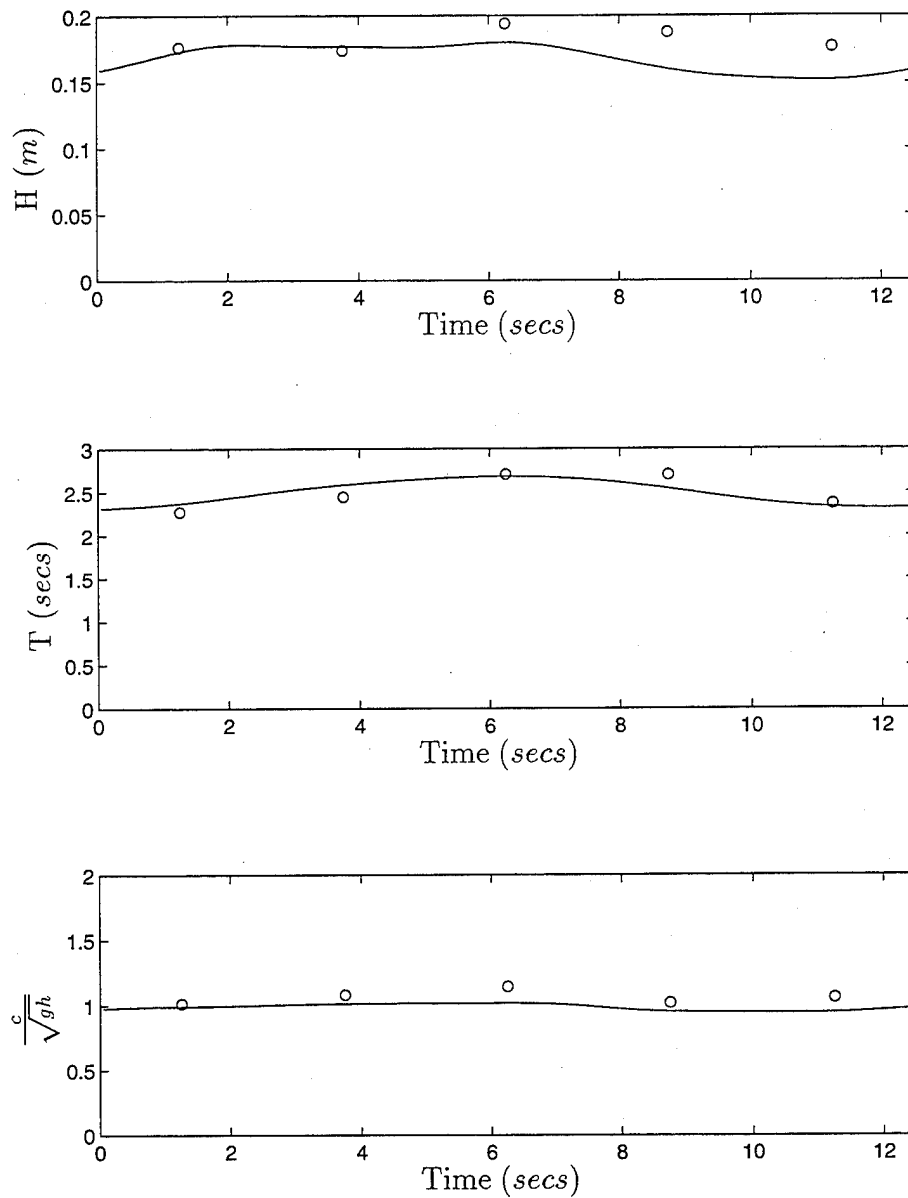
Figure 5.33: Comparison between model prediction of wave group profile
(———) and data (○) for Experiment W04 at $x = 18.60 \ m$
($h = 0.2082 \ m$). From the top, the figures are for wave height,
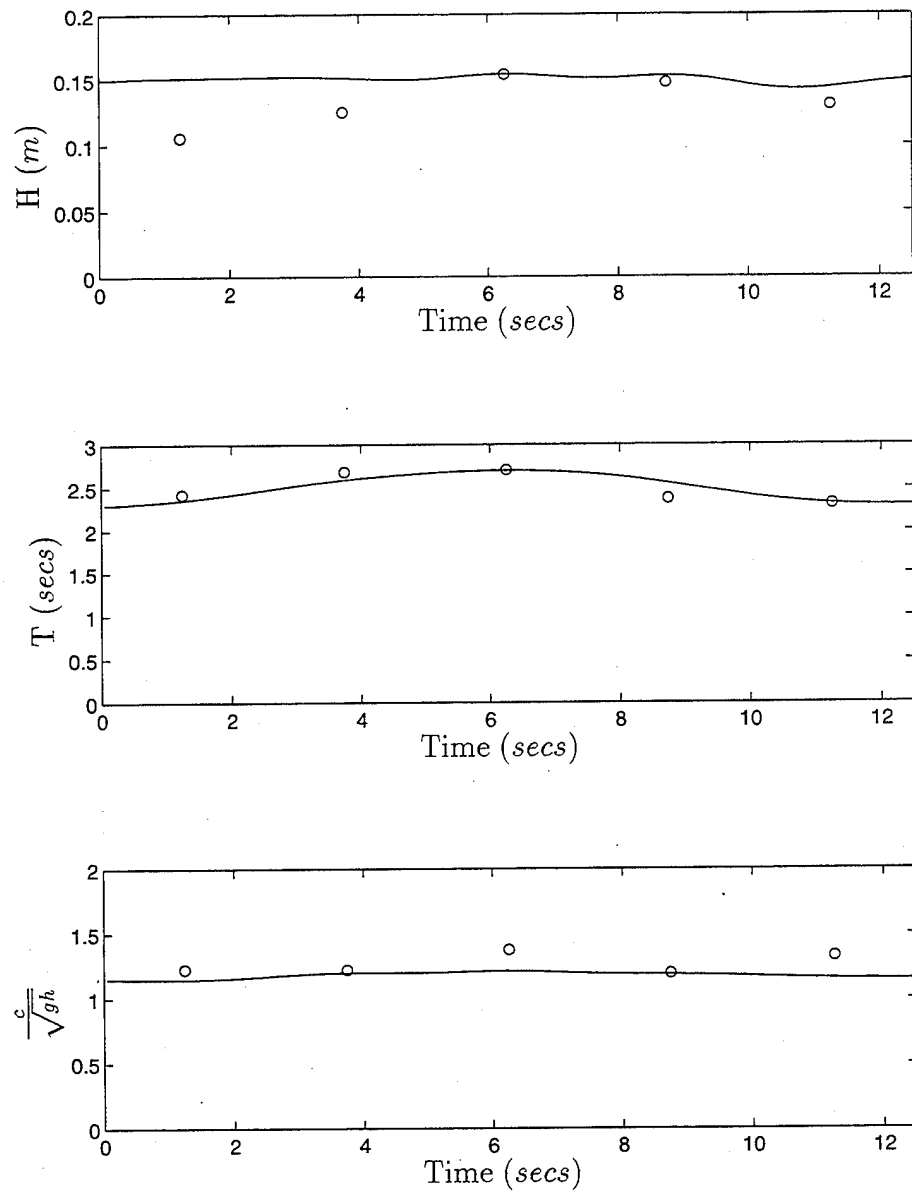wave period and normalized wave speed.

Figure 5.34: Comparison between model prediction of wave group profile (————) and data (○) for Experiment W04 at $x = 19.60$ m ($h = 0.1798$ m). From the top, the figures are for wave height, wave period and normalized wave speed.
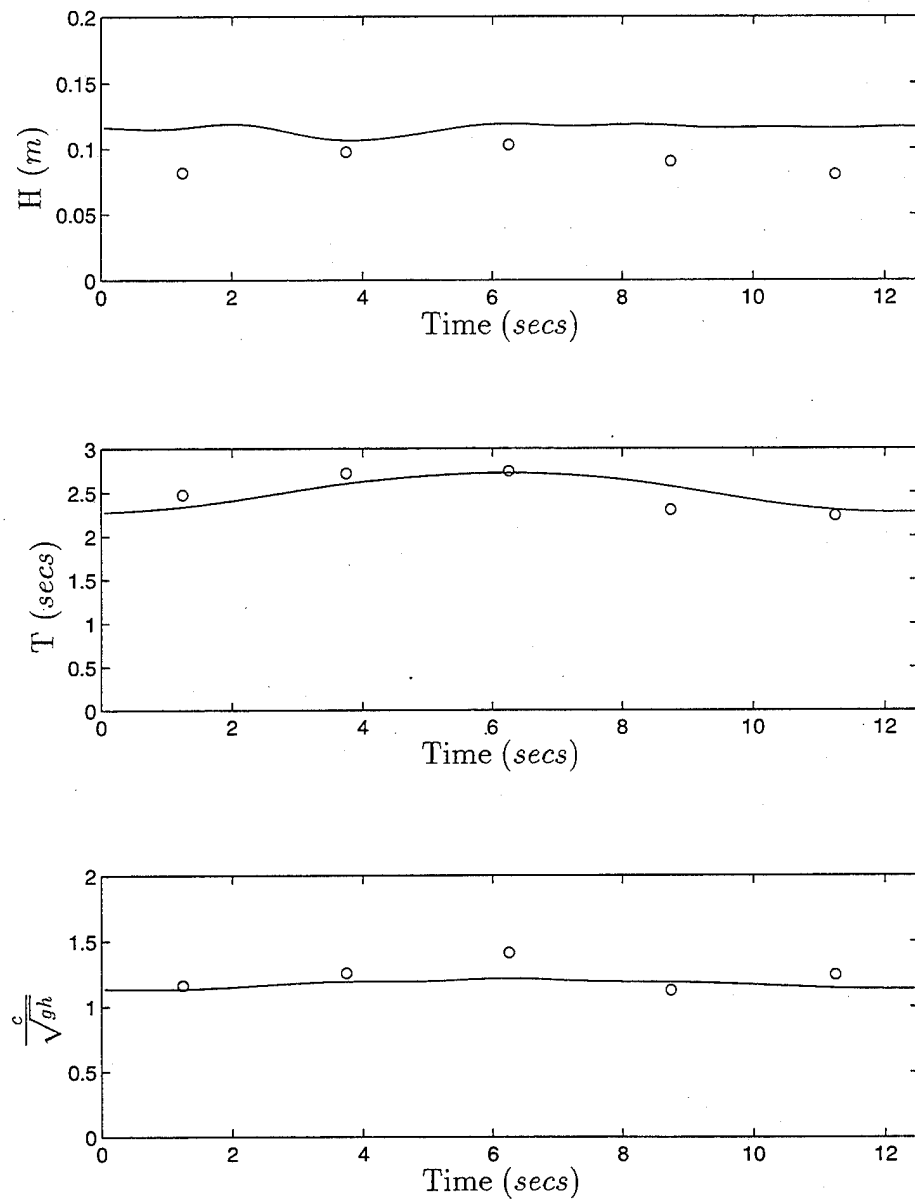
Figure 5.35: Comparison between model prediction of wave group profile
(——————) and data (∘) for Experiment W04 at $x = 20.90\ m$
($h = 0.1429\ m$). From the top, the figures are for wave height,
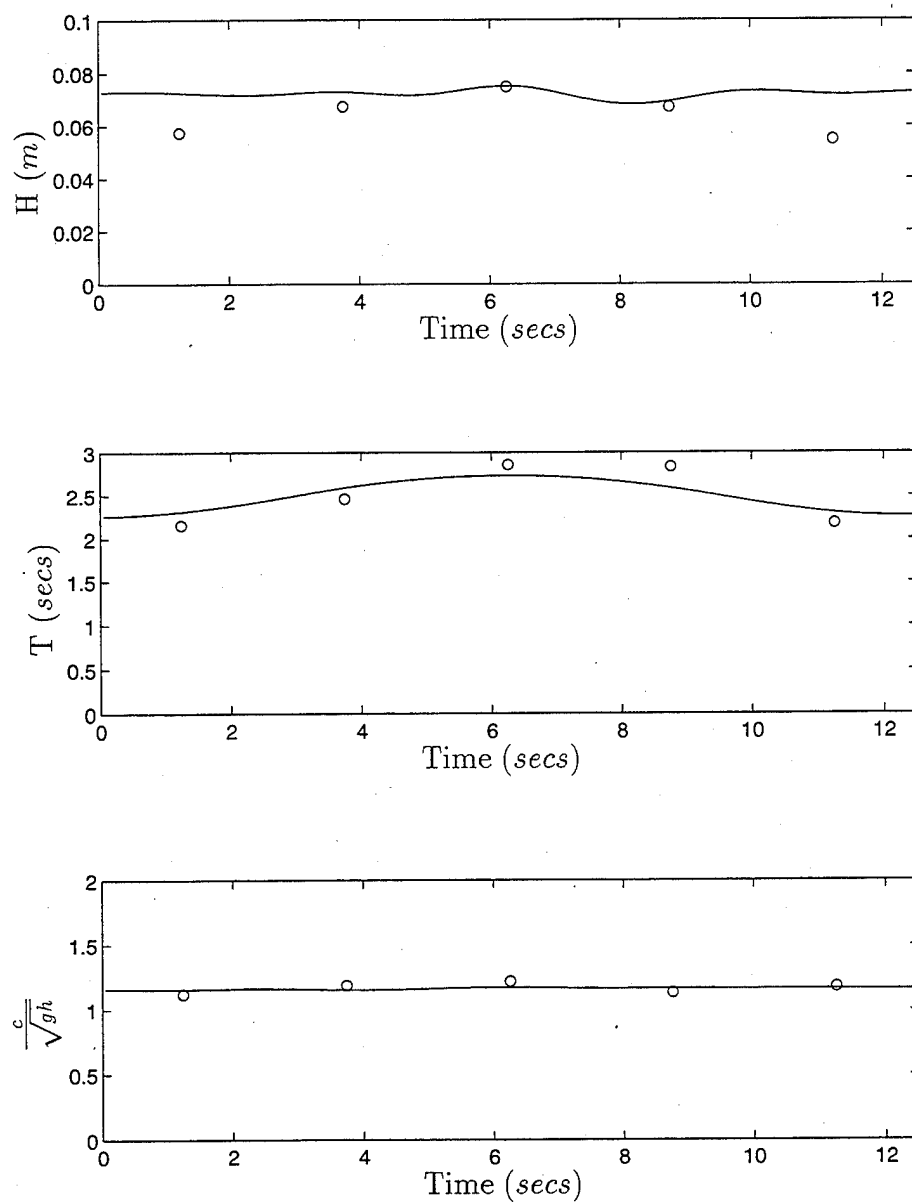wave period and normalized wave speed.

Figure 5.36: Comparison between model prediction of wave group profile
(————) and data (○) for Experiment W04 at $x = 22.70$ m
($h = 0.0918$ m). From the top, the figures are for wave height,
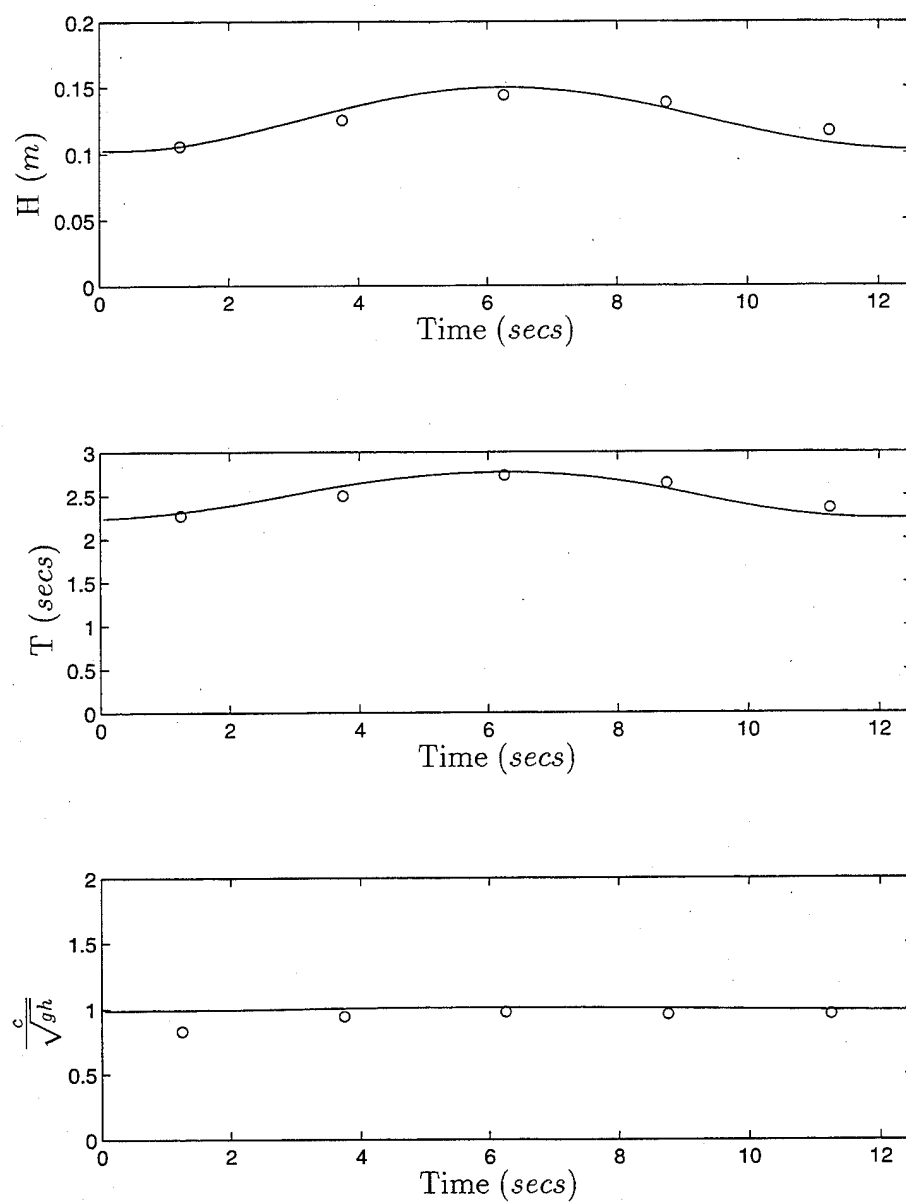wave period and normalized wave speed.

Figure 5.37: Comparison between model prediction of wave group profile (————) and data (○) for Experiment W05 at $x = 12.85$ m ($h = 0.3716$ m). From the top, the figures are for wave height, wave period and normalized wave speed.
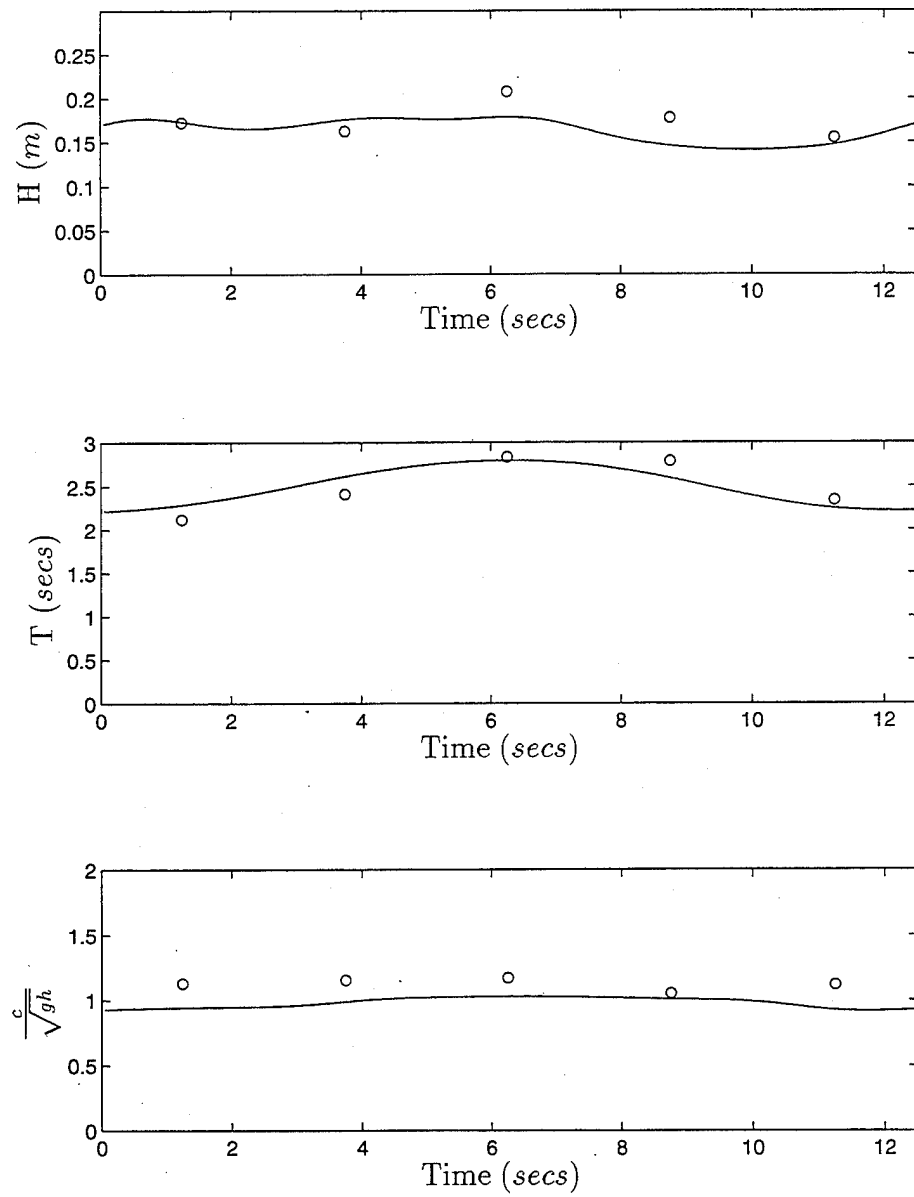
Figure 5.38: Comparison between model prediction of wave group profile (————) and data (○) for Experiment W05 at $x = 18.60\ m$ ($h = 0.2082\ m$). From the top, the figures are for wave height, wave period and normalized wave speed.
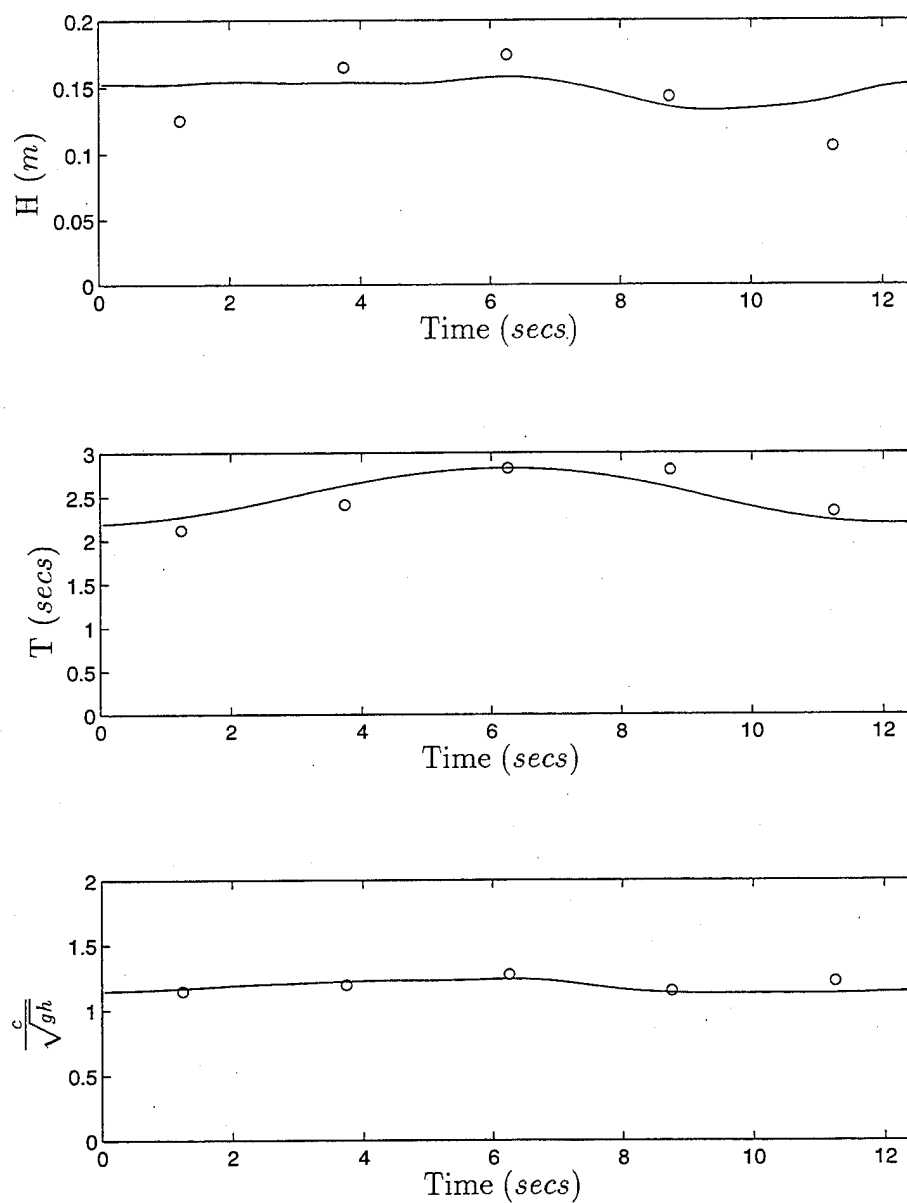
Figure 5.39: Comparison between model prediction of wave group profile
(———) and data (○) for Experiment W05 at $x = 19.60\ m$
($h = 0.1798\ m$). From the top, the figures are for wave height,
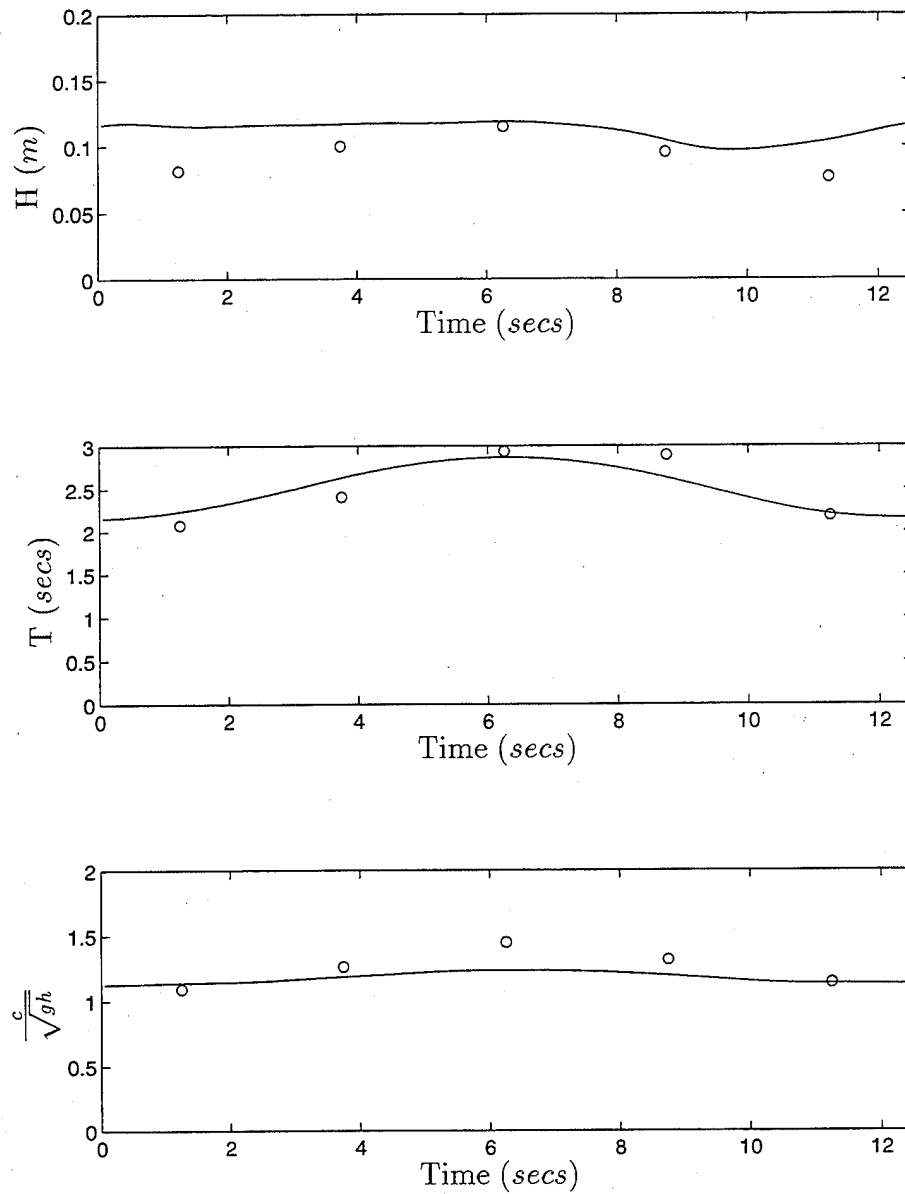wave period and normalized wave speed.

Figure 5.40: Comparison between model prediction of wave group profile (———) and data (○) for Experiment W05 at $x = 20.90\ m$ ($h = 0.1429\ m$). From the top, the figures are for wave height, wave period and normalized wave speed
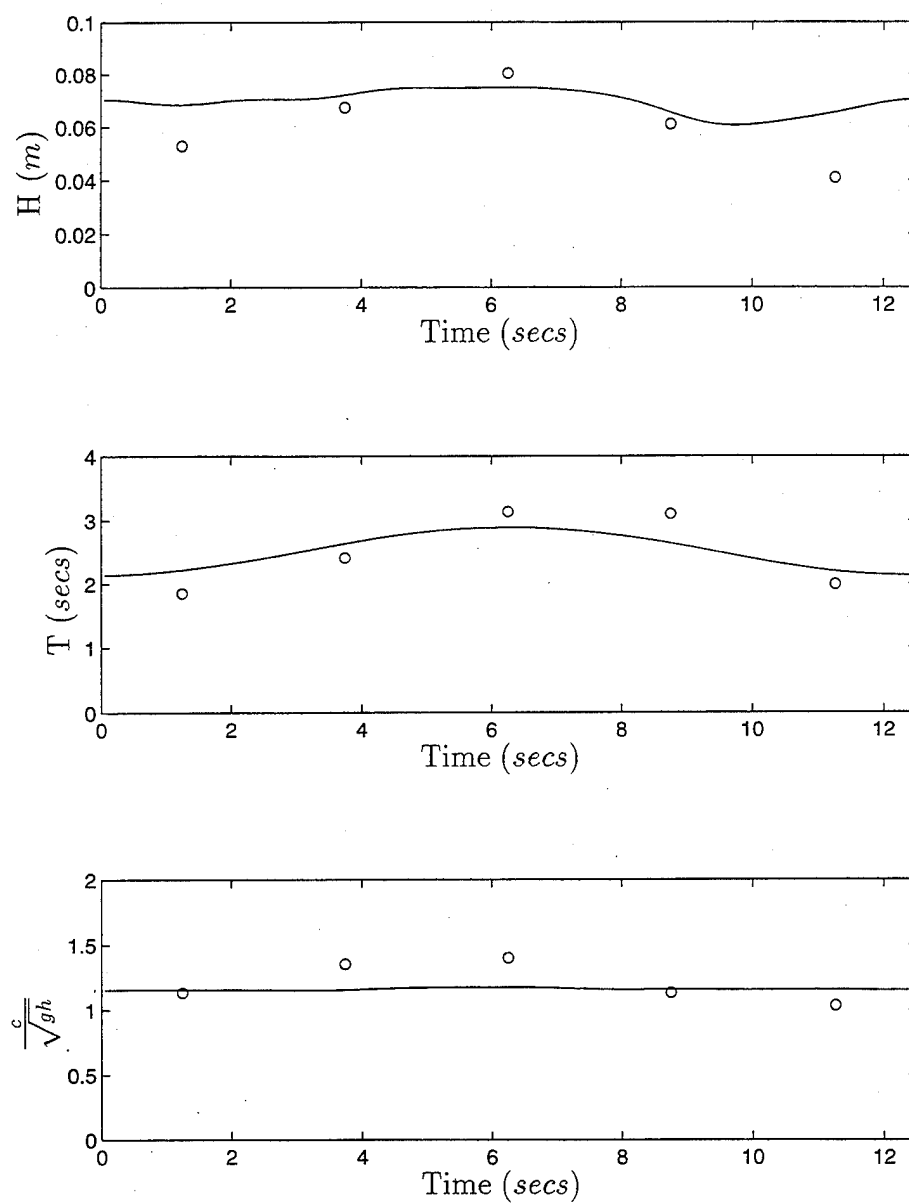
Figure 5.41: Comparison between model prediction of wave group profile (————) and data (○) for Experiment W05 at $x = 22.70\ m$ ($h = 0.0918\ m$). From the top, the figures are for wave height, wave period and normalized wave speed.

Chapter 6

CONCLUSIONS AND RECOMMENDATIONS

Wave groupiness is known to be one of the main mechanisms for the generation of long waves in the nearshore region. Improving the understanding of the propagation of wave groups helps improve the prediction of the long waves in the nearshore region.

A model, based on the wave conservation laws, to predict the time and space dependent behavior of the wave averaged quantities, c, ω and H, was developed. The non-linear effects of the wave near breaking are included in the dispersion relation. Experiments were conducted in the Precision Wave Tank at the Coastal Engineering Laboratory at the University of Delaware to provide the data to test the model. Wave groups formed by combining cnoidal waves of different wave heights were generated to study the time variation of the wave averaged quantities. The model was then compared to the data from these experiments.

The breaking of the waves in a group is found to be affected by the group structure, with the wave incident immediately after the largest wave breaking at a much higher depth. The ratio of breaker height to breaker depth is also found to be much higher for the waves in a group. As expected, the wave break point was found to vary with the wave height.

The wave groups for the experiments were created in a heuristic fashion by combining cnoidal waves of different heights and therefore are not of permanent form. The sieching periods of the tank were also found to be close to the group periods used in the experiments which resulted in energy transfer to the seiching mode of the tank. Although the seiching modes did not have the exact same frequency of the group, it is indistinguisable from the group frequency due to the limited time of data acquisition. From the experiments, it was found that considerable amount of groupiness is transferred into the surf zone, although inside the breaking region, the groupiness was less than that oberved in the shoaling region and much less than that oberved at the reference gage.

The model was tested against the individual waves in a group. It was found that the wave height prediction is good whereas the prediction of the wave speed inside the surf zone and that of the wave period for higher groupiness can be improved. Such an improvement would be achieved by the inclusion of wave-wave interactions as well as a better model for the surf zone wave speed.

Appendix A

GAGE LOCATIONS FOR THE EXPERIMENTS

The gage locations for the different runs of each experiment are tabulated here. The values along the rows are the distances of each gage, in meters, from the mean position of the wave maker.

Gage	Run number					
number	R01	R02	R03	R04	R05	R06
1	4.60	4.60	4.60	4.60	4.60	4.60
2	11.85	19.40	21.70	21.60	21.50	21.40
3	13.50	19.80	22.10	22.00	21.90	21.80
4	14.60	20.10	22.40	22.30	22.20	22.10
5	15.60	20.50	22.80	22.70	22.60	22.50
6	16.80	20.80	23.10	23.00	22.90	22.80
7	17.40	21.20	23.50	23.40	23.30	23.20
8	17.90	21.50	23.80	23.70	23.60	23.50
9	18.50	21.90	24.20	24.10	24.00	23.90
10	19.20	22.20	24.50	24.40	24.30	24.20

Table A.1: Gage distance from wavemaker (in meters) for case W01

Gage number	Run number						
	R01	R02	R03	R04	R05	R06	R07
1	4.60	4.60	4.60	4.60	4.60	4.60	4.60
2	11.85	18.00	18.10	18.20	18.05	18.15	21.10
3	12.85	18.30	18.40	18.50	18.35	18.45	21.40
4	13.75	18.70	18.80	18.90	18.75	18.85	21.80
5	14.75	19.00	19.10	19.20	19.05	19.15	22.10
6	15.65	19.40	19.50	19.60	19.45	19.55	22.50
7	16.50	19.70	19.80	19.90	19.75	19.85	22.80
8	17.20	20.10	20.20	20.30	20.15	20.25	23.20
9	18.00	20.40	20.50	20.60	20.45	20.55	23.50
10	18.65	20.80	20.90	21.00	20.85	20.95	23.90

Table A.2: Gage distance from wavemaker (in meters) for case W02

Gage number	Run number								
	R01	R02	R03	R04	R05	R06	R07	R08	R09
1	4.60	4.60	4.60	4.60	4.60	4.60	4.60	4.60	4.60
2	11.85	18.00	18.05	18.10	18.15	18.20	18.35	18.25	18.30
3	12.85	18.30	18.35	18.40	18.45	18.50	18.65	18.55	18.60
4	13.75	18.70	18.75	18.80	18.85	18.90	19.05	18.95	19.00
5	14.75	19.00	19.05	19.10	19.15	19.20	19.35	19.25	19.30
6	15.65	19.40	19.45	19.50	19.55	19.60	19.75	19.65	19.70
7	16.50	19.70	19.75	19.80	19.85	19.90	20.05	19.95	20.00
8	17.20	20.10	20.15	20.20	20.25	20.30	20.45	20.35	20.40
9	18.00	20.40	20.45	20.50	20.55	20.60	20.75	20.65	20.70
10	18.65	20.80	20.85	20.90	20.95	21.00	21.15	21.05	21.10

Table A.3: Gage distance from wavemaker (in meters) for case W03

Gage	Run number								
number	R01	R02	R03	R04	R05	R06	R07	R08	R09
1	4.60	4.60	4.60	4.60	4.60	4.60	4.60	4.60	4.60
2	11.85	18.00	18.05	18.10	18.15	18.20	18.25	18.30	18.35
3	12.85	18.30	18.35	18.40	18.45	18.50	18.55	18.60	18.65
4	13.75	18.70	18.75	18.80	18.85	18.90	18.95	19.00	19.05
5	14.75	19.00	19.05	19.10	19.15	19.20	19.25	19.30	19.35
6	15.65	19.40	19.45	19.50	19.55	19.60	19.65	19.70	19.75
7	16.50	19.70	19.75	19.80	19.85	19.90	19.95	20.00	20.05
8	17.20	20.10	20.15	20.20	20.25	20.30	20.35	20.40	20.45
9	18.00	20.40	20.45	20.50	20.55	20.60	20.65	20.70	20.75
10	18.65	20.80	20.85	20.90	20.95	21.00	21.05	21.10	21.15

Table A.4: Gage distance from wavemaker (in meters) for cases W04 and W05

Appendix B

THE VARIATION OF WAVE HEIGHT, FREQUENCY AND PHASE SPEED OF THE INDIVIDUAL WAVES IN A GROUP.
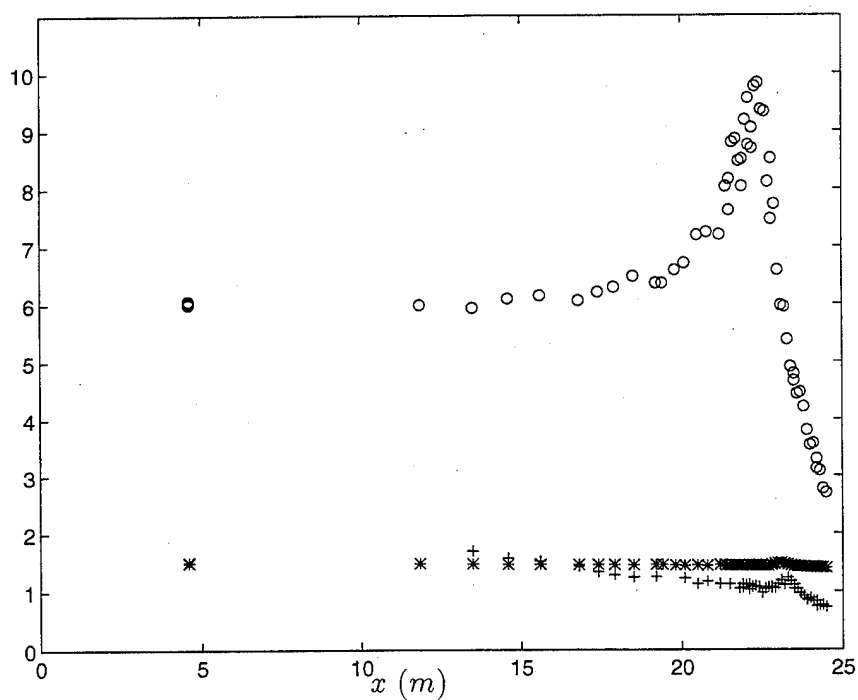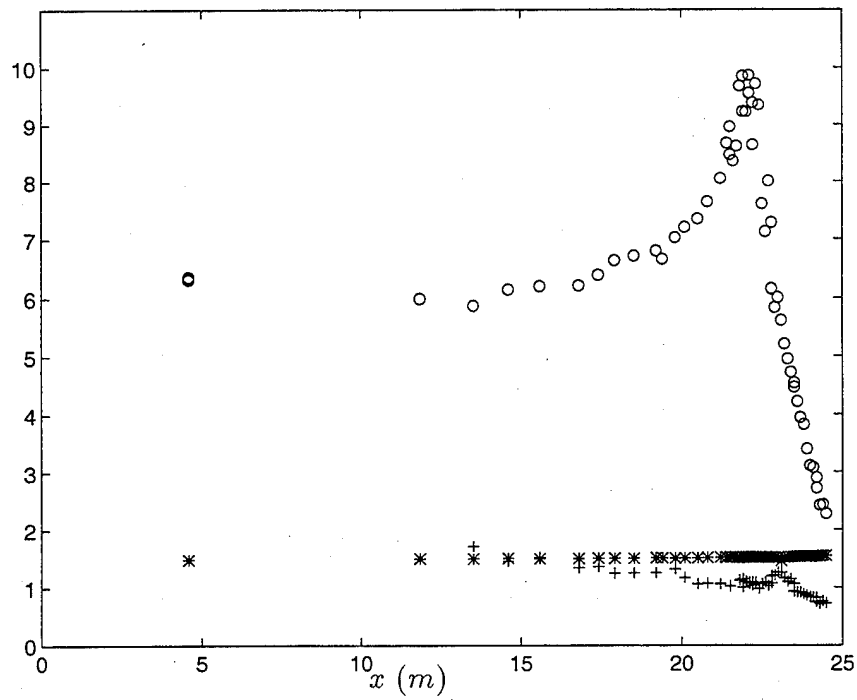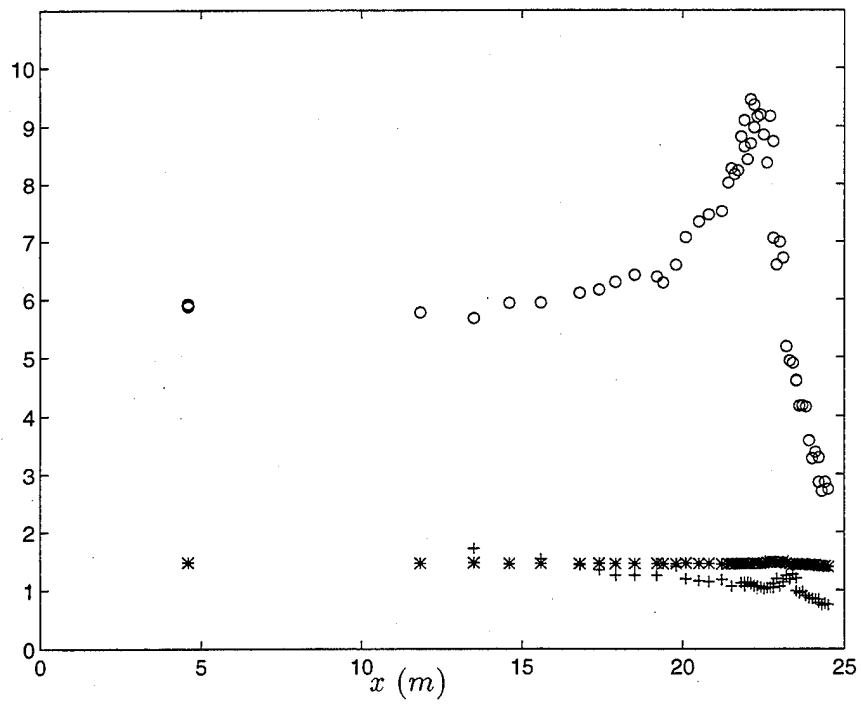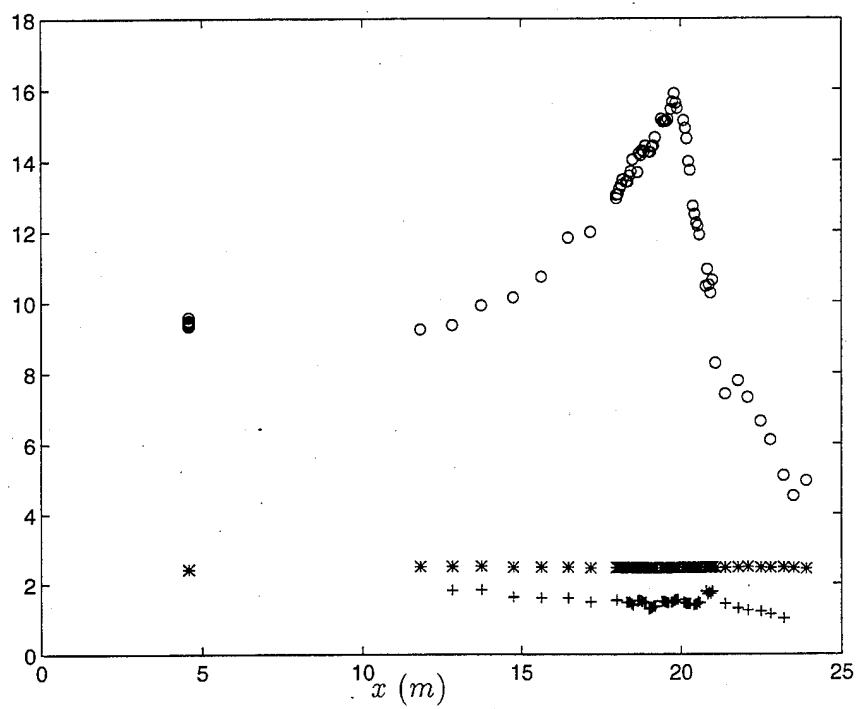

Figure B.1: Variation of wave height ('o'), wave period ('*') and phase speed ('+') for the first wave in Experiment W01
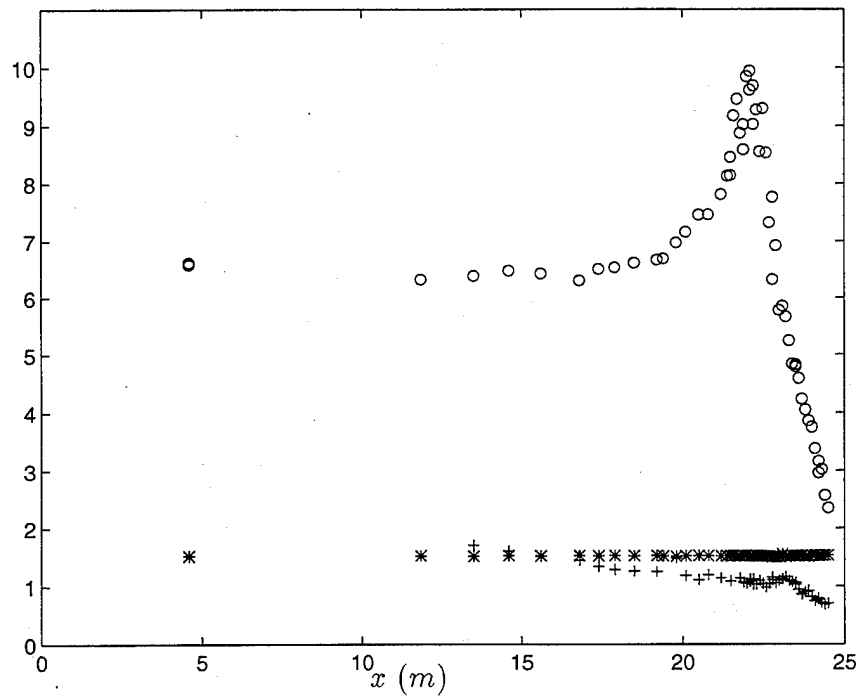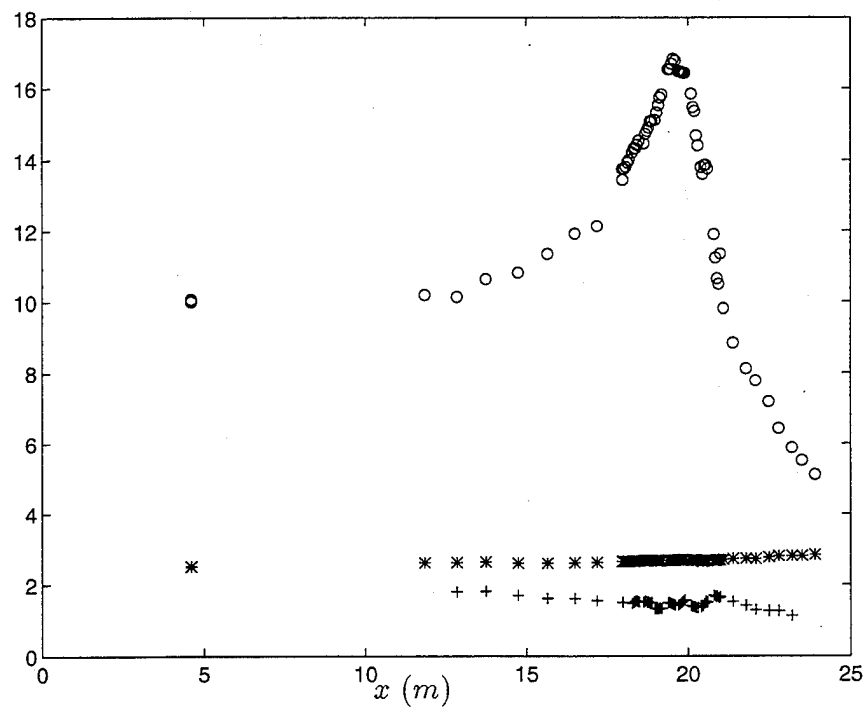
Figure B.2: Variation of wave height ('o'), wave period ('*') and phase speed ('+') for the second wave in Experiment W01
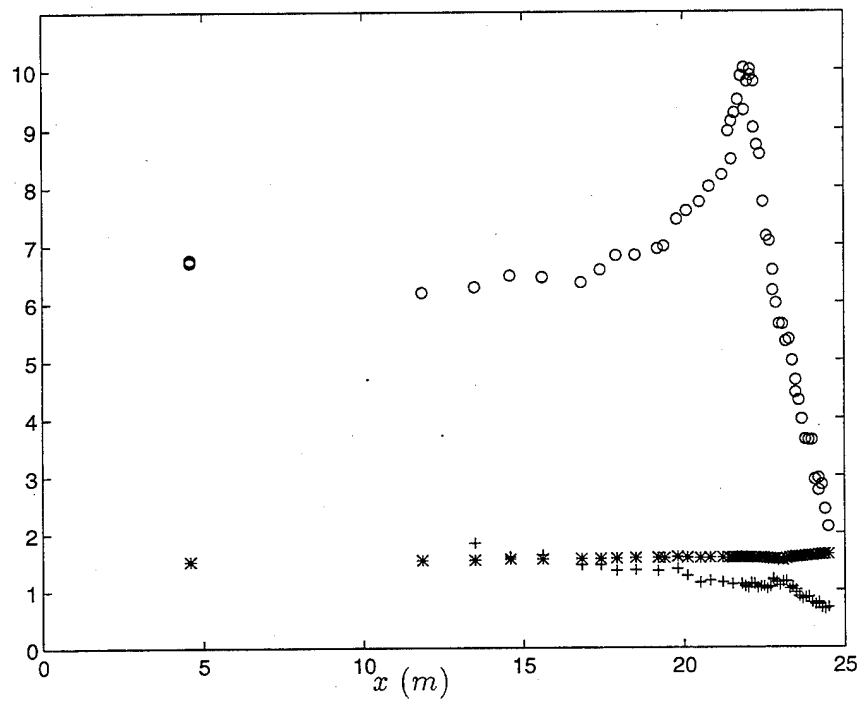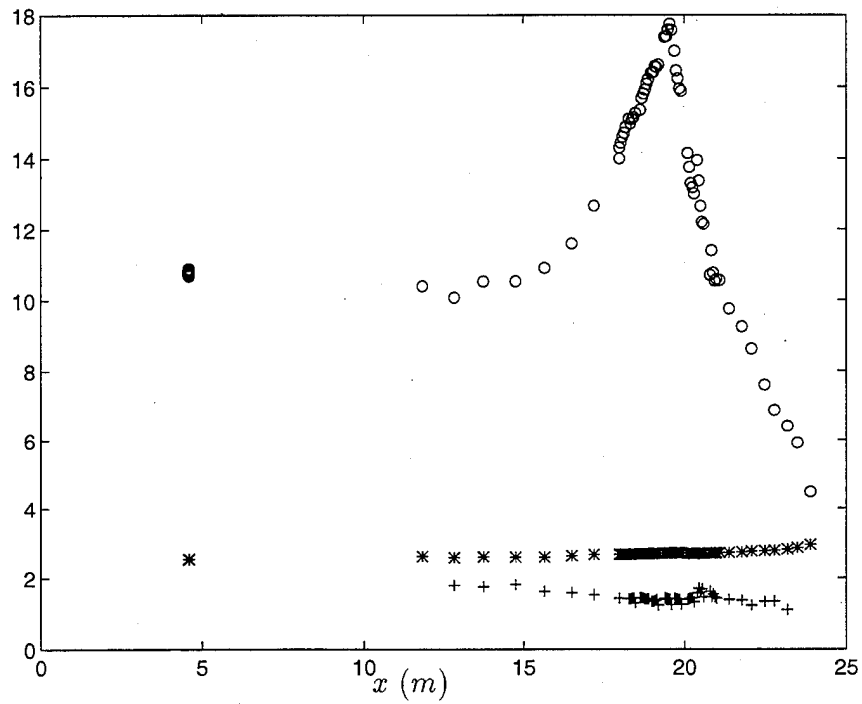
Figure B.3: Variation of wave height ('o'), wave period ('*') and phase speed ('+') for the third wave in Experiment W01
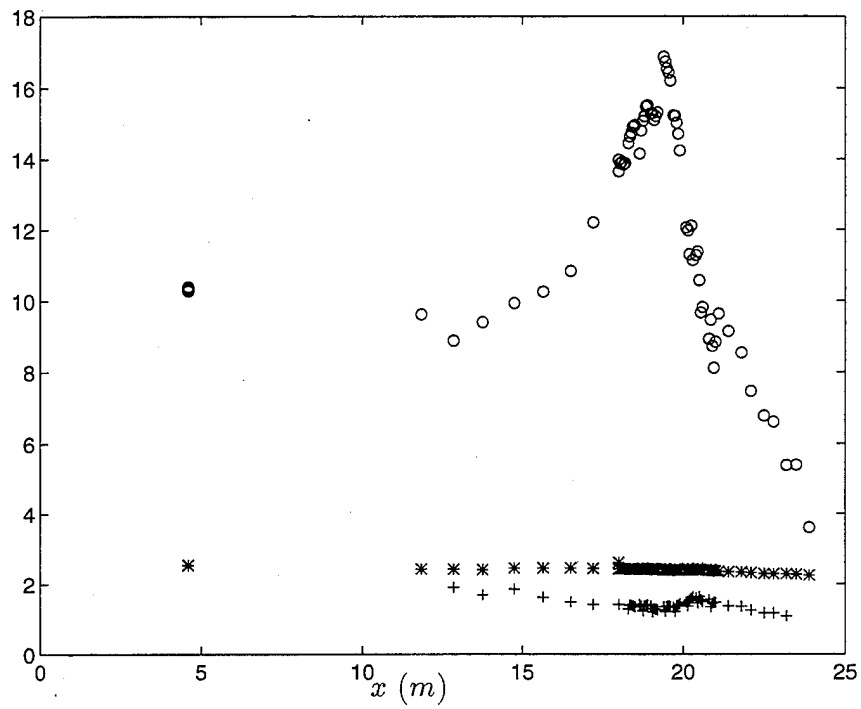
Figure B.4: Variation of wave height ('o'), wave period ('*') and phase speed ('+') for the fourth wave in Experiment W01

Figure B.5: Variation of wave height ('o'), wave period ('*') and phase speed ('+') for the fifth wave in Experiment W01

Figure B.6: Variation of wave height ('o'), wave period ('*') and phase speed ('+') for the first wave in Experiment W02
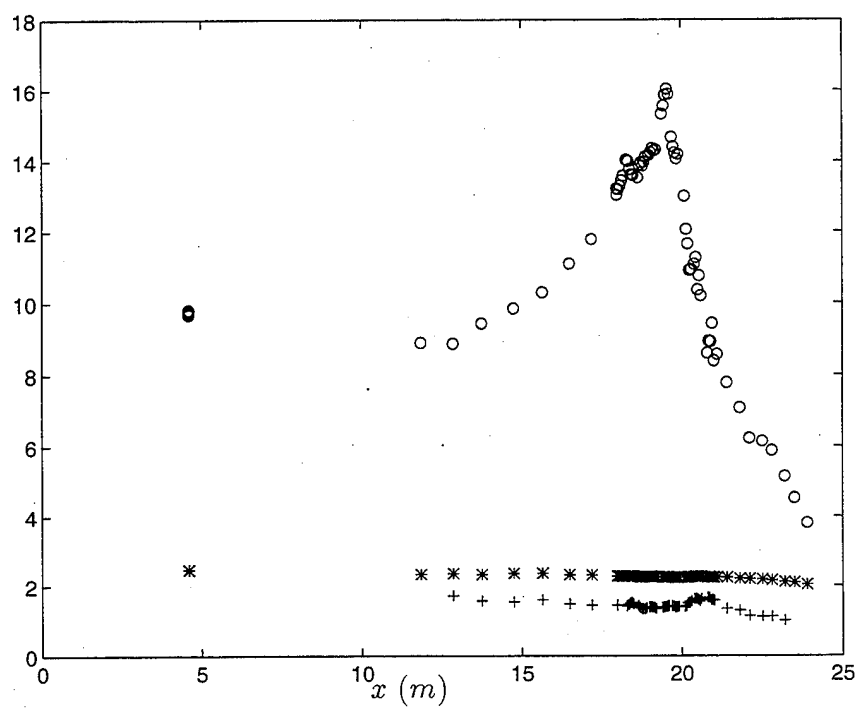
Figure B.7: Variation of wave height ('o'), wave period ('*') and phase speed ('+') for the second wave in Experiment W02

Figure B.8: Variation of wave height ('o'), wave period ('*') and phase speed ('+') for the third wave in Experiment W02

Figure B.9: Variation of wave height ('o'), wave period ('*') and phase speed ('+') for the fourth wave in Experiment W02
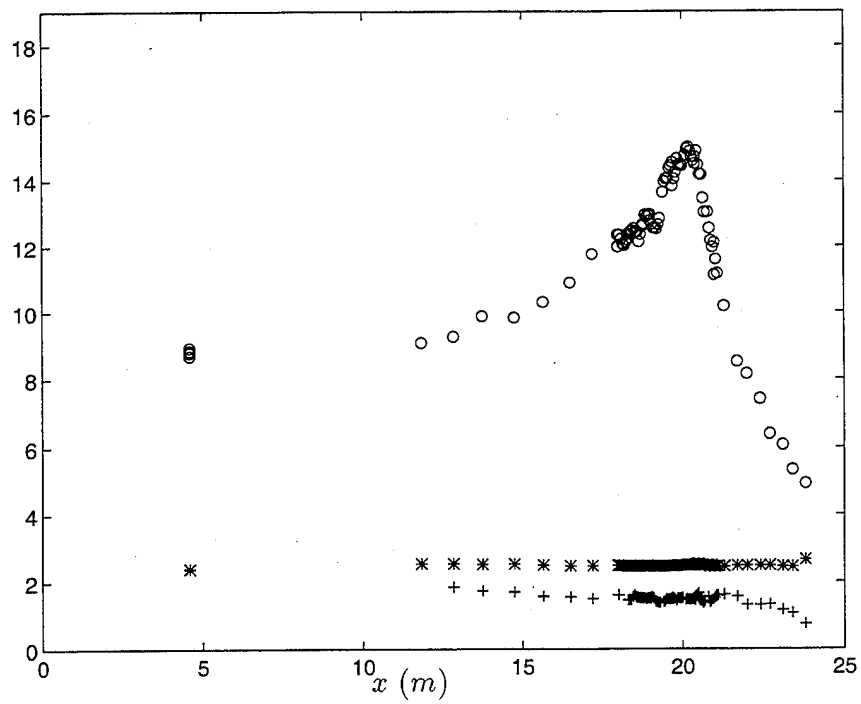
Figure B.10: Variation of wave height ('o'), wave period ('*') and phase speed ('+') for the fifth wave in Experiment W02

Figure B.11: Variation of wave height ('o'), wave period ('*') and phase speed ('+') for the first wave in Experiment W03
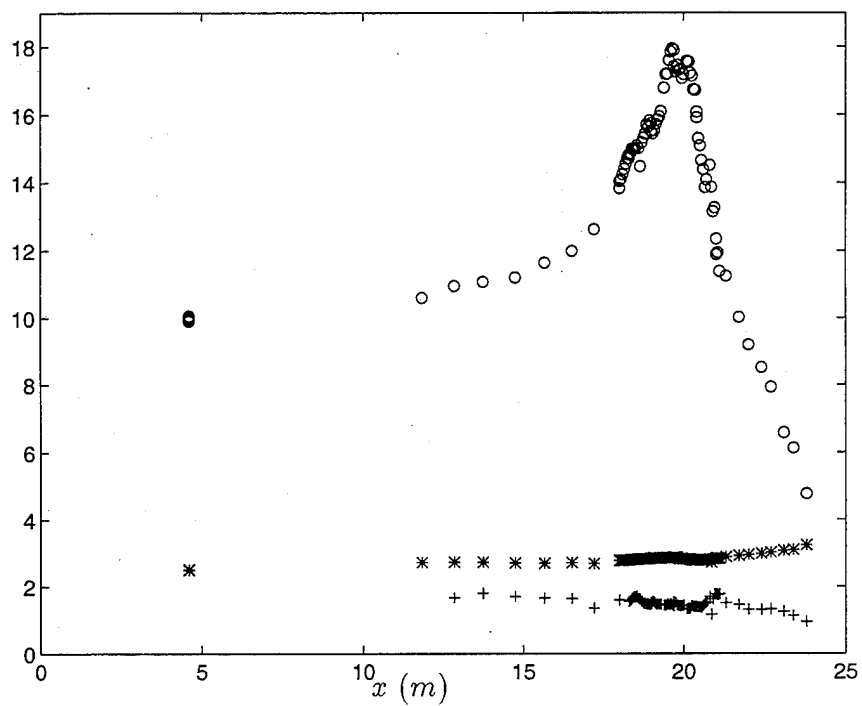
Figure B.12: Variation of wave height ('o'), wave period ('*') and phase speed ('+') for the second wave in Experiment W03
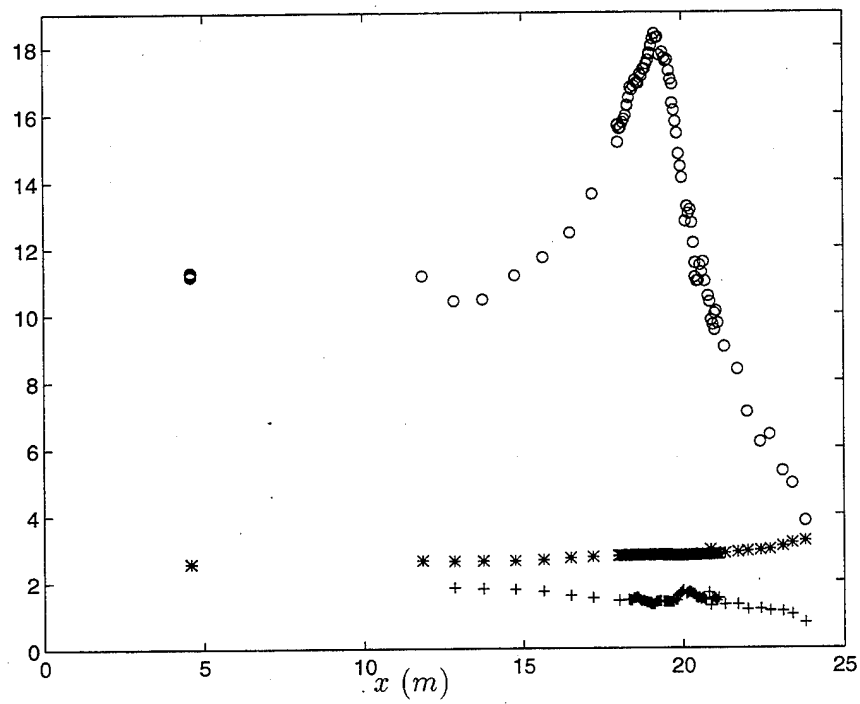
Figure B.13: Variation of wave height ('o'), wave period ('*') and phase speed
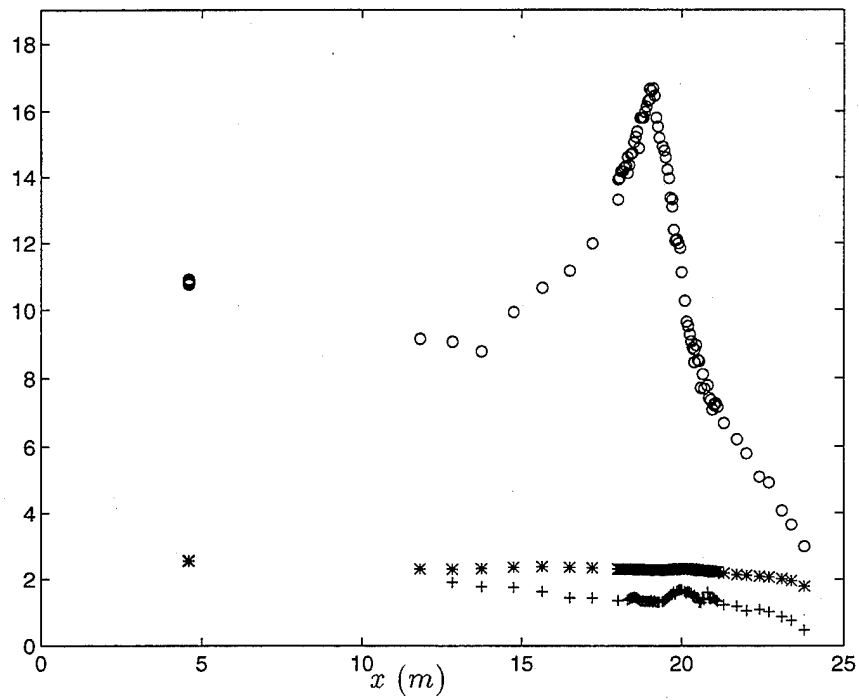('+') for the third wave in Experiment W03

Figure B.14: Variation of wave height ('o'), wave period ('*') and phase speed ('+') for the fourth wave in Experiment W03
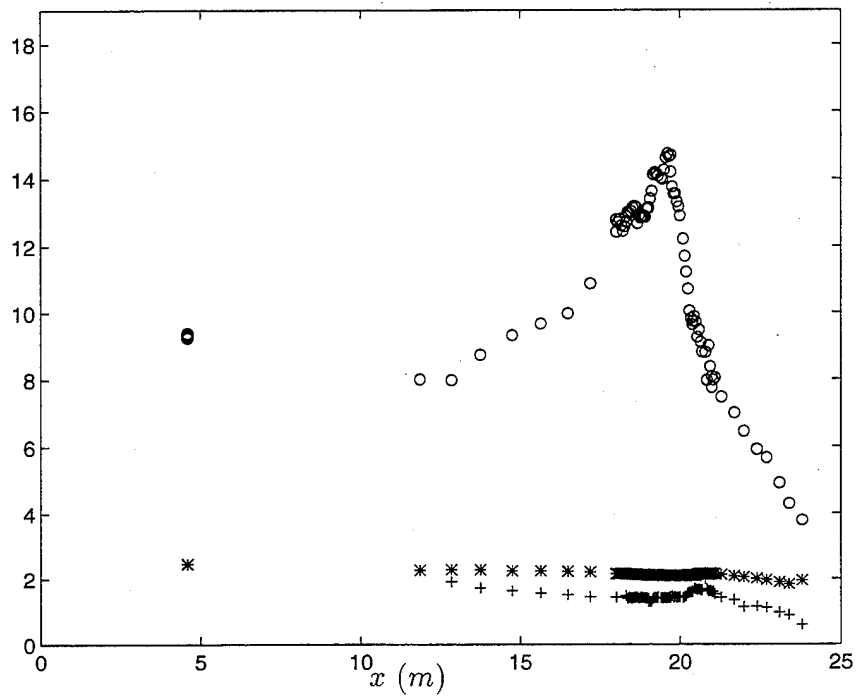
Figure B.15: Variation of wave height ('o'), wave period ('*') and phase speed ('+') for the fifth wave in Experiment W03
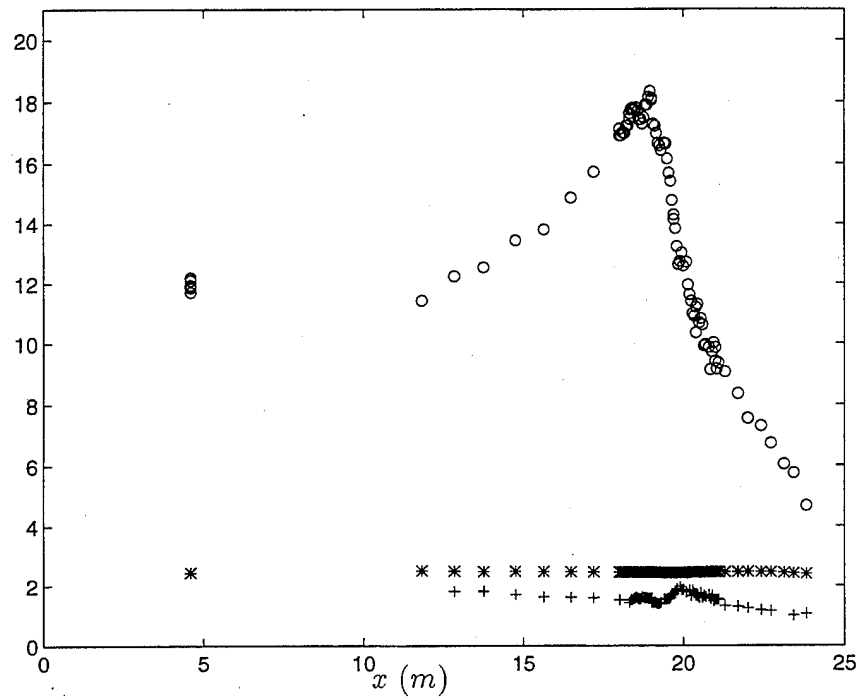
Figure B.16: Variation of wave height ('o'), wave period ('*') and phase speed ('+') for the first wave in Experiment W04
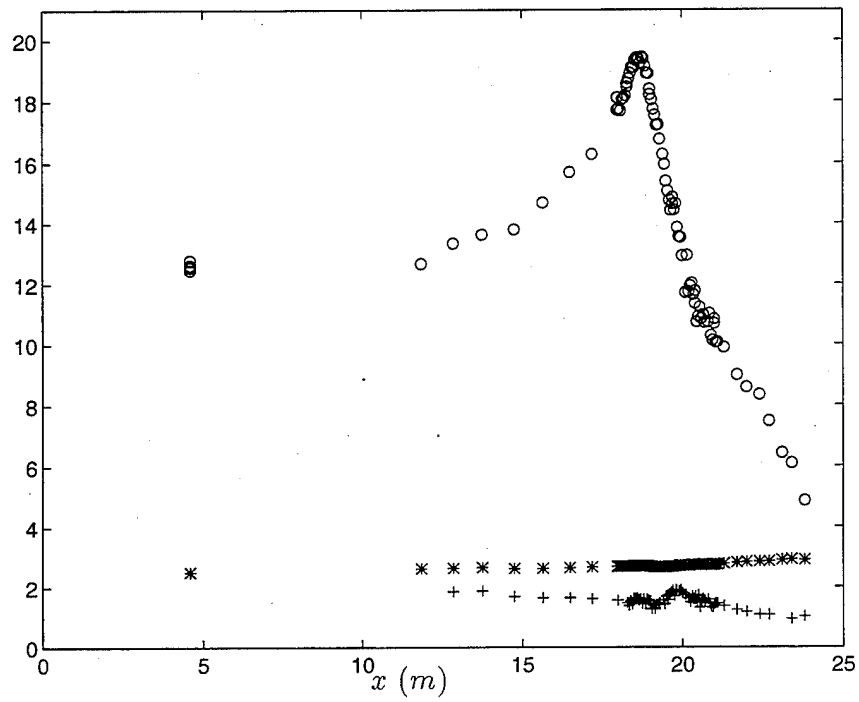
Figure B.17: Variation of wave height ('o'), wave period ('*') and phase speed ('+') for the second wave in Experiment W04

Figure B.18: Variation of wave height ('o'), wave period ('*') and phase speed ('+') for the third wave in Experiment W04

Figure B.19: Variation of wave height ('o'), wave period ('*') and phase speed ('+') for the fourth wave in Experiment W04

Figure B.20: Variation of wave height ('o'), wave period ('*') and phase speed ('+') for the fifth wave in Experiment W04
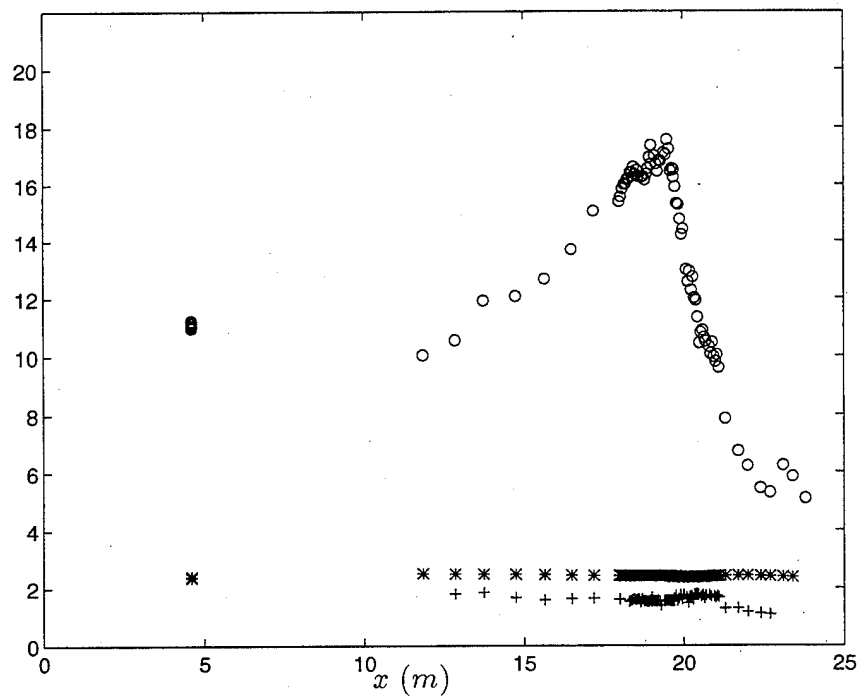
Figure B.21: Variation of wave height ('o'), wave period ('*') and phase speed ('+') for the first wave in Experiment W05

Figure B.22: Variation of wave height ('o'), wave period ('*') and phase speed ('+') for the second wave in Experiment W05
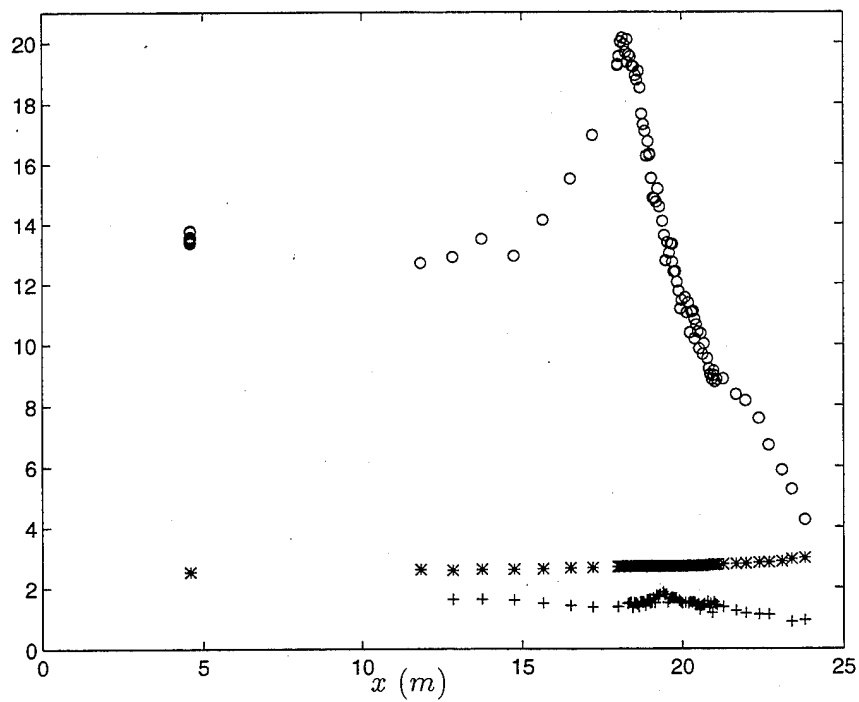
Figure B.23: Variation of wave height ('o'), wave period ('*') and phase speed ('+') for the third wave in Experiment W05
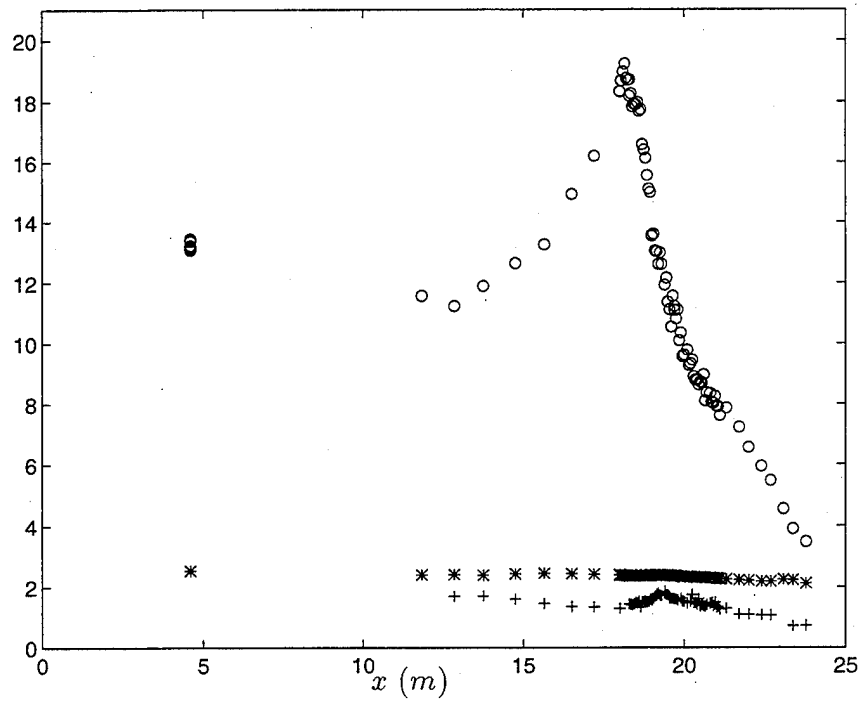
Figure B.24: Variation of wave height ('o'), wave period ('*') and phase speed ('+') for the fourth wave in Experiment W05
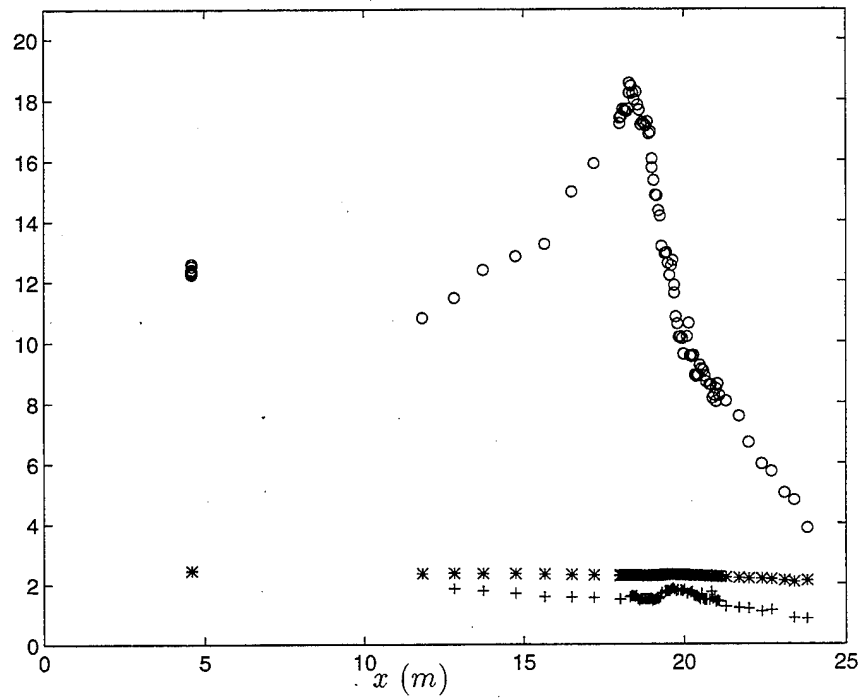
Figure B.25: Variation of wave height ('o'), wave period ('*') and phase speed ('+') for the fifth wave in Experiment W05
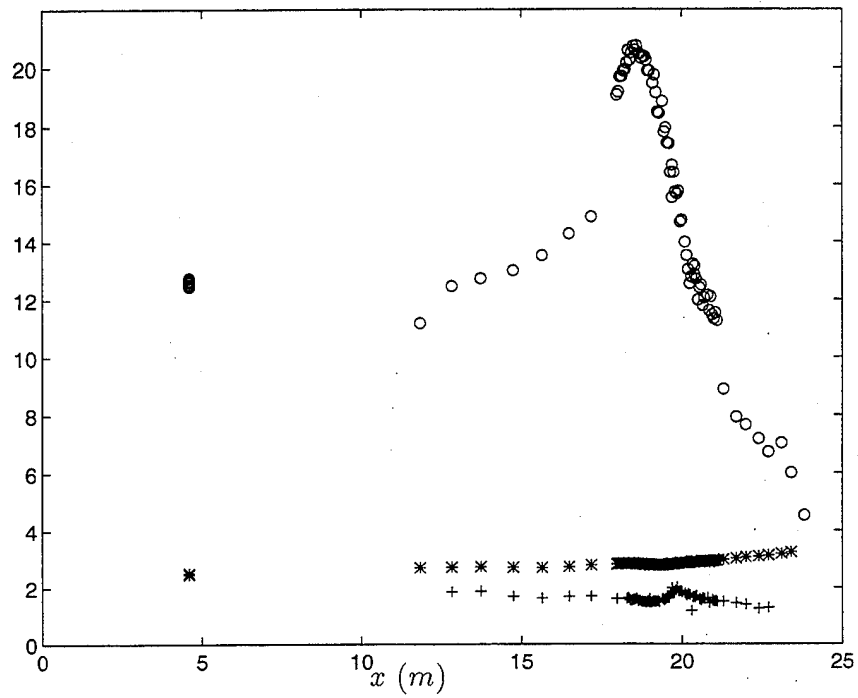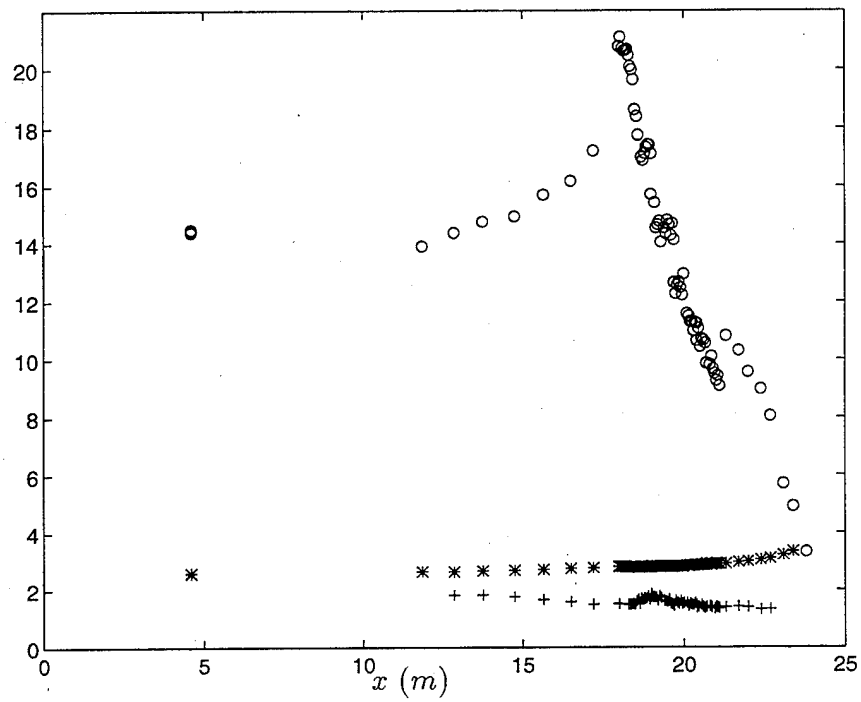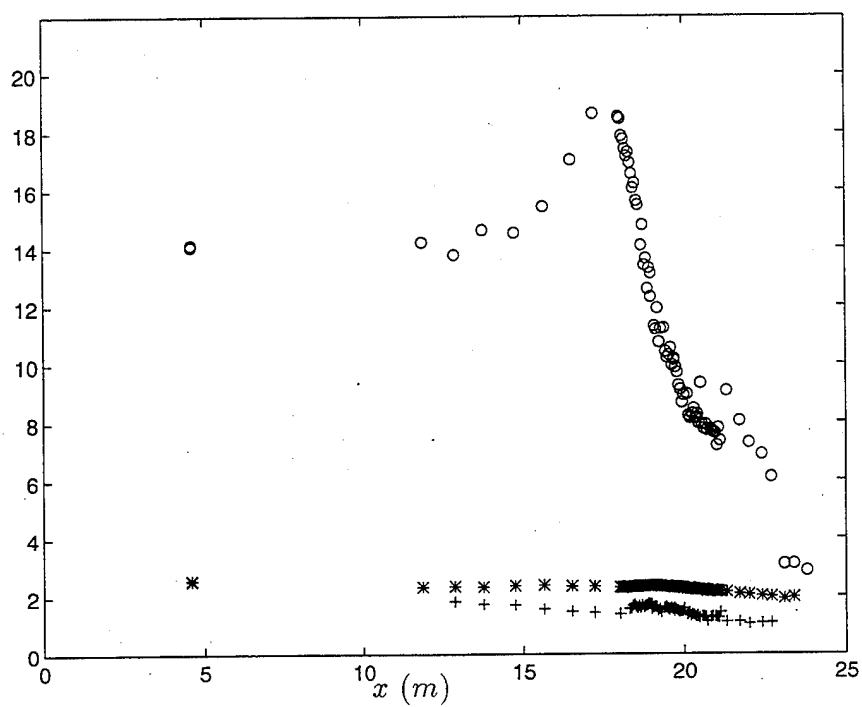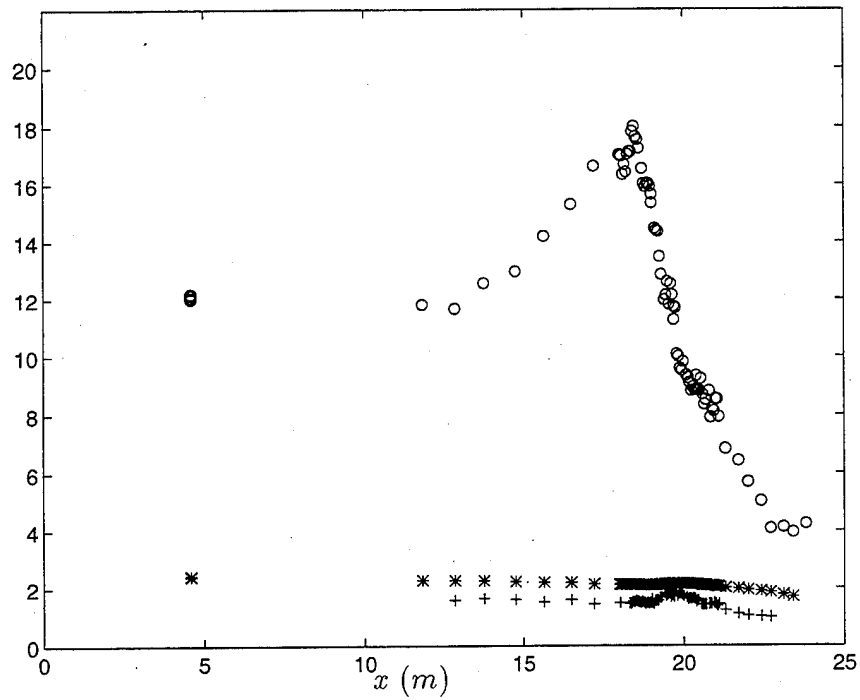
REFERENCES

Abdelrehman, S. M. and Thornton, E. B., 1988. Changes in the short wave amplitude and wave number due to the presence of infragravity waves. Proceedings of the ASCE Special Conference on Coastal Hydrodynamics, pp. 458-478.

Foote, Y., Huntley, D., Davidson, M., Russell, P., Hardisty, J. and Cramp, A., 1992. Incident wave groups and long waves in the nearshore zone. Proceedings of the 23rd International Conference on Coastal Engineering, pp. 974-989.

Dally, W. R., Dean, R. G., Dalrymple, R. A., 1984. A model for breaker decay on beaches. Proceedings of the 19th International Conference on Coastal Engineering, pp. 82-98.

Dally, W. R., Dean, R. G., Dalrymple, R. A., 1985. Wave height variation across beaches of arbitrary profile. Journal of Geophysical Research, Vol. 90, pp 11917-11927.

Funke, E. R. and Mansard, E. P. D., 1979. On the synthesis of realistic sea states in a laboratory flume. National Research Council of Canada, Hydraulic Laboratory Technical Report, LTR-HY-66.

Garrett, C. and Smith, J., 1976. On the interaction between long and short surface waves. Journal of Physical Oceanography, Vol. 6, pp. 925-930.

Goring, D. G., 1978. Tsunamis-The propagation of long waves onto a shelf. Rep. No. KH-R-38, W.M.Keck Lab. of Hydraulics and Water Res., CalTech, Pasadena, California.

Greenberg, M. D., 1988. Advanced Engineering Mathematics, Prentice Hall, Inc., New Jersey.

Hansen, J. B., 1990. Periodic waves in the surf zone : Analysis of experimental data. Coastal Engineering, Vol 14, pp. 19-41.

Henderson, F. M., 1966. Open Channel Flow. Macmillan Publ. Co., New York, pp. 61-79.

Huntley, D. A. and Kim, C-S., 1984. Is surf beat forced or free? Proceedings of the 19th International Conference on Coastal Engineering, Vol 9, pp. 1659-1676.

Kostense, J. K., 1984. Measurements of surf beat and set-down beneath wave groups. Proceedings of the 19th International Conference on Coastal Engineering, pp. 724-740.

Lippmann, T. C. and Holman, R. A., 1992. Wave group modulations in cross-shore breaking patterns. Proceedings of the 23rd International Conference on Coastal Engineering, pp. 918-931.

List, J. H., 1991. Wave groupiness variations in the nearshore. Coastal Engineering, Vol. 15, pp. 475-496.

List, J. H., 1992. A model for two-dimensional surf beat. Journal of Geophysical Research, Vol 97, pp. 5623-5635

Longuet-Higgins, M. S. and Stewart, R. W., 1962a. Radiation stresses in water waves; a physical discussion, with applications. Deep Sea Research, Vol 11, pp. 529-562.

Longuet-Higgins, M. S. and Stewart, R. W., 1962b. Radiation stress and mass transport in gravity waves, with application to surf beats. Journal of Fluid Mechanics, Vol. 13, pp. 481-504.

Longuet-Higgins, M.S. and Stewart, R. W., (1964). Radiation stress in water waves, a physical discussion with application. Deep Sea Research, 11, pp. 529-563.

Mansard, E. P. D. and Funke, E. R., 1980. The measurement of incident and reflected spectra using a least squares method. Proceedings of the 17th International Conference on Coastal Engineering, pp. 154-172.

Nakamura, S. and Kazumasa, K., 1992. Generation of infragravity waves in the breaking process of wave groups. Proceedings of the 23rd International Conference on Coastal Engineering, pp. 990-1003.

Peregrine, D. H., 1974. Water-wave interaction in the surf zone. Proceedings of the 14th International Conference on Coastal Engineering, pp. 500-517.

Phillips, O. M., 1980. The dynamics of the upper ocean. Cambridge University Press, Cambridge.

Roelvink, J. A., 1993a. Surf beat and its effect on cross-shore profiles. Thesis, Delft Hydraulics.

Roelvink, J. A., 1993b. Dissipation in random wave groups incident on a beach. Coastal Engineering, Vol 19, pp. 127-150.

Roelvink, J. A., Petit, H. A. H. and Kostense, J. K., 1992. Verification of one dimensional surfbeat model angainst laboratory data. Proceedings of the 23rd International Conference on Coastal Engineering, pp. 960-973.

Schäffer, H.A., 1993. Infragravity waves induced by short-wave groups. Journal of Fluid Mechanics, 247, pp. 551-588.

Schäffer, H. A., 1990. Infragravity water waves induced by short-wave groups. Series paper # 50, Institute of Hydrodynamics and Hydraulic Engineering, Technical University of Denmark.

Schäffer, H. A., Jonsson, I. G. and Svendsen, I. A., 1990. Free and forced cross-shore long waves. Water Wave Kinematics. pp. 367-385.

Schäffer, H. A. and Svendsen, I. A., 1988. Surf beat generation on a mild slope beach. Proceedings of the 21st International Conference on Coastal Engineering, pp. 1058-1072.

Southgate, H. N., 1993. Review of wave breaking in shallow water. HR published paper No. 71, Society of Underwater Technology conference on Wave Kinematics and Environmental forces, London.

Stive, M. J. F., 1984. Energy dissipation in waves breaking on gentle slopes. Coastal Engineering, Vol 8, pp. 99-127.

Svendsen, I. A., 1974. Cnoidal waves over a gently sloping bottom. Series paper # 6, Institute of Hydrodynamics and Hydraulic Engineering, Technical University of Denmark.

Svendsen, I. A., 1984. Wave heights and set-up in the surf zone. Coastal Engineering, 8, pp. 303-329.

Svendsen, I. A., 1987. Analysis of surf zone turbulence. Journal of Geophysical research, Vol. 92., pp. 5115-5124.

Svendsen, I. A. and Hansen, J. B. 1976. Deformation up to breaking of periodic waves on a beach. Proceedings of the 15th International Conference on Coastal Engineering, pp. 477-496.

Svendsen, I. A. and Hansen, J. B. 1988. Cross-shore currents in surf-zone modelling. Coastal Engineering, 12, pp. 23-42.

Svendsen, I. A. and Madsen, P. A., 1981. Energy dissipation in hydraulic jumps and breaking waves. Prog. rep. 55, Institute of Hydrodynamics and Hydraulic Engineering, Technical University of Denmark, pp. 39-47.

Symonds, G. Huntley, D. A. and Bowen, A. J., 1982. Two-dimensional surf beat: long wave generation by time varying break point. Journal of Geophysical Research, Vol. 87, pp. 492-498.

Wilson, B. S., 1966. Encyclopedia of Oceanography, R. W. Fairbridge, ed., Academic Press, New York.

Wilson, B. S., 1972. Seiches. Advances in Hydroscience, Vol 8, Academic Press, New York.

Whitham, J. B., 1974. Linear and Non-Linear Waves. Wiley Interscience Publication.